UNIVERSITY OF CALIFORNIA SAN DIEGO

Negative regulation of TLR4 signaling by GIV/Girdin shapes macrophage inflammatory responses

A dissertation submitted in partial satisfaction of the
requirements for the degree
Doctor of Philosophy

in

Biomedical Sciences

by

Lee Andrew Boland Swanson

Committee in charge:

Professor Pradipta Ghosh, Chair
Professor John Chang
Professor Victor Nizet
Professor Lawrence Prince
Professor Elina Zuniga

2020

The dissertation of Lee Andrew Boland Swanson is approved, and it is acceptable in quality and form for publication on microfilm and electronically:

_____

_____

_____

_____

_____

Chair

University of California San Diego

2020

DEDICATION

To:

Rebekah

TABLE OF CONTENTS

LIST OF FIGURES

ACKNOWLEDGEMENTS

This thesis is a body of work that represents my contributions to science over the past five and a half years. But a thesis is not done in isolation, and a scientist does not come into being without guidance and mentorship. During my graduate work I have had the privilege to work alongside talented individuals whose creative minds, drive to discover, and genuine love of science have helped me to hone my abilities and push my limits. All of the heated debates over contentious results, late nights sharing our crazy hypotheses, and beers consumed (after yet another failed experiment) are some of my most cherished memories. Thank you for helping me become the person and scientist I am today.

Chapter 2 in part is material being prepared to be submitted for publication in: **Swanson L**, Katkar GD, Chareddy Y, Tam J, Coates J, Sahoo D, Das S, Ghosh P. “Negative regulation of TLR4 signaling by GIV/Girdin shapes macrophage inflammatory responses.” The dissertation author was the primary author.

Chapter 3 in part a reprint of material submitted to be published in: Sahoo DS*, **Swanson L***, Sayed IM*, Katkar GD, Ibeawuchi SR, Lim BB, Mittal Y, Pranadinata RF, Tindle C, Fuller M, Stec DL, Chang JT, Sandborn WJ, Das S, Ghosh P. 2020. “Modeling disease continuum states from a clustered Boolean implication network”. *under review*. The dissertation author was the primary author.

VITA

2012	Bachelor of Science in Biochemistry, University of Minnesota-Twin Cities
2020	Doctor of Philosophy in Biomedical Sciences, University of California San Diego

PUBLICATIONS

Swanson L, Sanyaolu R, Gnoske T, Whelan CJ, Lonsdorf E, Cordeiro N. Differential response of nest predators to the presence of a decoy parent in artificial nests. Bird Study, 59(1):96-101. (2012).

El Ghazal R, Yin X, Johns SC, **Swanson L**, Macal M, Ghosh P, Zuniga EI, Fuster MM. Glycan Sulfation Modulates Dendritic Cell Biology and Tumor Growth. Neoplasia, 18(5), 294-306. doi:10.1016/j.neo.2016.04.00. (2016).

Ghosh P, Aznar N, **Swanson L**, Lo IC, Lopez-Sanchez I, Ear J, Rohena C, Kalogriopoulos NA, Joosen L, Dunkel Y, Sun N, Nguyen P, Bhandari D. Biochemical, Biophysical and Cellular Techniques to Study the Guanine Nucleotide Exchange Factor, GIV/Girdin. *Curr Protoc Chem Biol*. 8:265-298 (2016).

Dunkel Y, Diao K, Aznar N, **Swanson L**, Liu L, Zhu W, Mi XY, Ghosh P. Prognostic impact of total and tyrosine phosphorylated GIV/Girdin in breast cancers. FASEB J, 30(11), 3702-3713. doi:10.1096/fj.201600500. (2016).

Dallari S, Macal M, Loureiro ME, Jo Y, **Swanson L**, Hesser C, Ghosh P, Zuniga EI. Src family kinases Fyn and Lyn are constitutively activated and mediate plasmacytoid dendritic cell responses. Nat. Comm. doi: 10.1038/ncomms14830. (2017)

Getz M, **Swanson L**, Sahoo D, Ghosh P, Rangamani P. Guanine-nucleotide Exchange Modulator, GIV/Girdin, Serves as a Tunable Valve for Growth Factor-Stimulated Cyclic AMP Signals. MBoC. doi.org/10.1091/mbc.E18-10-0630. (2019)

Ghosh P, **Swanson L**, Sayed IM, Mittal Y, Lim BB, Ibeaquchi SR, Foretz M, Viollet B, Sahoo DS, Das S. The stress polarity signaling (SPS)-pathway serves as a marker and a target in the leaky gut barrier. Life Sci. Alliance. (2020).

ABSTRACT OF THE DISSERTATION

Negative regulation of TLR4 signaling by GIV/Girdin shapes macrophage inflammatory responses

by

Lee Andrew Boland Swanson

Doctor of Philosophy in Biomedical Sciences

University of California San Diego, 2020

Professor Pradipta Ghosh, Chair

Various insults (e.g. bacterial/viral infection, foreign bodies, or trauma) can trigger an acute inflammatory response which is generally protective; it contains and extinguishes the insult/trigger, removes damaged tissues, and prompts tissue repair. However, an uncontrolled or prolonged inflammatory response can lead to excessive tissue destruction and is a pathologic hallmark of inflammatory diseases including sepsis, arthritis, inflammatory bowel disease (IBD), organ fibrosis, type-II-diabetes, and cancers. Toll-like receptor 4 (TLR4) signaling in response to the Gram-negative bacterial antigen lipopolysaccharide (LPS) is a powerful inducer of in-

flammatory responses in macrophages and is critical for the control of bacterial infections and re-establishment of tissue homeostasis. However, uncontrolled activation of TLR4 can result in acute sepsis, and contribute to chronic inflammatory diseases. Therefore, understanding the intricate regulatory mechanisms of TLR4 inflammatory responses is essential for development of novel therapeutics combating inflammation-driven disease. In this dissertation, I describe a novel mechanism for negative regulation of TLR4 signaling by the Guanine Exchange Modulator (GEM) family member, GIV, and its impact on macrophage inflammatory responses both in vitro and in vivo animal models of inflammatory disease.

Chapter 1

Introduction

1.1 Macrophages: guardians of tissue homeostasis and champions of microbial defense

The initial discovery of macrophages by Ellie Metchnikoff in 1883 characterized the ”amoeboid cells” for their ability to ingest dead or dying cells or foreign bodies and was the first step to our current understanding of innate immune defense (Merien, 2016). Over a century of intense investigation has revealed that macrophages are found in all tissues of the body and play essential roles in diverse biological processes including development, tissue homeostasis, and immune defense through their ability to sense and adapt to changes in the local microenvironment (Murray and Wynn, 2011). A prime example of the diverse functions and fine-tuned sensing capabilities of macrophages is witnessed in the intestine, which house the largest pool of macrophages in the body and are positioned in close proximity to trillions of bacteria and foreign antigens in the gut lumen (Smith et al., 2011). Under steady state condi-

tions gut resident macrophages maintain tissue homeostasis by phagocytosing apoptotic cells and debris, promoting epithelial integrity and repair, and maintaining an non-reactive tissue environment through the production of IL-10 which antagonizes pro-inflammatory macrophage responses and promotes anti-inflammatory Treg function (Andrews et al., 2018, Gordon and Pluddemann, 2017, Gordon and Plüddemann, 2018). However, macrophages also act as sentinels for microbial infection and are constantly patrolling the body for potential threats. Tissue damage caused by microbial infection triggers blood monocytes to enter the tissue and differentiate into pro-inflammatory macrophages where they engulf and degrade invading microbes as well as dead cells and debris. In addition to their role as phagocytes, macrophages initiate a multifaceted anti-microbial response through secretion of anti-microbial peptides and proteases, reactive oxygen and nitrogen species, and pro-inflammatory cytokines such as TNFα, IL-1, IL-6, IL-12, and CCL2 which promote anti-microbial Th1 and Th17 immune responses (Rosenberger et al., 2004, Smith et al., 2011, Zhang and Mosser, 2008). The importance of pro-inflammatory macrophage responses in the control and clearance of pathogenic microbes has been demonstrated in many types of bacterial infection including Listeria monocytogenes, Salmonella, Mycobacterium tuberculosis, and chlamydial infection. (Rosenberger et al., 2004, Pfeffer et al., 1993, Rottenberg et al., 2002, Shaughnessy and Swanson). Therefore, it is not surprising that therapeutically enhancing macrophage antimicrobial function has proven to be a promising approach for combating infections. For example, mice treated with lipopeptide-2, an IL-8 family member cytokine, increased macrophage recruitment to the lung during pneumonia infection resulting in increased bacterial control and survival (Reppe et al., 2009). Other macrophage targeting therapeutic strategies include administering keratinocyte growth factor (KGF) to enhance phagolysosome fusion and nitric oxide production in *M. tuberculosis* and pulmonary *E.*

coli infection, and treatment of leukotriene B4 (LTB4) to enhance ROS production during *S. pyrogens* infection (Munguia and Nizet, 2017). Taken together, it is clear that macrophages play an essential role in sensing and responding to microbial infection and show promise as a therapeutic target for infectious disease. However, our understanding of macrophage antimicrobial responses is still far from complete, and new insights into mechanisms of macrophage inflammatory responses is needed to develop the next generation of macrophage targeting therapeutics.

Although a robust inflammatory response is required for efficient pathogen clearance, collateral damage to host tissue is inevitable, and therefore it is imperative that inflammatory responses be quickly shut down following pathogen clearance. Macrophages play essentials roles in both the initiation and resolution of inflammatory responses through their ability sense the needs of the tissue microenvironment and modulate immune responses accordingly. During the resolution phase of inflammation, pro-inflammatory macrophages either undergo apoptosis, or transition to an anti-inflammatory phenotype prompted by phagocytosis of apoptotic neutrophils (Ortega-Gómez et al., 2013, Scannell et al., 2007). Anti-inflammatory macrophages promote resolution by inhibiting leukocyte recruitment, promoting neutrophil apoptosis, and enhancing efferocytosis by macrophages through the production of lipid mediators (lipoxins, resolvins), proteins (Annexin A1, galectins), adenosine, and hydrogen sulphide (Headland and Norling, 2015). Failure of macrophages to transition to an anti-inflammatory phenotype can result in unchecked chronic inflammation associated with inflammatory diseases including atherosclerosis, asthma, rheumatoid arthritis, fibrosis, and inflammatory bowel disease (Wynn et al., 2013). In addition to resolving inflammation, macrophages help restore normal tissue function and are required for successful wound healing, tissue repair, regeneration, and fibrosis through the secretion

of pro-healing cytokines (IL-10), growth factors (TGF-β, WNT, VEGF), and extracellular matrix (ECM) remodeling proteases (MMPs and TIMPs) (Lucas et al., 2010, Ortega-Gómez et al., 2013, Saclier et al., 2013). Dysregulation of pro-healing macrophage functions leads to aberrant production of these mediators resulting in a state of chronic injury and development of pathological fibrosis (Wynn and Vannella, 2016). Therefore, the regulated transition of macrophages from pro-inflammatory to pro-healing phenotypes is essential for maintaining tissue health and homeostasis.

Taken together, macrophages are key mediators of tissue homeostasis and microbial defense that orchestrate the initiation, progression, and resolution of inflammatory responses. Their ability to rapidly morph their cellular programs to adapt to the specific needs of various tissue types makes them powerful tools in the immune defense arsenal. Although decades of research have yielded a rich understanding of macrophage inflammatory responses, we are only now beginning to uncover the intricate cellular and molecular mechanisms that govern macrophage function. It is my hope that we can build upon our current knowledge of macrophage biology with the ultimate goal of harnessing the power of macrophages as therapeutic weapons against inflammatory and infectious disease.

1.2 Toll-like receptors in pathogen sensing and inflammatory responses

Macrophage immune function was initially thought to be non-specific and focused solely on engulfment and destruction of pathogens, followed by antigen presentation and activation of adaptive immune cells. However, it is now clear that in addition to their role in pathogen

engulfment and antigen presentation, macrophages also mount pathogen specific immune responses. Unlike adaptive immune cells which confer specificity through cell surface receptors that are specific for a single antigen, macrophages have a variety of pathogen recognition receptors (PRRs) including Toll-like receptors (TLRs), nucleotide-binding oligomerization domain-like receptors (NLRs), C-type lectin receptors (CLRs), and RIG-1 like receptors (RLRs) that allow them to recognize various types of bacteria, viruses, yeast, and protozoa (Jang et al., 2015). Members of each of these PRR families recognize conserved molecular structures, or pathogen-associated molecular patterns (PAMPs) that have three core features; 1) they must be required for pathogen survival, 2) conserved across the entire class of pathogen, and 3) distinguishable from host structures (Mogensen, 2009). The repertoire of PRRs and the microbial targets they recognize are a product of millions of years of co-evolution between the host immune system and infectious microbes. Of all the PRRs, toll-like receptors have been the most well studied and have transformed our understanding of innate immune recognition.

Currently, there are 10 identified TLRs in humans, and 13 in mice, that are able to recognize a variety of microbial products including peptidoglycan and lipoproteins (TLR2), double-stranded RNA (TLR3), lipopolysaccharide and lipoteichoic acids (TLR4), bacterial flagellin (TLR5), and CpG DNA (TLR9) (Medzhitov, 2001). Professional antigen presenting cells (APCs) (i.e. macrophages, dendritic cells, and B-cells) are the dominant cell types that express TLRs, however TLR expression has been observed in many other cell types including non-immune cells (Muzio et al., 2000). Of all TLRs, Toll-like receptor 4 (TLR4) has been the most extensively studied since its discovery as the immune sensor for Lipopolysaccharide (LPS), a critical component of the outer cell membrane of Gram-negative bacteria, and stands out as a key signaling system which dictates major pro-inflammatory and anti-inflammatory cellular programs

in macrophages (Poltorak et al., 1998, Raetz and Whitfield, 2002). Interestingly, TLR4 is unable to directly bind LPS and requires the accessory proteins LPS binding protein (LBP), CD14, and MD2 to initiate receptor activation (Lu et al., 2008). Binding of LPS causes homodimerization of TLR4 monomers, recruitment of key adaptor proteins (MyD88, Mal, TRIF, and TRAM), and subsequent activation of downstream signaling pathways including the IRAK-TRAF, MAPK, PI3K-AKT, and TBK1 pathways. These signaling events converge on the transcription the transcription factors NFκB, AP-1, CREB, and IRF3 which drive expression of inflammatory cytokines (TNFα, IL-1β, IL-6, IL-12), type-I interferons, and antimicrobial factors required for initiation and propagation of the inflammatory response (Lu et al., 2008).

The first, and most critical, step in TLR4 activation is receptor dimerization and recruitment of adaptor proteins, which are both facilitated by Toll/interleukin-1 receptor (TIR) domains which are found in the cytoplasmic region of TLRs and TLR adaptor proteins MyD88, MAL, TRIF, TRAM, and SARM (Ve et al., 2015). TIR domains are comprised of 125-200 residues and have three conserved regions Box 1, Box 2, and Box 3, of which Box 2 is the most highly conserved across TIR-domain containing proteins and has been shown to play essential roles in TLR signaling (Li et al., 2005, Slack et al., 2000). Structural analysis has revealed that TIR domains adopt a flavodoxin-like fold, featuring a central five-stranded parallel β-sheet surrounded by five α-helices (Xu et al., 2000). Although the general topology of TIR domains is conserved, structural differences in α-helix positioning and orientation is thought to influence adaptor protein requirements and differing signaling profiles between TLRs (Ve et al., 2015). In addition to the core structure, the surface exposed BB-loop located in Box 2 of TIR domains, containing an invariant proline residue (P712 in TLR4), forms an essential interface for TLR homodimerization and adaptor recruitment (Li et al., 2005). In fact, the discovery of TLR4 as the receptor

for LPS was prompted by the characterization of C3H/HeJ mice which are unresponsive to LPS due to a P712H mutation within the BB-loop of TLR4 (Poltorak et al., 1998). The importance of the BB-loop in antimicrobial inflammatory responses is exemplified by the ability of some pathogenic bacteria to evade innate immune activation by secreting proteins with homology to the BB-loop region of TIR domains to block TIR dimerization and activation (Cirl et al., 2008, O'Neill, 2008). Additionally, engineered cell-permeating "decoy peptides" corresponding to the BB-loop of TIR domains have been used as a research tool and have been proposed for therapeutic intervention in inflammatory diseases involving overactive TLR signaling (Toshchakov et al., 2011, Toshchakov and Vogel, 2007).

As with any inflammatory response, negative regulation of LPS/TLR4 responses is necessary to limit pro-inflammatory cytokine production and prevent prolonged hyperinflammation that can result in excessive tissue damage and sepsis. Negative regulation of TLR4 can occur at multiple levels of the signaling cascade including the extracellular domain of TLR4(RP105, soluble decoy TLRs), TIR-adaptor recruitment and activation (STL2, SIGIRR, TRIAD3a, and SOCS1), and TLR4 activated kinases (IRAK-M, IRAK2c, MyD88s, TRAF1/4, and A-20) (Brint et al., 2004, Qin et al., 2005, Wald et al., 2003, Kobayashi et al., 2002, Divanovic et al., 2005). In addition to these direct mechanisms of inhibition, TLR responses are subject to negative feedback mechanisms such as internalization and degradation of TLR4 or in some cases apoptosis via both caspase-dependent and caspase-independent mechanisms (Liew et al., 2005). The intricate layers of TLR4 negative regulation speak to the destructive potential of unchecked TLR4 inflammatory responses. Understanding these mechanisms further will facilitate the development of novel strategies to combat TLR-mediated inflammatory disease.

1.3 Heterotrimeric G-protein signaling in inflammation

In addition to TLR signaling, G-protein signaling plays a critical role in multiple aspects of macrophage inflammatory responses. Heterotrimeric G proteins (henceforth, trimeric) work as molecular switches that control the flow of information from extracellular cues to a wide array of intracellular effector proteins (Gilman, 1987, Morris and Malbon, 1999). Activation of trimeric G proteins by G-protein-coupled Receptors (GPCRs) has two signaling components 1) alpha-subunit activation which modulates adenylate cyclase (AC) $\rightarrow$ cAMP pathway, and 2) release of 'free; G$\beta\gamma$-heterodimers which directly bind and initiate multiple signaling pathways (i.e. PLCγ2, P-REX, and Class 1 PI3Ks). Both components of G protein signaling have been implicated in key inflammatory signaling pathways including activation of NFκB (Ye, 2001) and signaling via the MAPK-AP-1 pathway (Karin, 1995), two key events within the LPS/TLR4 signaling network. In the context of injury, inflammation and repair, activation of G proteins by GPCRs is important for macrophage chemotaxis, neutrophil degranulation, superoxide generation, endothelial permeability, and inflammatory gene expression [reviewed in (Sun and Ye, 2012)]. Among the multitude of ligands that are known to initiate G protein signaling, chemokines and their receptors have emerged as attractive tractable targets for the pharmaceutical industry in combating inflammation (Proudfoot, 2002, Wells et al., 1998). In addition to canonical activation by GPCRs, G-proteins have been shown to play a role in LPS stimulated inflammatory responses (Fan et al., 2005, Ferlito et al., 2002, Dauphinee et al., 2011). Specifically, genetic ablation of Gαi resulted in high circulating levels of TNFα and increases in infiltrating neutrophils in both the gut and lung when mice were challenged with LPS (Fan et al., 2005), suggesting that activation of Gαi inhibits pro-inflammatory responses. Another study found that rapid cytokine production in bladder epithelial cells in response to LPS is dependent on a rapid increase in cAMP levels that

induce cytokine production via activation of the transcription factor CREB (Song et al., 2007), again pointing to non-canonical activation of G-proteins in the regulation of LPS/TLR4 inflammatory responses. However, it is still unknown how G-proteins activation is achieved downstream of LPS stimulated TLR4.

1.4 The role of GIV/Girdin in cell signaling

GIV is a multimodular signal transducer and a member of the non-receptor Guanine Exchange Modulator (GEM) family of proteins (Ghosh et al., 2017). Unlike the canonical GPCR/G protein pathway, in which G proteins engage exclusively with ligand-activated GPCRs, GEMs like GIV can bind and modulate G protein activity downstream of a diverse variety of ligand-activated receptors (Ghosh et al., 2017, Garcia-Marcos et al., 2015, Ghosh, 2015a, Ghosh, 2015b). This unique function is facilitated by an evolutionarily conserved short motif (30-aa) that directly binds and modulates two subtypes of trimeric G proteins [activates GNAI as a GEF, and inhibits GNAS as a GDI (Gupta et al., 2016). The impact of such dual modulation of opposing G proteins is sustained suppression of the cAMP→pCREB axis (Ghosh et al., 2017). Studies from our lab and others employing a selective GEM-deficient GIV mutant (F1685A) have demonstrated that the signaling network triggered in cells with wild-type GIV is a mirror image of the network in cells expressing a GEM-deficient mutant GIV; signals that are enhanced in cells that are GEM-proficient are suppressed in cells that are GEM-deficient, and vice versa. In addition to the GEM module, the C-terminus of GIV features multiple binding motifs that allow GIV to bind multiple classes of cell surface receptors (i.e. SH2-domain→RTK, PTB→Integrins, PBM→frizzled receptors) (Ghosh et al., 2017). Together, the GEM motif and the C-terminal binding modules allow GIV to facilitate G-protein activation downstream of non-GPCR recep-

tors.

Over a decade of research by our lab and others has revealed the diverse biological processes impacted by non-canonical G-protein activation by GIV including cell motility, golgi structure and secretory function, autophagy, endosome maturation, cell survival, cell polarity, cell division, endo- and exocytosis, and cell-cell junctions (Lopez-Sanchez et al., 2014, Garcia-Marcos et al., 2010, Garcia-Marcos et al., 2009, Lo et al., 2015, Beas et al., 2012, Ichimiya et al., 2015, Sasaki et al., 2015). GIV-dependent signaling has also been implicated in a number of pathophysiologic conditions that suggest GIV-GEM may modulate inflammatory signaling. GIV mRNA and protein increases after dermal wounds (Dunkel et al., 2012), nephrotic injury (Wang et al., 2015), and fibrogenic insults to the liver (Lopez-Sanchez et al., 2014) and activation of GIV is indispensable for healing after vascular injury (Miyachi et al., 2015, Miyachi et al., 2014), myocardial infarction (Hayano et al., 2015), dermal wounds (Piao et al., 2015), and podocyte survival after nephotic injury (Wang et al., 2015). In the context of immune cells, GIV is highly expressed in multiple lymphoid tissues including spleen and lymphnode (Le-Niculescu et al., 2005). Additionally, GIV expression increases 18-fold during macrophage differentiation and is required for macrophage chemotaxis (Ghosh et al., 2008). Our lab also found that Gαi is activated in response to LPS and that GIV-GEM function is required for the enhancement of PI3K-Akt signals in liver-resident myofibroblasts (Lopez-Sanchez et al., 2014). Another group has recently shown that the GIVSTAT3 signaling axis is required for angiogenesis in response to the proinflammatory cytokine IL-17(Pan et al., 2015). Taken together, it appears that GIV plays a role in modulating inflammatory responses in multiple contexts. However, GIV's impact on the regulation of TLR4 signaling and macrophage inflammatory responses has not been rigorously explored.

1.5 Outline of the dissertation

Our understanding of macrophage biology as progressed immensely since their initial discovery in 1883. Over a century of discovery and technological advancement in the fields of cell biology, biochemistry, genetics, and immunology have fueled our inquiry into the mechanisms governing macrophage function and their contribution to human health and disease. However, a complete understanding of macrophage physiological function and regulatory mechanisms is still far from reality. The vast heterogeneity of macrophages subsets, the signaling pathways that instruct them, and the transcriptional programs that define them are only now beginning to be elucidated. With these new discoveries has come an appreciation for the role of macrophages in maintaining tissue homeostasis in every part of the body, as well as the realization that dysregulated macrophage function contributes to a plethora of inflammatory diseases. Therefore, it is imperative that we continue to push our understanding of macrophage regulatory mechanisms, especially in the context of disease, to develop novel therapeutic strategies to combat these diseases.

The remainder of my dissertation will be dedicated to describing my Ph.D. work and how it has focused on elucidating the intricate signaling events that govern macrophage inflammatory responses. I will start with a description of my main work on the discovery and characterization of GIV as novel regulator of TLR4 signaling, its consequences for macrophage inflammatory responses, and the impact dysregulation of this pathway has on inflammatory diseases (Chapter 2). I will then dedicate a section to describing my work on the identification and validation of a therapeutic target for fixing defects in gut barrier function and its implication in treating inflammatory bowel disease (Chapter 3). Finally, I will discuss how my thesis work has advanced the field, and future directions of the work (Chapter 4).

Chapter 2

Negative regulation of TLR4 signaling by GIV/Girdin shapes macrophage inflammatory responses

Various insults (e.g. bacterial/viral infection, foreign bodies, or trauma) can trigger an acute inflammatory response which is generally protective; it contains and extinguishes the insult/trigger, removes damaged tissues, and prompts tissue repair. However, an uncontrolled or prolonged inflammatory response can lead to excessive tissue destruction and is a pathologic hallmark of inflammatory diseases including sepsis, arthritis, inflammatory bowel disease (IBD), organ fibrosis, type-II-diabetes, and cancers. Toll-like receptor 4 (TLR4) signaling in response to the Gram-negative bacterial antigen lipopolysaccharide (LPS) is a powerful inducer of inflammatory responses in macrophages and is critical for the control of bacterial infections and re-establishment of tissue homeostasis. However, uncontrolled activation of TLR4 can re-

sult in acute sepsis, and contribute to chronic inflammatory diseases. Therefore, understanding the intricate regulatory mechanisms of TLR4 inflammatory responses is essential for development of novel therapeutics combating inflammation-driven disease. In this work, we describe a novel mechanism for negative regulation of TLR4 signaling by the Guanine Exchange Modulator (GEM) family member, GIV, and its impact on macrophage inflammatory responses both in vitro and in vivo animal models of inflammatory disease.

2.1 Introduction

Like most diseases, pathogenic inflammation is a disorder of signal transduction. Of the multitude of signaling pathways linked to the initiation of inflammation, Toll-like receptor-4 (TLR4), which is activated by lipopolysaccharide (LPS), an integral component of gram-negative bacteria, stands out as a key signaling system which dictates major pro-inflammatory and anti-inflammatory cellular programs in macrophages. TLR4 is a member of the larger TLR family which recognize a wide variety of Pathogen Associated Molecular Patterns (PAMPS) and initiates acute inflammation through production of inflammatory cytokines and type 1 interferons (Moynagh, 2005). Specialized TLRs for each class of PAMP allow fine tuning of the inflammatory response for efficient removal of the pathogen, with minimal host tissue destruction.

TLR4 efficiently detects gram-negative bacterial infections through recognition of the bacterial membrane component, LPS. Binding of LPS to TLR4 causes homodimerization of TLR4 monomers, recruitment of key adaptor proteins (MyD88, TIRAP, TRIF, TRAM) using the conserved Toll-interleukin-1 receptor (TIR) domain, and activation of transcription factors (NFκB, IRF3, AP-1) (Lu et al., 2008). These signaling events result in the production of proinflammatory cytokines(TNFα, IL-1β, IL-6, IL-12) and type-I interferons required for pathogen destruction and

propagation of the inflammatory response (Lu et al., 2008). Although many components of the TLR signaling pathway have been well characterized, the intricate regulatory mechanisms balancing pro-inflammatory and anti-inflammatory responses remain incompletely understood.

GIV is a multimodular signal transducer and a member of the non-receptor Guanine Exchange Modulator (GEM) family of proteins (Ghosh et al., 2017). Unlike the canonical GPCR/G protein pathway, in which G proteins engage exclusively with ligand-activated GPCRs, GEMs, like GIV, can bind and modulate G protein activity downstream of a diverse variety of ligand-activated receptors (Ghosh et al., 2017, Garcia-Marcos et al., 2015, Ghosh, 2015a, Ghosh, 2015b). This unique function is facilitated by an evolutionarily conserved short motif ($\sim$30-aa) that directly binds and modulates two subtypes of trimeric G proteins [activates GNAI as a GEF, and inhibits GNAS as a GDI (Gupta et al., 2016). The impact of such dual modulation of opposing G proteins is sustained suppression of the cAMP$\rightarrow$pCREB axis (Ghosh et al., 2017). Studies from our lab and others employing a selective GEM-deficient GIV mutant (F1685A) have demonstrated that the signaling network triggered in cells with wild-type GIV is a mirror image of the network in cells expressing a GEM-deficient mutant GIV; signals that are enhanced in cells that are GEM-proficient are suppressed in cells that are GEM-deficient, and vice versa. In addition to the GEM module, the C-terminus of GIV features multiple binding motifs that allow GIV to bind multiple classes of cell surface receptors (i.e. SH2-domain$\rightarrow$RTK, PTB$\rightarrow$Integrins, PBM$\rightarrow$frizzled receptors) (Ghosh et al., 2017). Together the GEM motif and the C-terminal binding modules allow GIV to facilitate G-protein activation downstream of non-GPCR receptors.

Previous work from our lab and others has unraveled a series of clues that suggest GIV-GEM may modulate inflammatory signaling. First, GIV mRNA and protein increases after dermal wounds (Dunkel et al., 2012), nephrotic injury (Wang et al., 2015), and fibrogenic insults

to the liver (Lopez-Sanchez et al., 2014) and activation of GIV is indispensable for healing after vascular injury (Miyachi et al., 2015, Miyachi et al., 2014), myocardial infarction (Hayano et al., 2015), dermal wounds (Piao et al., 2015), and podocyte survival after nephotic injury (Wang et al., 2015). In the context of immune cells, GIV is highly expressed in multiple lymphoid tissues including spleen and lymphnode (Le-Niculescu et al., 2005). Additionally, GIV expression increases 18-fold during macrophage differentiation and is required for macrophage chemotaxis (Ghosh et al., 2008). Our lab also found that Gαi is activated in response to LPS and that GIV-GEM function is required for the enhancement of PI3K-Akt signals in liver-resident myofibroblasts stimulated with LPS (Lopez-Sanchez et al., 2014). Another group has recently shown that the GIVSTAT3 signaling axis is required for angiogenesis in response to the proinflammatory cytokine IL-17(Pan et al., 2015). Taken together, it appears that GIV plays a role in modulating inflammatory responses in multiple contexts. However, GIV's impact on the regulation of TLR4 signaling and macrophage inflammatory responses has not been rigorously explored.

2.2 Results and Discussion

GIV/Girdin is highly expressed in immune tissues and cell types

We first started by asking if GIV is expressed in immune tissues and cell types. Using publically available protein expression databases (The Human Protein Atlas) we found that GIV is highly expressed in several immune tissues including lymph nodes, appendix, spleen, bone marrow, and tonsil (Figure 2-1A). Next we asked if GIV expression is enriched in a particular immune cell type. Using publicly available RNAseq datasets (Immgen), we found that GIV is highly expressed in myeloid cell types (macrophages and dendritic cells), moderately

expressed in B-cells and natural killer (NK) cells, and lowly expressed in T-cell populations (Figure 2-2A). Next we wanted to explore possible functions of GIV in macrophages. One major function of macrophages is to survey tissue sites for invading pathogens and cellular damage and mount tailored responses to clear infection and restore tissue homeostasis(Murray, 2017). Macrophages do this by adopting distinct cellular programs, commonly referred to as polarization, which have classically been studied using a simplified M1 (pro-inflammatory) vs. M2 (anti-inflammatory/healing) model. Interestingly, analysis of publicly available RNA-seq datasets (Beyer et al., 2012) revealed that GIV expression was significantly decreased in LPS stimulated (M1) but not IL-4 stimulated (M2) macrophages compared to controls (Figure 2-2B). To confirm these results, we stimulated RAW 264.7 macrophages with either LPS or IL-4 and immunoblotted for GIV (Figure 2-2C). We found that in addition to GIV protein levels being decreased in LPS stimulated macrophages, GIV levels were also increased in IL-4 stimulated macrophages. This observation was confirmed by analysis of four additional RNAseq datasets from both mouse and human macrophage populations (Figure 2-1B). From these data we conclude that GIV is expressed in tissues with important immune functions, and that high expression is seen in myeloid lineage cells including macrophages and dendritic cells. Additionally, based on changes in GIV mRNA and protein expression under polarizing conditions, we hypothesized that GIV may play a role in macrophage inflammatory responses.

GIV/Girdin depleted macrophages have enhanced inflammatory gene signature in response to LPS

Since GIV levels were reduced in pro-inflammatory (M1) polarized macrophages and increased in anti-inflammatory (M2) polarized macrophages we hypothesized that GIV may inhibit

pro-inflammatory responses and promote anti-inflammatory/healing programs in macrophages. To study the role of GIV in macrophage inflammatory responses, we generated two model systems; 1) a GIV-depleted RAW 264.7 macrophage cell line using short-hairpin RNA (shRNA) (Figure 2-2D) and 2) a myelomonocytic specific conditional GIV knockout mouse, generated by crossing Girdin floxed mice(Asai et al., 2012) to LysM-cre mice (Jax labs), which express nuclear-localized cre recombinase under the endogenous lysozyme 2 (Lyz2) promoter/enhancer elements. To validate GIV depletion in macrophages from these mice, we generated thioglycolate induced peritoneal macrophages and measured GIV protien levels by immunoblot (Figure 2-3).

The first question we asked was whether the transcriptional response to the pro-inflammatory stimulus LPS was altered in GIV depleted macrophages. To address this, WT and GIV depleted RAW macrophages were stimulated with LPS (100ng/ml) for 6hr and relative transcript expression levels were assessed by RNA sequencing. We found that 150 genes were significantly upregulated and 26 genes were significantly downregulated in GIV depleted macrophages compared to WT controls (Figure 2-2E). Gene ontology analysis (DAVID GO) of upregulated genes revealed 29 significantly enriched biological processes, where downregulated genes were not significantly enriched in any biological process (Figure 2-2F). Of the enriched pathways, we noticed a large proportion were involved in inflammatory signaling and cytokine responses (highlighted in red) including cellular response to TGFβ stimulus, MAPK cascade, cytokine mediated signaling pathway, positive regulation of IL6 production, myeloid dendritic cell differentiation, microglial cell proliferation, defense response to protozoan, inflammatory response, immune response, fever generation, positive regulation of NO biosynthesis, cellular response to LPS, Th17 cell lineage commitment, and positive regulation of cell prolif-

eration in bone marrow. A closer look at the gene transcripts within each of these GO terms revealed several pro-inflammatory cytokines and chemokines including IL-6, IL-1α, IL-1β, IL-23α, IL-17A, IL-12A, CXCL2, and IFNβ1 that were significantly upregulated in GIV-depleted macrophages compared to controls (Figure 2-2G).

To confirm these findings we used quantitative PCR (qPCR) to measure pro-inflammatory cytokine transcript levels in both RAW and peritoneal macrophages depleted of GIV. We found significant increases in IL-6, IL-1β, and IFNβ in GIV-depleted RAW macrophages compared WT controls (Figure 2-4a). Interestingly, GIV-depleted RAW macrophages had a significant decrease in the anti-inflammatory cytokine IL-10 which suggests GIV may also play a role in regulating anti-inflammatory gene programs. Similar results were seen in RAW macrophages with significant increases in IL-6, IL1β, and TNFα, but not IFNβ (Figure 2-4B). Opposite of RAW macrophages, peritoneal macrophages had an increase in IL-10 but did not reach statistical significance. Differences in functional responses to TLR-ligands between macrophage model systems has been documented(Berghaus et al., 2010) and must be considered when interpreting results. However, it is clear that both RAW and peritoneal macrophages have an enhanced pro-inflammatory cytokine signature when GIV is depleted. To assess if increases in pro-inflammatory cytokine transcript levels translate to secreted protein, we used ELISA to measure secretion of IL-6 and TNFα in RAW and peritoneal macrophages stimulated with LPS. We found that both TNFα and IL-6 were significantly upregulated in GIV depleted RAW and peritoneal macrophages (Figure 2-4C-D). Since GIV appears to be involved in regulating pro-inflammatory cytokine responses, we next asked if GIV plays a role in either sensitivity or tolerance to LPS induced cytokine responses. Using an LPS titration approach, we found that GIV-depleted macrophages showed increased sensitivity to lower amounts of LPS compared to

controls (Figure 2-4E), where GIV depletion did not significantly influence LPS induced tolerance (Figure 2-5A). Taken together we conclude that GIV depletion in macrophages results in an enhanced pro-inflammatory gene signature, increased production of pro-inflammatory cytokines, and increased sensitivity to LPS stimulation. These results support the hypothesis that GIV is a negative regulator of LPS responses in macrophages.

GIV depletion enhances pro-inflammatory cytokine response and exacerbates sepsis induced death during live microbe infection

One of the major functions of macrophages is the detection of microbial infection and initiation of immune responses to clear the infection and restore tissue homeostasis. Our initial results show that depletion of GIV results in enhanced pro-inflammatory cytokine responses to lipopolysaccharide, an essential component of the outer membrane of gram-negative bacteria. To test if this hyperinflammatory phenotype is observed in response to live-microbe infection, we infected RAW macrophages with two stains of gram-negative bacteria, *E. coli* or *Salmonella*, and measured cytokine response by qPCR and ELISA. In line with results from LPS stimulation, GIV-depleted macrophages infected with *E. coli* had significantly increased transcript levels of IL-6, IL-1β, TNFα, and IFNβ (Figure 2-6A), and secreted IL-6 and TNFα (Figure 2-6B) compared to WT controls. Similar increases in IL6, IL1β, and IFNβ transcript levels were seen during *Salmonella* infection but did not reach statistical significance (Figure 2-7A). However, significant increases in secreted IL-6 and TNFα were observed using ELISA (Figure 2-6D). From these data we conclude that GIV-depleted macrophages exhibit enhanced pro-inflammatory cytokine responses during infection with live-microbes. To explore the consequences of myeloid specific GIV-depletion during acute inflammatory responses in vivo, we examined the kinetics and out-

come of sepsis-induced death caused by intraperitoneal (i.p.) injection of Gram-negative *E. coli* bacteria into GIV$^{fl/fl}$LysMcre^{+} or WT control mice. In line with increased cytokine responses, we found that GIV-depleted mice succumbed to sepsis-induced death faster than controls (Figure 2-6E). These results extend our initial finding that GIV is a negative regulator of macrophage inflammatory responses to include two models of live microbe infection and a mouse model of acute inflammation. Our findings lay the groundwork for future studies examining GIV in the context of human sepsis and validation of GIV as a potential therapeutic target to treat sepsis.

Conditional depletion of GIV in myeloid cells exacerbates disease in DSS colitis

In addition to sepsis, inflammatory bowel disease (IBD; Crohn's disease and Ulcerative Colitis) is in part initiated and perpetuated by inappropriate immune responses to intestinal microbes. Intestinal macrophages play a critical role in intestinal homeostasis by both maintaining tolerance to non-pathogenic antigens and protecting the gut against pathogenic infection(De Schepper et al., 2018). Dysregulation of macrophage inflammatory responses by either over activation of inflammatory responses, or a block in the resolution of inflammation, have been associated with IBD development and progression (Na et al., 2019) (Smith et al., 2009, Kamada et al., 2008). In light of our findings implicating GIV as a negative regulator of macrophage inflammatory responses, we hypothesized that depletion of GIV in macrophages will exacerbate IBD. To test GIV's role in IBD we used the dextran sodium sulfate (DSS) mouse model of colitis using our myeloid-specific GIV knockout mice (GIV$^{fl/fl}$LysMcre^{+}). Mice were treated with DSS in drinking water for 7 days followed by 7 days recovery (Figure 2-8A), and monitored for changes in weight, stool consistency, bleeding, colon length, colon tissue destruction, and immune infiltrates. We found that GIV$^{fl/fl}$LysMcre^{+} mice had significantly more weight loss (Figure 2-8B)

and fibrotic shortening of the colon (Figure 2-8C) compared to littermate controls. Disease activity index (DAI) was also increased in GIV$^{fl/fl}$LysMcre^{+} mice compared to controls but did not reach statistical significance (Figure 2-8D). Histomorphological analysis of colon tissue sections revealed increased destruction of crypt architecture and immune infiltrates compared to littermate controls (Figure 2-8E-F). From these data we conclude that conditional knockout of GIV in myeloid cells exacerbates multiple metrics of DSS colitis. It is known that in addition to gene depletion in macrophages the lysMcre system causes various levels of depletion in other cell types including granulocytes, neutrophils, and dendritic cells(Clausen et al., 1999); all of which are known to express GIV and play a role in the pathogenesis of IBD(Bernardo et al., 2018, Wéra et al., 2016). Therefore, our experiments cannot rule out the contribution of GIV depletion in these cell type. However, the results from DSS colitis, acute sepsis, and in vitro cell stimulation assays together suggest that GIV depleted macrophages are likely playing a role.

GIV depletion in macrophages enhances pro-inflammatory signaling pathways during LPS response

Next we wanted to investigate potential mechanisms responsible for the enhanced pro-inflammatory phenotype observed in GIV-depleted macrophages. Extensive effort has gone into elucidating the signaling events that occur downstream of TLR4, the receptor for LPS(Poltorak et al., 1998). Binding of LPS causes homodimerization of TLR4 monomers, recruitment of adaptor proteins (MyD88, TIRAP, TRIF, TRAM) via the Toll-interleukin-1 receptor (TIR) domain, which act as a signaling platform for downstream signaling cascades (IRAK-TRAF, AKT, MAPK, PKA), resulting in activation of transcription factors (NFκB, IRF3, AP-1) (Lu et al., 2008a). These signaling events result in the production of pro-inflammatory cytokines (TNFα, IL-1β, IL-6, IL-

12) and type-I interferons required for pathogen destruction and propagation of the inflammatory response (Lu et al., 2008b)(Figure 2-9A). Previous studies from our lab and others have shown GIV to be responsible for modulating a diverse range of signaling pathways through its ability to link G-protein signaling, via its GEM motif, to a multitude of cell surface receptors (reviewed here (Aznar et al., 2016)). Specifically, GIV acts as a scaffold to recruit and activate G-proteins (Gαi) independently of G-protein coupled receptors (Garcia-Marcos et al., 2009). In the context of inflammation, numerous studies have demonstrated GIV's role in modulating inflammatory signaling in a variety of contexts including dermal wounds (Dunkel et al., 2012, Piao et al., 2015), nephrotic injury (Wang et al., 2015), liver fibrosis (Lopez-Sanchez et al., 2014), vascular injury (Miyachi et al., 2015, Miyachi et al., 2014), and myocardial infarction (Hayano et al., 2015). Since we found GIV to negatively regulate cytokine production in response to LPS, we hypothesized that GIV may also modulate LPS-TLR4 signaling through enhancement of pro-inflammatory signaling pathways.

To test this, we stimulated GIV-depleted RAW macrophages, or WT controls, with LPS and monitored signaling dynamics of key pathways (NFκB, CREB, AKT, and MAPK) by immunoblot (Figure 2-9B). To better visualize signaling kinetics, we plotted densitometry values of NFκB and CREB signaling from our immunoblots (figure 2-9C). We found that after 30min of LPS stimulation all pathways showed increased activation in GIV-depleted macrophages compared to controls. Interestingly, this enhanced activation was maintained even after 60min, suggesting that GIV-depletion may inhibit negative feedback mechanisms required to dampen TLR4 signaling. We also observed enhanced CREB signaling in GIV-depleted macrophages at 5min, before any detectable signaling could be observed in WT cells, suggesting faster signaling kinetics when GIV is depleted. This result is in line with our earlier finding that GIV depletion in-

creases macrophage sensitivity to LPS (Figure 2-9E). To confirm that increased phosphorylation of NFκB corresponds to functional activation, we transfected either WT or GIV-depleted RAW macrophages with a NFκB luciferase reporter construct and monitored NFκB activity after 6hrs LPS stimulation (Figure 2-9D). We observed $\sim$2-fold increase in NFκB activity in GIV-depleted macrophages compared to controls confirming that increased NFκB phosphorylation results in increased activity. CREB phosphorylation is induced downstream of TLR4 signaling by two parallel pathways; the cAMP-PKA pathway, and the p38-MAPK pathway (Avni et al., 2010). Results from our immunoblot show upregulation of the MAPK-ERK pathway, which could explain CREB phosphorylation. However, cAMP has also been shown to increase in response to LPS (Avni et al., 2010), but how cAMP is induced downstream of TLR4 is unknown. Since GIV is known to negatively regulate cAMP production via activation of Gαi (Getz et al., 2019, Gupta et al., 2016), we hypothesized that GIV-depletion in macrophages would result in an increase in cellular cAMP levels. Using an ELISA based cAMP assay, we found that cAMP level were in fact elevated in GIV-depleted macrophages after LPS stimulation (Figure 2-9D). Numerous studies investigating canonical activation of G-proteins by GPCRs in macrophages have identified cAMP as an anti-inflammatory second messenger (reviewed here (Peters-Golden, 2009)). However, other studies have shown elevated levels of cAMP in response to LPS is responsible for rapid induction of IL-6 production (Song et al., 2007, Song et al., 2009). Therefore, GIV's suppression of cAMP downstream of TLR4 stimulation may represent a novel role for cAMP in macrophage inflammatory responses and is an area of interest for future studies.

GIV directly interacts with TLR4 using a TIR-like loop (TILL) motif within its C-terminus and physically links TLR4 and Gαi

Next we wanted to dive deeper into the mechanisms of TLR4 regulation by GIV. GIV's unique ability to activate G-protein signaling downstream of a diverse array of non-GPCR receptors is mediated by short linear interaction motifs (SLIMs) in the C-terminus of GIV, including distinct modules that couple GIV to receptor tyrosine kinases (RTKs), Integrins, and frizzled receptors (reviewed in (Ghosh et al., 2017))(Figure 2-10). We hypothesized that GIV binds TLR4 through a unique SLIM and facilitates formation of a ternary complex with Gαi. To determine if GIV interacts with TLR4 in macrophages, we immunoprecipitated endogenous TLR4 from RAW macrophages and found that GIV co-immunoprecipitates with TLR4 (Figure 2-11a) To determine if the interaction between GIV and TLR4 is direct via GIV's C-terminus, we purified various fragments of recombinant His-GIV-CT and conducted an in vitro pulldown assay with GST-tagged TIR-domain of TLR4 (aa 676-835) (Figure 2-11B). We found that binding between GIV and TLR4 is direct and mediated via a 110aa stretch in GIV's C-terminus. To determine if GIV facilitates formation of a TLR4-GIV-Gαi ternary complex, we conducted an in vitro pulldown assay with GST-TLR4-TIR and His-Gαi3 in the presence or absence of His-GIV-CT (Figure 2-11C). We found that TLR4 and Gαi3 are only able to form a complex in the presence on GIV, suggesting that GIV acts as a physical link between TLR4 and Gαi as it does multiple other receptor classes.

Because TLR4 signaling relies on the Toll/interleukin-1 receptor (TIR) homology domain to assemble multimeric post-receptor complexes, we hypothesized that GIV may contain a TIR-like domain within its C-terminus that mediates interaction with TLR4. Using an online sequence alignment tool (Clustal Omega) we identified a 12aa stretch in GIV's C-terminus with sequence

homology to the BB-loop region of TIR domains(Figure 2-11D). The BB-loop is essential for both TLR dimerization and recruitment of TIR-adaptors, and mutations in this domain have been shown to inhibit TLR signaling (Ohnishi et al., 2009). Interestingly, IL17RA also has a TIR-like motif that corresponds to the BB-loop of TIR-domains (TIR-like loop or TILL) that is essential for NFκB and MAPK activation in response to IL17RA ligands (Gaffen, 2009), adding support to the idea that BB-loop motifs alone can impact inflammatory responses. To remain consistent with the IL17RA nomenclature we will refer to GIV's putative BB-like loop as GIV's "TILL" motif. To test if GIV's interaction with TLR4 is dependent on GIV's TILL motif, we substituted critical residues within GIV-TILL with alanine (K1749A, EFL1751-53AAA, PG1754-55AA) and found that all three mutants failed to bind TLR4, but that a mutation in an nearby SLIM (PTB domain mutant) had no effect on binding (Figure 2-11E). This further supports that GIV binds TLR4 via its putative TILL motif.

The TIR-domain containing adaptors MAL, TRAM, TRIF, and MyD88 can either directly, or indirectly, interact with TLRs to propagate inflammatory signaling responses. However, there is selectivity in TIR-TIR interactions. For example, the TIR adaptor MAL is required for recruitment of MyD88 to the receptor tail of some TLRs (TLR1/2, TLR2/6, and TLR4) but not all (TLR5, TLR7/8, TLR9, TLR11/12) (Medzhitov, 2001). To assess the selectivity are promiscuity of GIV binding to TIR-domain containing proteins we conducted GST pulldown assays with other TLRs (TLR2, TLR1, TLR6) as well as TIR-adaptor proteins (Mal, TRAM, TRIF, MyD88). We found that TLR4 was the only TLR tested that could bind GIV (Figure 2-11F). Additionally, we found that GIV binds the TIR adaptors MAL and TRAM but not MyD88 (Figure 2-11G), and mutations in GIV's TILL domain are sufficient to disrupt these interactions (Figure 2-11H). These results demonstrate that GIV's TILL motif is able to bind multiple TIR-domain containing proteins

(promiscuity), but can bind only a single TLR, TLR4 (specificity). To explore the consequences of these interaction patterns, we conducted a TLR-ligand screen where GIV-depleted or WT RAW macrophages were stimulated with ligands for various TLRs (Figure 2-12A). As with the TLR4 ligand LPS, we saw increased cytokine transcript production in GIV-depleted macrophages stimulated ligands for TLR1/2, TLRR2/6, and TLR3 compared to controls (Figure 2-12B). However, this pattern was not seen for ligands to TLR5. TLR7/8, and TLR9. Interestingly, TLRs impacted by GIV depletion are ones that require the TIR-adaptors MAL, TRAM, and TRIF for signaling. This suggests GIV's role as a negative regulator of TLR inflammatory responses could occur by multiple mechanisms. One hypothesis is that GIV inhibits TLR4 responses by directly binding to the receptor tail and either prevents dimerization of TLR4 homodimers or the recruitment of TIR-adaptors. Another possibility is that GIV binds TIR-adaptor proteins MAL and TRAM and sequesters them from the receptor tail of multiple TLRs. This hypothesis is consistent with the mechanism used by other negative regulators of TLR signaling STL2 (IL1R1) and SIGIRR, which sequester TIR-adaptors in the cytoplasm by interacting with their TIR-domains (Brint et al., 2004, Qin et al., 2005, Wald et al., 2003). Understanding in more detail the TIR-domain binding specificity and exact mechanisms GIV uses to inhibit various TLR responses will be explored in future work.

Structural characterization of GIV-TLR4 binding interface and design of therapeutic peptides

Binding of LPS to TLR4 causes homodimerization of TLR4 monomers through interaction of their TIR domains resulting in the formation of a secondary TIR interface for binding of TIR-adaptor molecules Mal and TRAM (Bovijn et al., 2012) that allows recruitment of additional

adaptors MyD88 and TRIF, again via TIR-TIR interactions. Using structural, biochemical, and computational approaches, work from several groups has identified multiple interaction sites for TIR-TIR interactions during TLR homodimerization and adaptor recruitment (Bovijn et al., 2012, Ve et al., 2017, Bovijn et al., 2013). These studies and others found that TIR-TIR interactions can occur between two BB-loop regions (Homotypic interaction) or between the BB-loop of one TIR domain and the C-terminal helix of another TIR-domain (heterotypic interaction). To gain deeper insight into the mechanism of binding between GIV's TILL motif and TLR4 TIR-domains, we took a homology modeling approach to predict the binding interface and identify key residues that facilitate binding.

First, we asked if the interaction between TLR4 and GIV happens in a homotypic or heterotypic fashion? To investigate this, we derived homology models of GIV's TILL motif binding to TLR4 in both modes (Figure 2-13A, Figure 2-14A). Since the structure of the TLR4 TIR-domain is not available, models were built by homology using the TIR-domain structures of TLR1 (Xu et al., 2000), TLR6 (Nyman et al., 2008), and TLR10 (Jang and Park, 2014) as templates. Analysis of the homotypic binding model revealed key residue contacts that facilitate binding including GIV's K1750, P1756, and R1759 with TLR4's Q683, Y709, and Y709 respectively (Figure 2-13B-C). The identification of K1750 and P1756 of GIV as important binding residues is supported by GIV-TLR4 GST pulldown assays that show loss of binding upon mutation of either of these residues to alanine (Figure 2-13E). Additionally, P1756 within GIV's TILL motif corresponds to proline 712 (P714 in humans) in TLR4's BB-loop that is essential for TIR-TIR interactions (Poltorak et al., 1998). Published work has also found Y709 to form essential contacts in the TIR-TIR binding interface in the context of both TLR homodimerization as well as adaptor recruitment (Basith et al., 2011, Ronni et al., 2003). This site is of particular interest since

it opens the possibility of a phospho-regulated binding mechanism between GIV and TLR4, however phosphorylation of Y709 has not yet been demonstrated (www.Phosphosite.org). Next we wanted to know if any of the key binding residues could explain the specificity of GIV's interactions with TIR-modules observed in our biochemical assays (Figure 2-11 F-H). Alignment of the BB-loop sequences of TLR4, MyD88, Mal, TRAM, TLR1, TLR2, and TLR6 highlighting GIV contact sites revealed Q683, E685, and Y709 as contact sites that could be specific to the GIV−TLR4 interface (Figure 2-13D). Mutagenesis experiments assessing the impact of each of these sites on GIV-TLR4 binding will need to be done to confirm these observations. Analysis of the heterotypic binding model (Figure 2-14A) revealed that binding between GIV and TLR4 in a heterotypic fashion could be accommodated. However, analysis of predicted contact residues did not identify any contact sites that could explain the binding specificity observed in our biochemical assays. Therefore, although it is possible the GIV can form both heterotypic and homotypic interactions with TLR4's TIR-domain, we conclude that homotypic binding is the more likely binding mode.

Next we wanted to use the structural insights gained from our homology model to test if we could experimentally disrupt the GIV-TLR4 interaction. Engineered cell-permeating "decoy peptides" corresponding to the BB-loop of TIR domains have been used as a research tool and have been proposed for therapeutic intervention in inflammatory diseases involving overactive TLR signaling (Toshchakov et al., 2011, Toshchakov and Vogel, 2007). We used a similar approach by designing a cell-penetrable peptide corresponding to the homotypic BB-loop interface of GIV. To test if our GIV TILL peptide could disrupt the GIV-TLR4 interaction, we used a GST pulldown assay with recombinant purified His-GIV-CT and GST-tagged TLR4 with increasing amounts of GIV TILL peptide or a scrambled control peptide (Figure 2-13F). We found that our

GIV TILL peptide was able to disrupt GIV-TLR4 binding at all concentrations tested with no impact of our scrambled control peptide. To assess if GIV-TLR4 disruption could be achieved in cells, we incubated RAW macrophages with either GIV TILL peptide or scrambled control peptide, immunoprecipitated endogenous TLR4, and immunoblotted for GIV and Gαi3 (Figure 2-13G). We found that incubation with TILL peptide was sufficient to disrupt both GIV and Gαi from the TLR4 complex. Next we investigated the impact of GIV TILL peptide disruption of the GIV$-$TLR4 interaction on LPS inflammatory responses in macrophages. RAW macrophages were incubated with GIV TILL-peptide or scrambled control peptide for 1hr, followed by 6hr LPS stimulation, and measurement of pro-inflammatory cytokine transcripts by qPCR (Figure 2-13H). We found that macrophages incubated with GIV TILL peptide had reduced expression of inflammatory transcripts compared to scrambled control. These results show that the GIV TILL peptide can bind the GIV-TLR4 binding interface, displace GIV, and inhibit pro-inflammatory responses upon LPS stimulation in macrophages. These findings add support to the claim that GIV's TILL motif facilitates binding to TLR4 and provides proof-of-principle for therapeutically targeting the GIV-TLR4 interface to treat inflammatory diseases.

2.3 Concluding remarks

A proper immune response requires a balance between pro-inflammatory and anti-inflammatory responses which must remain under tight control. Perturbed balance leads to pathogenesis of a multitude of diseases, and therefore understanding the cellular processes that maintain this balance are paramount to developing novel immunomodulatory therapies. In this work we have identified and characterized GIV as novel negative regulator of TLR4 signaling in macrophages and demonstrate the impact of disrupting this regulatory mechanism in two an-

imal models of inflammatory disease. Additionally, we delineate the biochemical and structural mechanism of GIV's interaction with TLR4 and were able to experimentally target this interaction using a cell-penetrating peptide. Overall, this work adds to the growing body of knowledge on the regulation of inflammatory responses in macrophages and opens the door for investigating the GIV-TLR4 signaling axis as a therapeutic target for inflammatory diseases.

2.4 Materials and Methods

Plasmid constructs

Cloning of GIV-CT (aa 1623-1870, 1660-1870, and 1790-1870) into pET28b (His-GIV CT) were previously described (Garcia-Marcos et al., 2009). His-GIV-CT mutants (detailed in table) were generated by site-directed mutagenesis using QuickChange kit (Stratagene) and specific primers (sequence available upon request) as per the manufacturer's protocols. Cloning of Gαi3 into pET28b was previously described (Ghosh et al., 2008). GST-tagged TLR4 was obtained from Yun Soo Bae (Park et al., 2004). GST-tagged MyD88-TIR was obtained from Bernadette Byrne (Carlsson et al., 2016). GST-tagged TRAM and MAL, and NFκB reporter plasmids were obtained from Andrew Bowie (Lysakova-Devine et al., 2010). GST-tagged TLR1, TLR2, and TLR6 were cloned by amplifying TIR regions (detailed in table) from THP-1 macrophage (human) cDNA and subcloned into pGEX-6p1 using BamHI and EcoRI restriction sites. His-tagged TLR4 was generated by subcloning human TLR4 (from GST-TLR4 construct described above) into pET28b using BamHI and EcoRI restriction sites. Cloning of GIV shRNA constructs (detailed in table) was previously described (Bhandari et al., 2015).

Protein expression and purification

Both GST and His-tagged proteins were expressed in E. coli strain BL21 (DE3) and purified as previously described (Garcia-Marcos et al., 2009, Ghosh et al., 2008). Briefly, cultures were induced using 1mM IPTG overnight at 25C. Cells were then pelleted and resuspended in either GST lysis buffer (25mM Tris-HCL (pH 7.4), 20mM NaCl, 1mM EDTA, 20% (vol/vol) glycerol, 1% (vol/vol) Triton X-100, protease inhibitor cocktail) or His lysis buffer (50mM NaH2PO4 (pH7.4), 300mM NaCl, 10mM imidazole, 1% (vol/vol) Triton-X-100, protease inhibitor cocktail). Cells were lysed by sonication, and lysates were cleared by centrifugation at 12,000 X g at 4°C for 30 mins. Supernatant was then affinity purified using glutathione-Sepharose 4B beads or HisPur Cobalt Resin, followed by elution, overnight dialysis in PBS, and then storage at -80°C.

Cell culture, transfection, lysis, and immunoblotting

The RAW 264.7 cell line was obtained from and cultured according to American Type Culture Collection (ATCC) guidelines. Transfection, lysis, and immunoblotting were carried out as described previously (Ghosh et al., 2016). Whole-cell lysates were prepared after washing cells with cold PBS before resuspending and boiling them in sample buffer. For immunoblotting, protein samples were separated by SDS-PAGE and transferred to polyvinylidene fluoride membranes. Membranes were blocked with 5% nonfat milk or 5% BSA (when probing for phosphorylated proteins) in PBS. The membrane was stained with Ponceau S to visualize bait proteins, washed, blocked, and incubated with primary antibody solutions overnight at 4°C (dilutions for each primary antibody detailed in table). Washed blots were then incubated with infrared secondary antibodies (detailed in table) for 1 hr at room temperature. Infrared imaging with two-color detection and quantification were performed using a Li-Cor Odyssey imaging system and

analysis was performed with Image Studio Lite software.

In vitro Pulldown and Co-immunoprecipitation (Co-IP)

For in vitro pulldown assays, Purified GST-tagged proteins from E. coli were immobilized onto glutathione-Sepharose beads by incubating with binding buffer (50mM Tris-HCl (pH 7.4), 100mM NaCl, 0.4% (vol/vol) Nonidet P-40, 10mM MgCl2, 5mM EDTA, 2mM DTT) for 60 min at 4°C. GST-protein bound beads were washed and incubated with purified His-tagged proteins re-suspended in binding buffer for 4 hrs at 4°C. After binding, bound complexes were washed four times with 1ml phosphate wash buffer (4.3 mM Na2HPO4, 1.4 mM KH2PO4(pH 7.4), 137mM NaCl, 2.7mM KCl, 0.1% (vol/vol) Tween-20, 10mM MgCl2, 5mM EDTA, 2mM DTT, 0.5mM sodium orthovanadate) and eluted by boiling in Laemmli buffer (5% SDS, 156mM Tris-Base, 25% glycerol, 0.025% bromophenol blue, 25% β-mercaptoethanol). For immunoprecipitation assays, cell were lysed in cell lysis buffer (20mM HEPES (pH 7.2), 5mM Mg-acetate, 125mM K-acetate, 0.4% Triton X-100, 1mM DTT, 0.5mM sodium orthovanadate, Tyr phosphatase inhibitor cocktail, Ser/Thr phosphatase inhibitor cocktail, and protease inhibitor cocktail) using a 28G syringe, followed by centrifugation at 10,000 X g for 10 min. Cleared supernatants were then incubated with mouse anti-TLR4 or mouse IgG control antibodies at 4°C overnight. Protein A agarose beads were added to immunobound lysates and incubated for 1 hr at 4°C. Immuno-complex bound beads were washed with wash buffer (4.3 mM Na2HPO4, 1.4 mM KH2PO4(pH 7.4), 137mM NaCl, 2.7mM KCl, 0.1% (vol/vol) Tween-20, 10mM MgCl2, 5mM EDTA, 2mM DTT, 0.5mM sodium orthovanadate) and eluted by boiling in Laemmli buffer (5% SDS, 156mM Tris-Base, 25% glycerol, 0.025% bromophenol blue, 25% β-mercaptoethanol).

Computational modeling of GIV-TLR interactions

Since the structure of the TLR4 TIR-domain is not available, models were built by homology using the TIR-domain structures of TLR1(Xu et al., 2000), TLR6(Nyman et al., 2008), and TLR10(Jang and Park, 2014) as templates. Homology modeling was performed in ICM as done previously (Abagyan et al., 1997, Abagyan and Totrov, 1994). The position of the conserved Pro-Gly motif of the GIV(1749-1761) peptide was inherited from the corresponding BB-loop motif in the homotypic TIR-domain homodimer of TLR10 (Nyman et al., 2008) and the heterotypic TIR-domain homodimer of MAL/TIRAP (Ve et al., 2017)The peptide was built ab initio, tethered to the respective Pro-Gly positions, and its conformations were extensively sampled ($>$ 108 steps) by biased probability Monte Carlo (BPMC) sampling in internal coordinates , with the TLR4 TIR domain represented as a set of energy potentials precalculated on a 0.5 Å 3D grid and including Van der Waals potential, electrostatic potential, hydrogen bonding potential, and surface energy. Following such grid-based docking, the peptide poses were merged with full-atom models of the TLR4 TIR domain, and further sampling was conducted for the peptide and surrounding side chains of the TLR4 residues.

Generation of stable cell lines

ShRNA control and shRNA GIV RAW 264.7 stable cells lines were generated by lentiviral transduction followed by selection with puromycin as described previously (Midde et al., 2018). Lentiviral packaging was performed in HEK293T cell by co-transfecting shRNA constructs with psPAX2 and pMD2G plasmids (4:3:1 ratio) using Mirus LT1. The medium was changed after 24 hr, and virus-containing media was collected after 36-48 hr, centrifuged, and filtered through a 0.45 μM filter. Fresh virus-containing media was diluted 1:4 with RAW media (DMEM, 10% FBS)

and polybrene (6 μg/ml final concentration) was added. Lentiviral mixture was added to RAW macrophages (2.5x10^5 cells seeded in 6-well plate), spun at 800xG at room temperature for 30 min, and transferred to cell culture incubator and media was changed after 4 hrs. Puromycin (2.5 μg/ml) was added 48 hrs post-transduction for selection. Depletion of endogenous GIV was confirmed by immunobloting with GIV-CC (ABT80) rabbit antibody.

Generation of conditional GIV KO mouse lines

All breeding and mouse experimentation was done in accordance with the rules and regulations of the Institutional Animal Care and Use Committee (IACUC), and all measures were taken to use animal subjects efficiently and humanely. Girdin floxed mice were a generous gift from Dr. Masahide Takahashi (Nagoya University, Japan) and were described previously (Asai et al., 2012). LysMcre mice (B6.129P2-Lyz2tm1(cre)Ifo/j) were purchased from The Jackson Laboratory. Girdin floxed x LysMcre mice were generated by us and were maintained as homozygous floxed (fl/fl) and heterozygous LysMcre. Mice were genotyped by PCR (primers in table).

Lipopolysaccharide (LPS) stimulation and Bacterial infection

For LPS stimulation experiments, cells were seeded (12-well plate: 2.5x10^5 cells, 6-well plate: ^{5}) and incubated overnight at 37°C before stimulation with LPS (dose and stimulation times indicated in figures and legends). For live microbe infection experiments (*E. coli* and *Salmonella*), bacteria was maintained and cultured in accordance with ATCC protocols as was previously described (Das et al., 2015). For bacterial culture, a single colony was inoculated into LB broth and grown for 8 hr under aerobic conditions in an orbital shaking incubator at

150 rpm and then under oxygen-limiting conditions overnight. Under these conditions, bacteria correspond to 5-7x10^8 colony forming units (CFU), where OD 0.5 is equivalent to 5x10^8. Cells were infected at a multiplicity of infection (moi) of 1 for *E. coli* and 10 for *Salmonella*. For RNA readouts, cells were washed once with 1X PBS and 0.5ml Trizol was added directly to the well before collection and storage at -80°C. For supernatant cytokine analysis (ELISA), supernatant was collected at indicated times, centrifuged at 13,000xg for 10 min, and absolute levels of IL-6, IL-10, and TNFα were quantified using ELISA MAX or OtpEIA ELISA kits (details in table) using manufacturers protocols. For cell lysate analysis (Western blot), cells were washed 1X with PBS, scraped from well, and processed as described above.

RNA isolation, quantitative PCR, and RNA sequencing

All RNA was isolated using Direct-zol RNA Miniprep Kit using manufactures protocol from samples collected in Trizol reagent. RNA concentration and purity were quantified using a Nanodrop Microvolume Spectrophotometer. 500ng RNA was used for RT-PCR using qScriptä cDNA SuperMix kit and manufacturers protocol. cDNA was diluted 1:5 with ddH2O and qPCR was carried out using 2X PowerUp SYBR Green Master Mix. The cycle threshold (Ct) of target genes was normalized to 18s housekeeping gene, relative expression of mRNA was calculated using the $\Delta\Delta$Ct method, and results expressed as fold-change. Paired-end RNA-Seq data were aligned to the reference mouse genome(mmGRCh38_94_k) using kallisto software with default parameters. Log normalization was applied on the TPM values. We summarized gene expression table from the transcription table by adding all the transcription values for each gene and keep them as a single entry. Gene symbols were added from the UCSC Table Browser and kgXref table. Differentially expressed genes were discovered by DESeq2 package.

Measurement of cellular cAMP levels

RAW 264.7 cells (2.5x10^5 cells/well in 12-well plate) were incubated with 200 μM isobutylmethylxanthine (IBMX) for 20 min, followed by 1 hr LPS (100 ng/ml) stimulation. Cells were lysed and cAMP levels assessed by cAMP-Screen Cyclic AMP Immunoassay System using manufacturers protocols, and data expressed as pmol cAMP/ml.

NFκB reporter assay

RAW 264.7 cells (5x10^4 cells/well in 96-well plate) were transfected with 100ng NFκB reporter plasmid and 20ng Renilla control plasmid. 24hr after transfection, cells were stimulated with LPS (100ng/ml) for 6hr and NFκB activity was assessed using the Duel-luciferase Reporter Assay System using manufacturers protocol.

DSS colitis

7-8 week-old GIV$^{fl/fl}$LysMcre^{+} or GIV $^{fl/fl}$ littermate controls were given either normal drinking water or 2% dextran sodium sulfate (DSS) for 7 days, followed by 7 days recovery with normal drinking water. Water levels were monitored to ensure equal volumes of water were consumed between treatment groups. Weight was monitored daily. Disease activity index (DAI) was calculated using by scoring stool consistency (0-4), rectal bleeding (0-4), and weight loss (0-4) as previously published(Kim et al., 2012). Mice were sacrificed on the day 14, and colon length was measured. Colon samples were prepared as Swiss-rolls, fixed in formalin, embedded in paraffin, and cut into sections. Sections were stained with hematoxylin and eosin and evaluated for mononuclear infiltrates, submucosal edema, surface erosions, inflammatory exudates, and presence of crypt abscesses and scored as done previously (Das et al., 2015)

Statistical Analysis and Replications

Statistical significance between datasets with three or more experimental groups was determined using one-way (or two-way in the case of DSS weight analysis) analysis of variance (ANOVA) including a Tukey's test for multiple comparisons. Statistical difference between two experimental groups was determined using a two-tailed unpaired t-test. For all tests, a p-value of 0.05 was used as the cutoff to determine significance. All experiments were repeated a least three times, and p-values are indicated in each figure. All statistical analysis was performed using GraphPad prism 8.

Acknowledgements

This research was funded by NIH (R01AI141630), as well as a T32 training grant DK00720243.

Chapter 2 in part is a reprint of material to be submitted to be published in: **Swanson, L.**, Katkar, G.D., Chareddy, Y., Tam, J., Coates, J., Behroozikhah, M., Sahoo, D., Das, S., Ghosh, P.. "Negative regulation of TLR4 signaling by GIV/Girdin shapes macrophage inflammatory responses.". The dissertation author was first author.

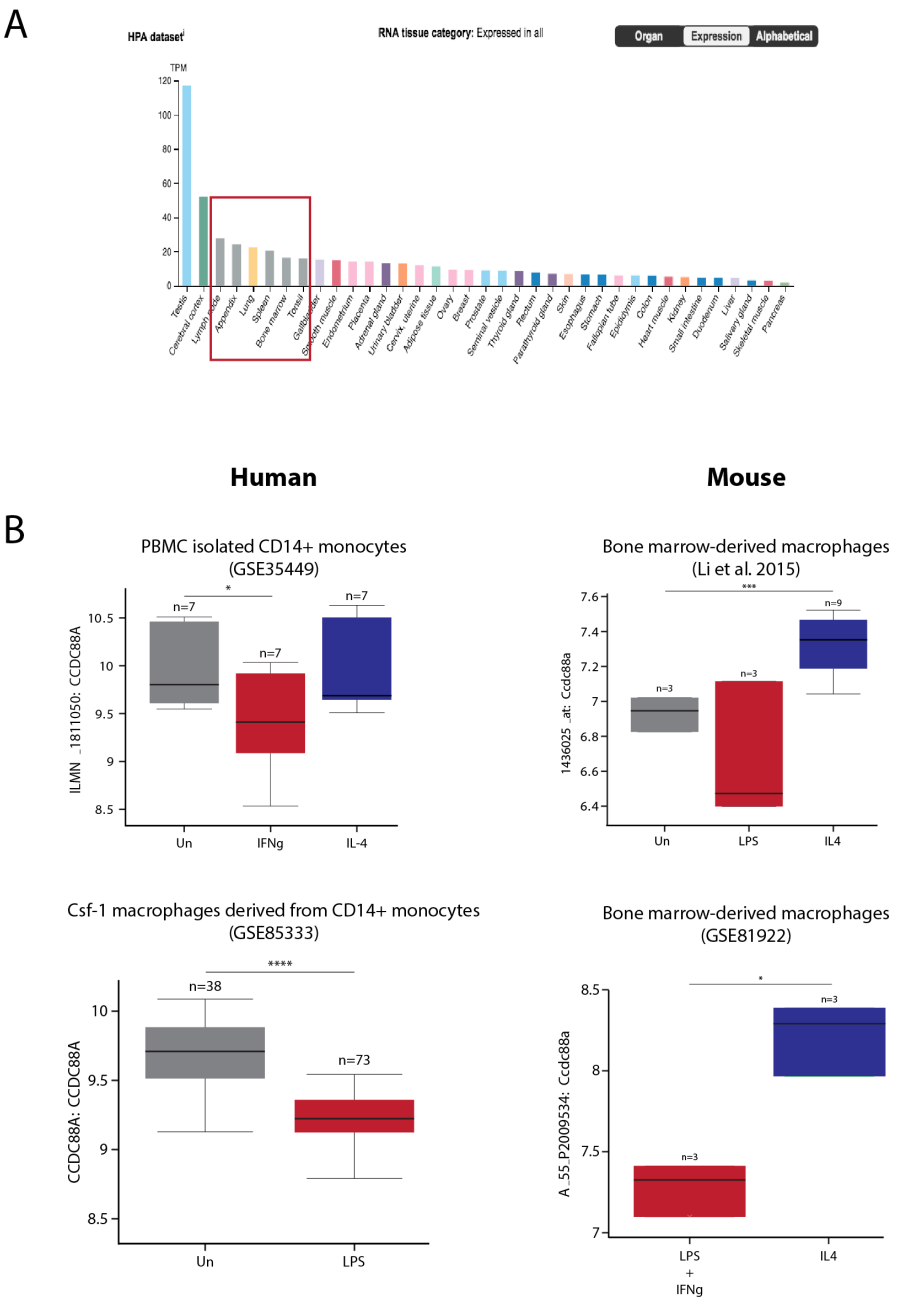

Figure 2.1: GIV expression in immune tissues and polarized macrophages. (A) Bar graph, generated using Human Protein Atlas (www.proteinatlas.org), showing GIV transcript levels from various human tissues. Red box highlights GIV expression in immune tissues. (B) Box plots of GIV transcript levels, curated from publicly available RNAseq datasets (Gene Expression Omnibus [GEO]), in human and mouse macrophages polarized under indicated pro- or anti-inflammatory conditions.

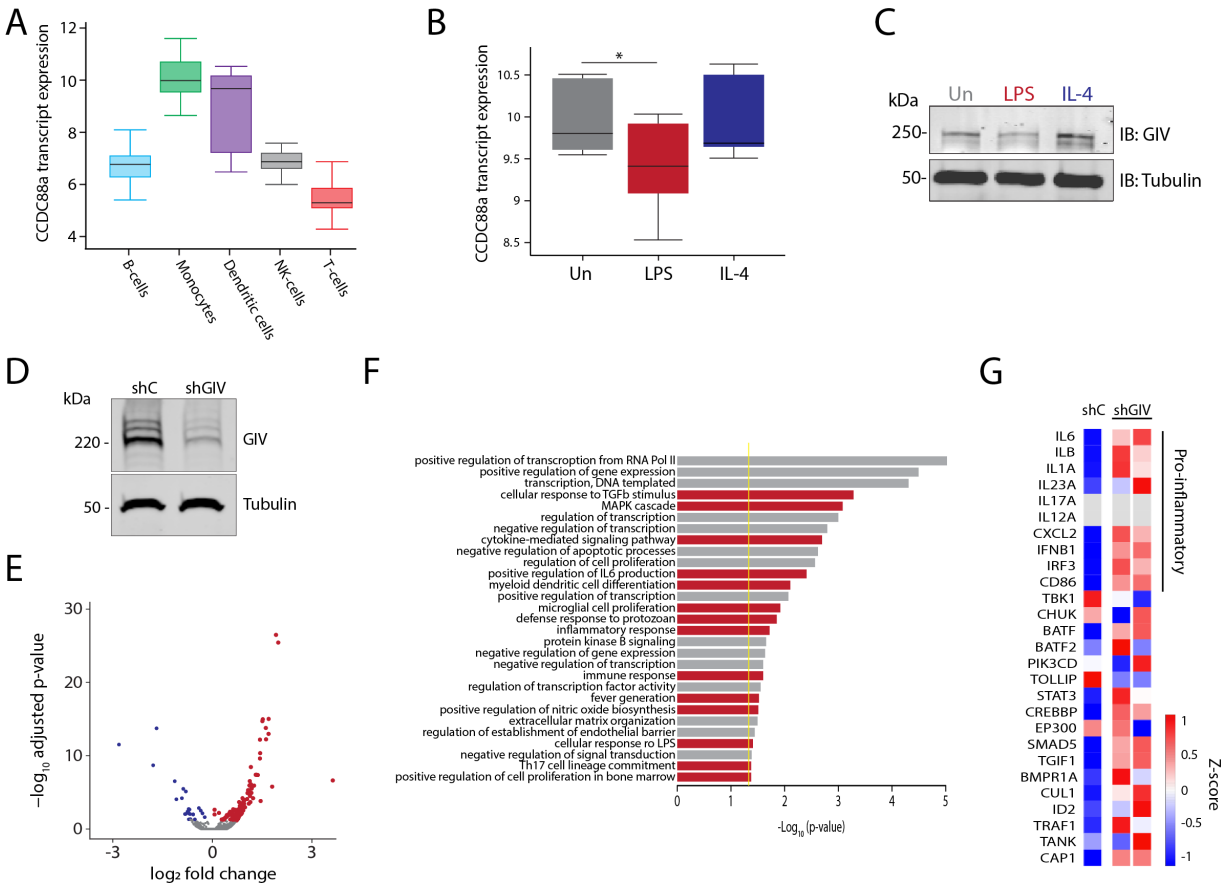

Figure 2.2: GIV/Gidrin expression is associated with pro-inflammatory gene programs in macrophages. (A) Box plots representing GIV (CCDC88a) transcript levels in various immune cell populations. (B) Box plots representing GIV transcript levels in polarized macrophages stimulated with either LPS or IL-4. (C) Immunoblot of GIV protein expression in polarized macrophages stimulated with either LPS or IL-4. (D) Immunoblot of RAW 264.7 macrophages depleted of GIV using shRNA. (E) Volcano plot of significantly upregulated (red) and downregulated (blue) gene transcripts in GIV-depleted macrophages compared to WT controls. (F) Bar graph of significantly enriched biological processes determined by gene ontology (GO) analysis. Yellow line designates p=0.05 cutoff. (G) Heatmap of significantly upregulated gene transcripts identified in GO analysis.

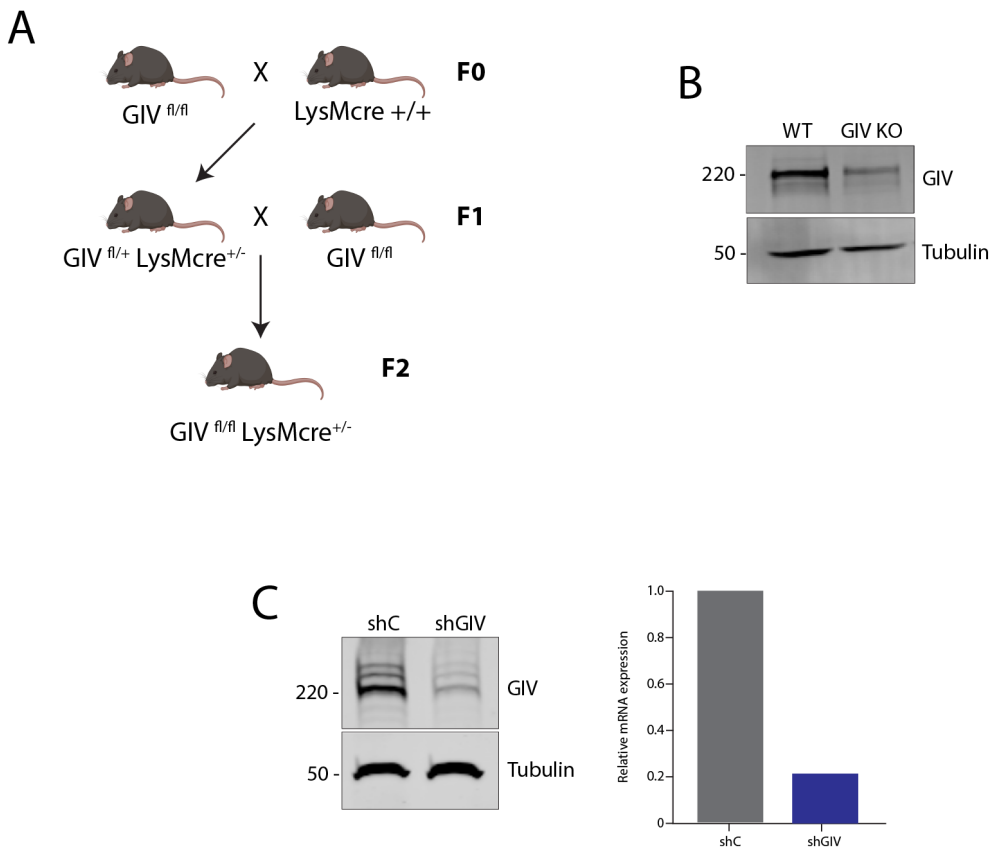

Figure 2.3: Validation of GIV-depletion model systems. (A) Schematic of breeding scheme used to generate conditional myeloid-cell specific (LysMcre) GIV knockout mice. (B) Immunoblot confirming protein depletion in peritoneal macrophages isolated from GIV$^{fl/fl}$$LysMcre^{+}$ mice. (C). Immunoblot confirming protein depletion in RAW 264.7 macrophage cell line using shRNA. (D) Bar graph of GIV mRNA levels in shRNA GIV-depleted macrophages relative to WT controls.

Figure 2.4: GIV depletion increases the magnitude and sensitivity of cytokine responses to LPS. (A-B) Bar graphs displaying cytokine transcript levels (qPCR) in GIV-depleted RAW macrophages (A) or peritoneal macrophages (B) stimulated with LPS (100ng/ml, 6hr) compared to WT controls. (C-D) Bar graphs showing levels of secreted pro-inflammatory cytokines (ELISA) in GIV-depleted or WT RAW (C) or peritoneal (D) macrophages stimulated with LPS. (E) Line graphs comparing sensitivity of cytokine response to increasing doses of LPS in GIV-depleted RAW macrophages compared to WT controls. All qPCR and ELISA results are from 3 independent experiments and displayed as mean $\pm$ S.E.M.. Students t-test was used for two-parameter statistical analysis (A-B) and two-way ANOVA using Sidak's multiple comparisons test was used for multi-parameter statistical analysis (C-E). (*;$p \leq 0.05$, **;$p \leq 0.01$, ***;$p \leq 0.001$, ****;$p \leq 0.0001$).

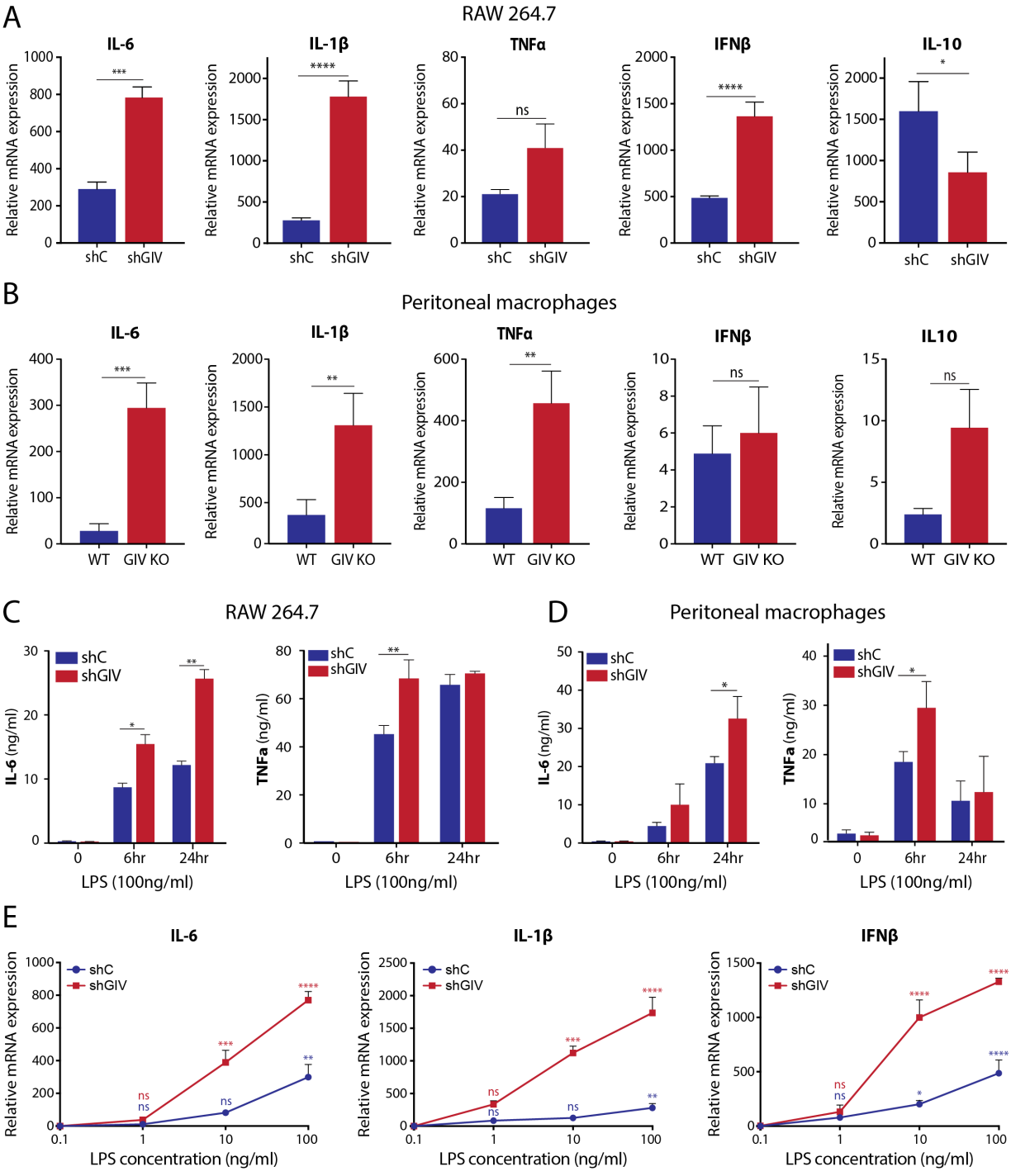
A
RAW 264.7
IL-6
IL-1β
TNFα
IFNβ
IL-10
Relative mRNA expression
shC
shGIV
B
Peritoneal macrophages
IL-6
IL-1β
TNFα
IFNβ
IL10
WT
GIV KO
C
RAW 264.7
D
Peritoneal macrophages
IL-6 (ng/ml)
TNFa (ng/ml)
LPS (100ng/ml)
0
6hr
24hr
E
IL-6
IL-1β
IFNβ
LPS concentration (ng/ml)

A

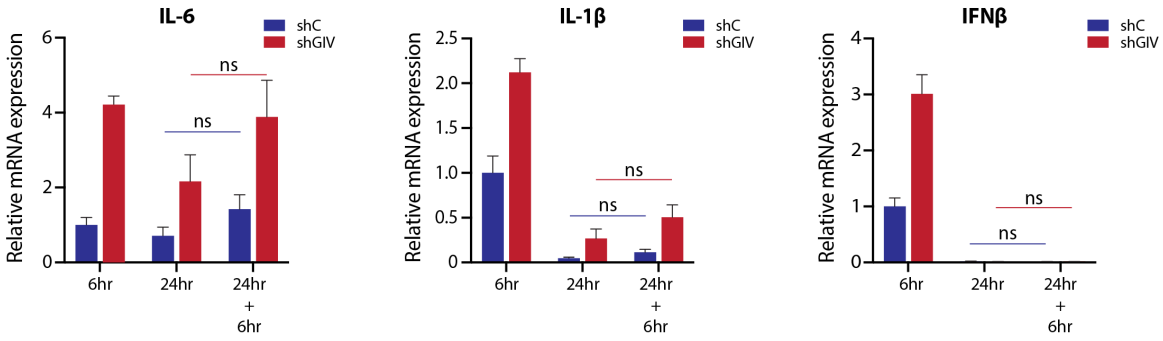

Figure 2.5: GIV depletion is not required for LPS induced tolerance in macrophages. (A) Bar graphs showing transcript levels of pro-inflammatory cytokines in WT or GIV-depleted macrophages either 1) simulated with LPS (100ng/ml) for 6hrs, 2) stimulated with LPS (100ng/ml) for 24hrs, or 3) stimulated with LPS (100ng/ml) for 24hr before re-challenge with LPS (100ng/ml) for 6hrs. Results were from 3 independent experiments and displayed as mean $\pm$ S.E.M.. two-way ANOVA using Sidak's multiple comparisons test was used for multi-parameter statistical analysis.

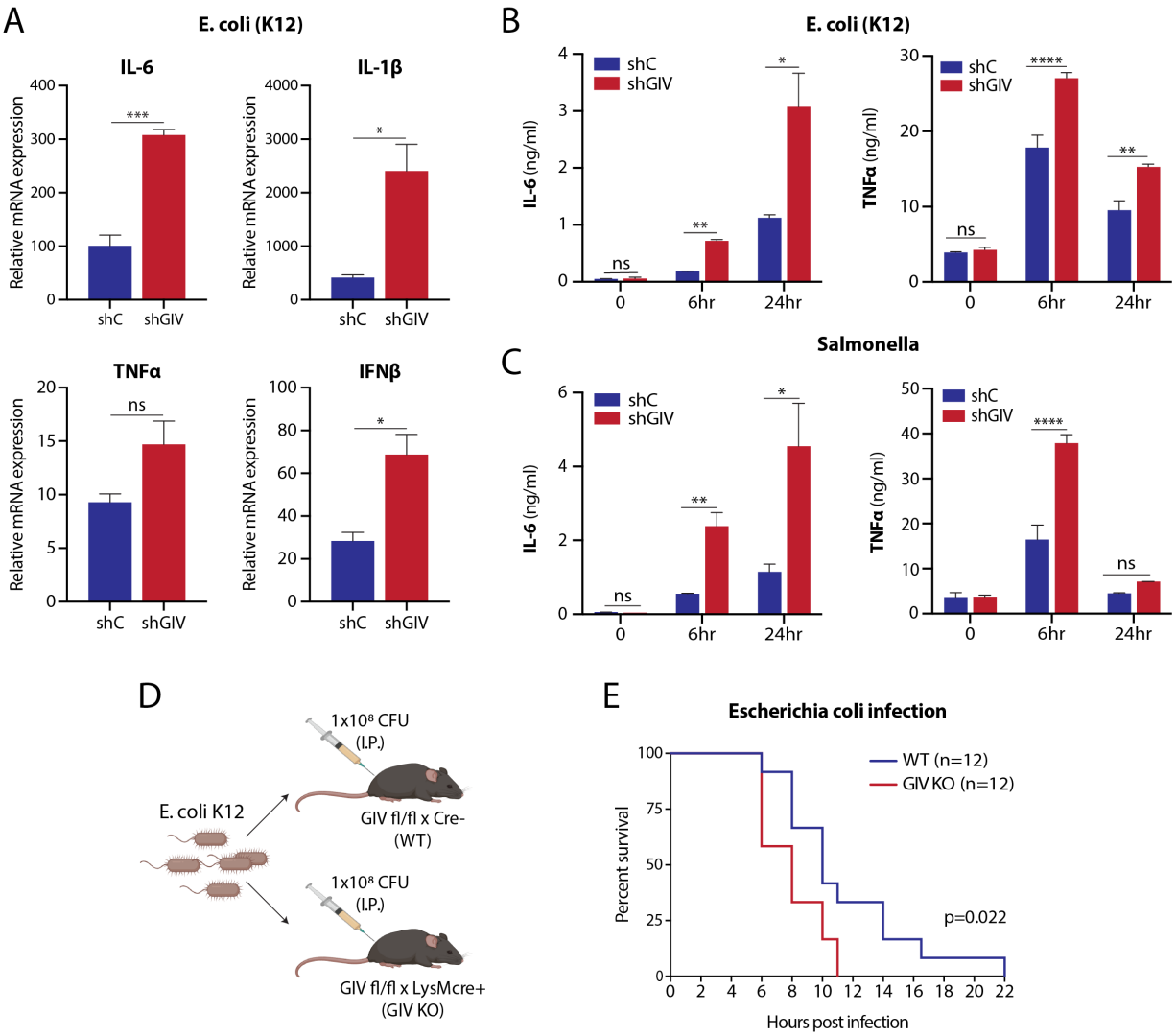

Figure 2.6: GIV depletion enhances pro-inflammatory cytokine response during live-microbe infection. (A) Bar graphs displaying cytokine transcript levels (qPCR) in GIV-depleted RAW macrophages infected with live *E. coli* K12 (MOI=1) for 6hrs compared to WT controls. (B-C) Bar graphs showing levels of secreted pro-inflammatory cytokines (ELISA) in GIV-depleted or WT RAW macrophages infected with either *E. coli* K12 (MOI=1) or *Salmonella* (MOI=10) for 6hrs. All qPCR and ELISA results are from 3 independent experiments and displayed as mean ± S.E.M.. Students t-test was used for two-parameter statistical analysis (A-B) and two-way ANOVA using Sidak's multiple comparisons test was used for multi-parameter statistical analysis (B-C). (D) Schematic of sepsis induced death mouse model. (E) Survival curve of mice i.p. infected with E. coli. Values expressed as percent survival. (*;$p \leq 0.05$, **;$p \leq 0.01$, ***;$p \leq 0.001$, ****;$p \leq 0.0001$).

A

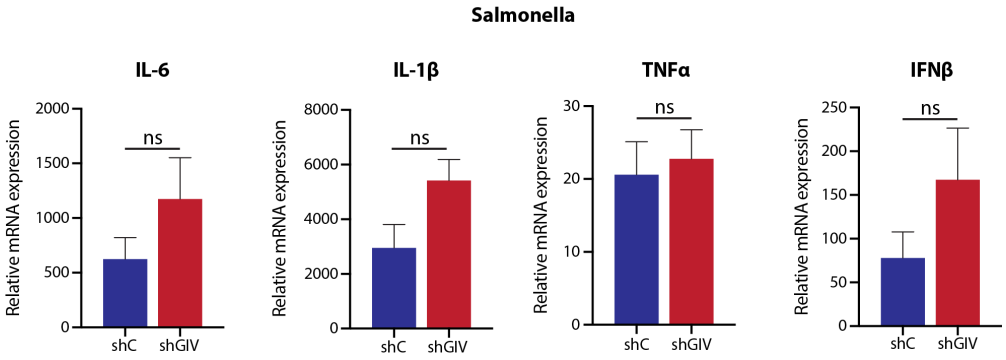

Figure 2.7: GIV depletion enhances pro-inflammatory cytokine response during live-microbe infection. (A) Bar graphs displaying cytokine transcript levels (qPCR) in GIV-depleted RAW macrophages infected with live *Salmonella* (MOI=10) for 6hrs compared to WT controls. Results were from 3 independent experiments and displayed as mean ± S.E.M.. Students t-test was used for statistical analysis.

Figure 2.8: Myeloid cell specific GIV depletion exacerbates disease in DSS colitis. (A) Schematic outlining experimental design of DSS colitis model. (B) Line graph showing body weight change monitored daily during the course of acute DSS colitis. (C) Scatter plot of colon length assessed at d14 of DSS experiment. (D) Line graph of disease activity index (DAI) using stool consistency (0-4), rectal bleeding (0-4), and weight loss (0-4) as scoring criteria. (E) Scatter plot of histomorphological evaluation of inflammation by HE stained colon tissues using inflammatory cell infiltrate (1-3), and epithelial architecture (1-3) as scoring criteria. (E) Representative images of colon tissue stained with HE. Data displayed as mean $\pm$ S.E.M. and either one-way or two-way ANOVA using Tukey's or Sidak's multiple comparisons test was used to determine significance. (*;$p \leq 0.05$, **;$p \leq 0.01$, ***;$p \leq 0.001$, ****;$p \leq 0.0001$).

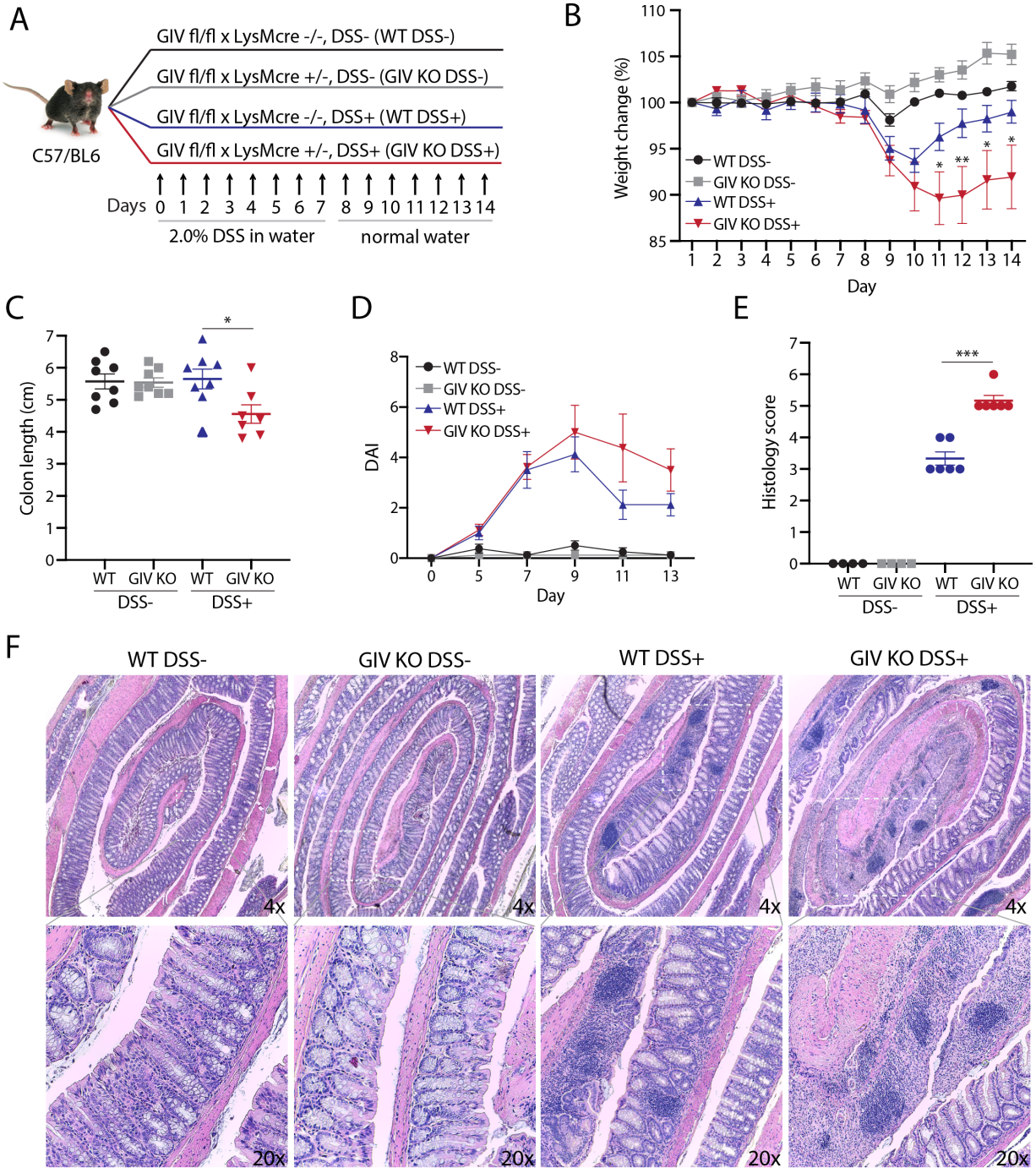
A
GIV fl/fl x LysMcre -/-, DSS- (WT DSS-)
GIV fl/fl x LysMcre +/-, DSS- (GIV KO DSS-)
GIV fl/fl x LysMcre -/-, DSS+ (WT DSS+)
GIV fl/fl x LysMcre +/-, DSS+ (GIV KO DSS+)
C57/BL6
Days 0 1 2 3 4 5 6 7 8 9 10 11 12 13 14
2.0% DSS in water
normal water
B
Weight change (%)
WT DSS-
GIV KO DSS-
WT DSS+
GIV KO DSS+
Day
C
Colon length (cm)
WT GIV KO WT GIV KO
DSS- DSS+
D
DAI
WT DSS-
GIV KO DSS-
WT DSS+
GIV KO DSS+
Day
E
Histology score
WT GIV KO WT GIV KO
DSS- DSS+
F
WT DSS-
GIV KO DSS-
WT DSS+
GIV KO DSS+
4x
20x

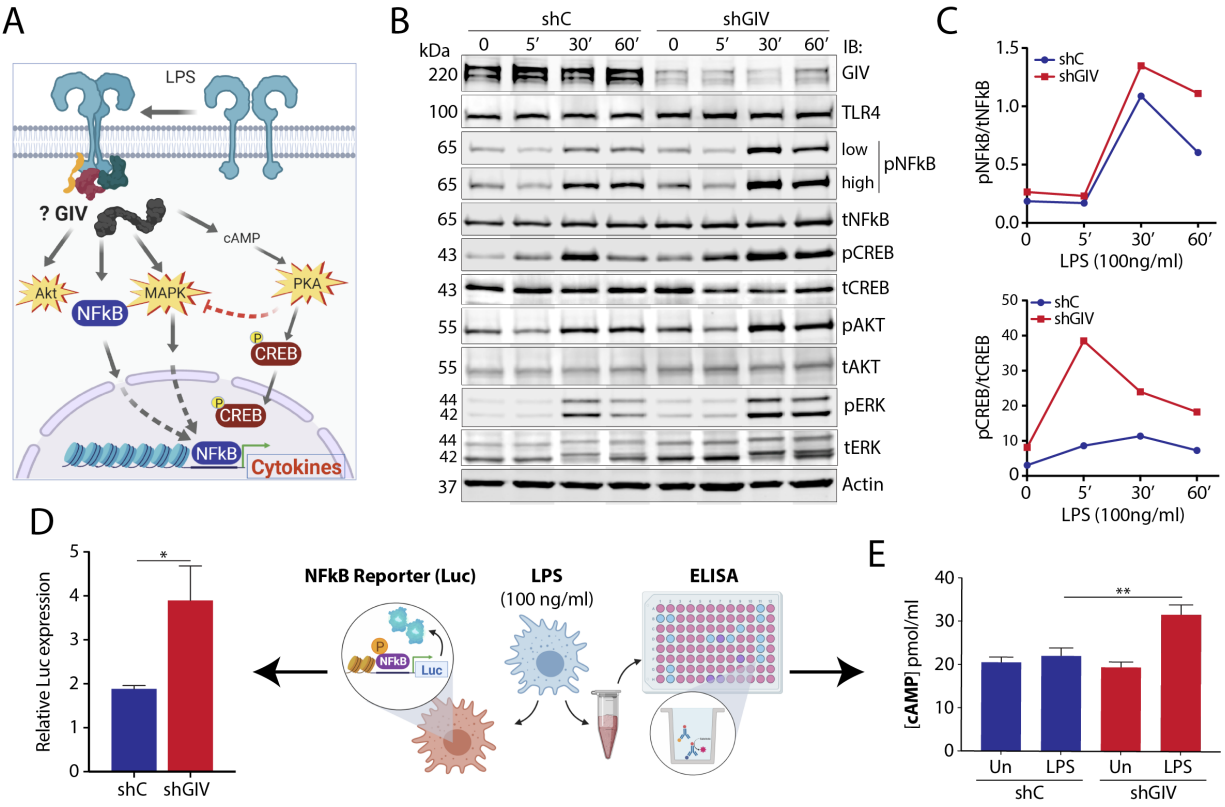

Figure 2.9: GIV depletion in macrophages enhances pro-inflammatory signaling pathways during LPS response. (A) Schematic highlighting GIV's potential role in modulating signaling pathways downstream of TLR4. (B) Immunoblot of whole-cell lysates from GIV-depleted or WT control RAW macrophages stimulated with LPS (100ng/ml) and probed for activation indicated signaling pathways. (C) Line graphs of densitometry values taken from representative signaling immunoblots. (D) Bar graph of relative NFκB activity in WT and GIV-depleted RAW macrophages determined using NFκB luciferase reporter assay. (E) Bar graph of intracellular cAMP levels in LPS stimulated (100ng/ml) WT and GIV-depleted RAW macrophages. Results are from 3 independent experiments and displayed as mean $\pm$ S.E.M.. Students t-test was used for two-parameter statistical analysis (A-B) and two-way ANOVA using Sidak's multiple comparisons test was used for multi-parameter statistical analysis (C-E). (*;p$\leq$0.05, **;p$\leq$0.01, ***;p$\leq$0.001, ****;p$\leq$0.0001).

A

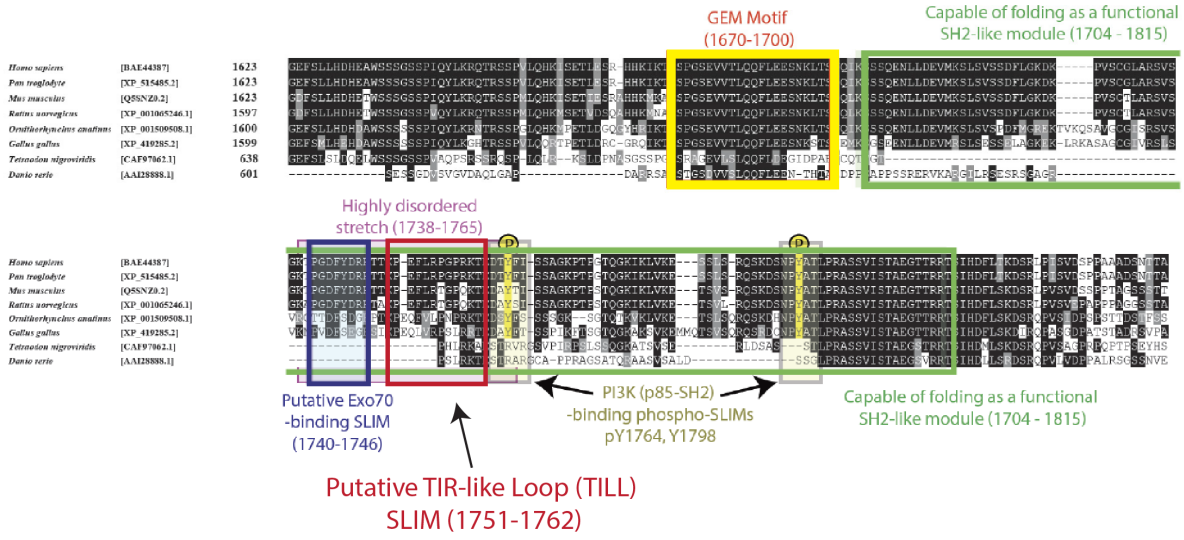

Figure 2.10: Short linear interaction motifs (SLIMs) within GIV's C-terminus. (A) Sequence of GIV's C-terminus showing all currently identified SLIMs. Putative TIR-like Loop (TILL) SLIM is highlighted in red.

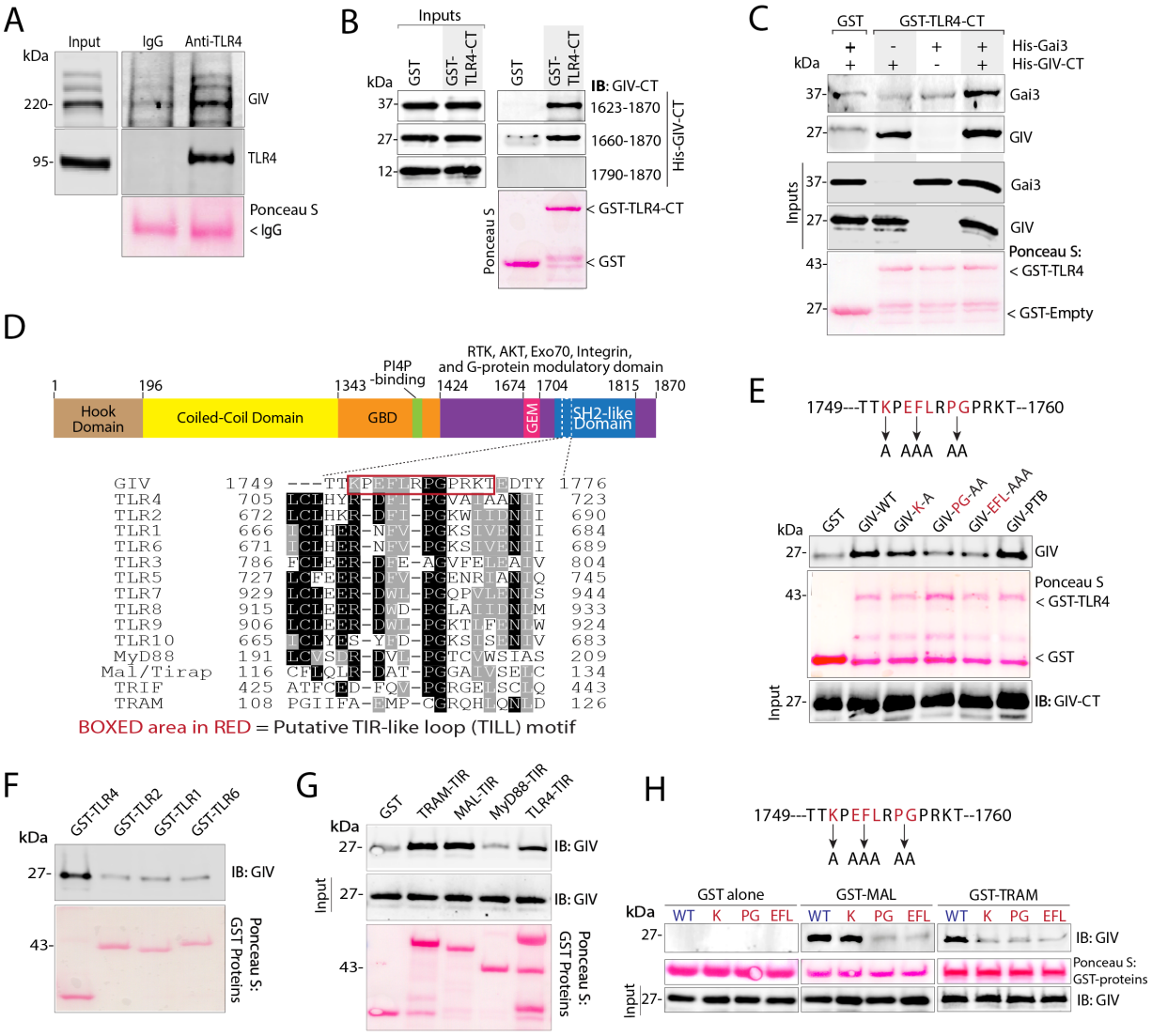

Figure 2.11: GIV directly interacts with TLR4 using a TIR-like loop (TILL) motif within its C-terminus, and physically links TLR4 and Gαi. (A) Endogenous TLR4 was immunoprecipitated from RAW lysates, and bound complexs of TLR4 and GIV were visualized by immunoblot. Equal loading of IgG and anti-TLR4 were confirmed by Ponceau S staining. (B) Various constructs of recombinant His-GIV-CT (3μg) were used in GST pulldown assays with GST or GST-TLR4-TIR and bound GIV was visualized by immunoblot. (C) Recombinant His-GIV-CT (3μg) and His-Gαi3 (3μg) were used in a GST pulldown assay with GST or GST-TLR4-TIR and bound GIV and Gαi were visualized by immunoblot. (D) Sequence alignment showing short linear TIR-like loop (TILL) motif that is conserved between GIV and TIR containing proteins. (E) Recombinant His-GIV-CT or TILL mutants were used in a GST pulldown assay with GST or GST-TLR4 and bound GIV was visualized by immunoblot. (F-G) Recombinant His-GIV-CT (3μg) was used in a GST pulldown assay with various GST-TLR proteins (F), GST-TIR adaptors (G), and bound GIV was detected by immunoblot. (H) Recombinant His-GIV-CT TILL mutants were used in GST pulldown assays with TIR adaptor proteins and bound GIV was visualized by immunoblot. For all recombinant GST pulldown assays equal loading of GST proteins were confirmed by Ponceau S staining.

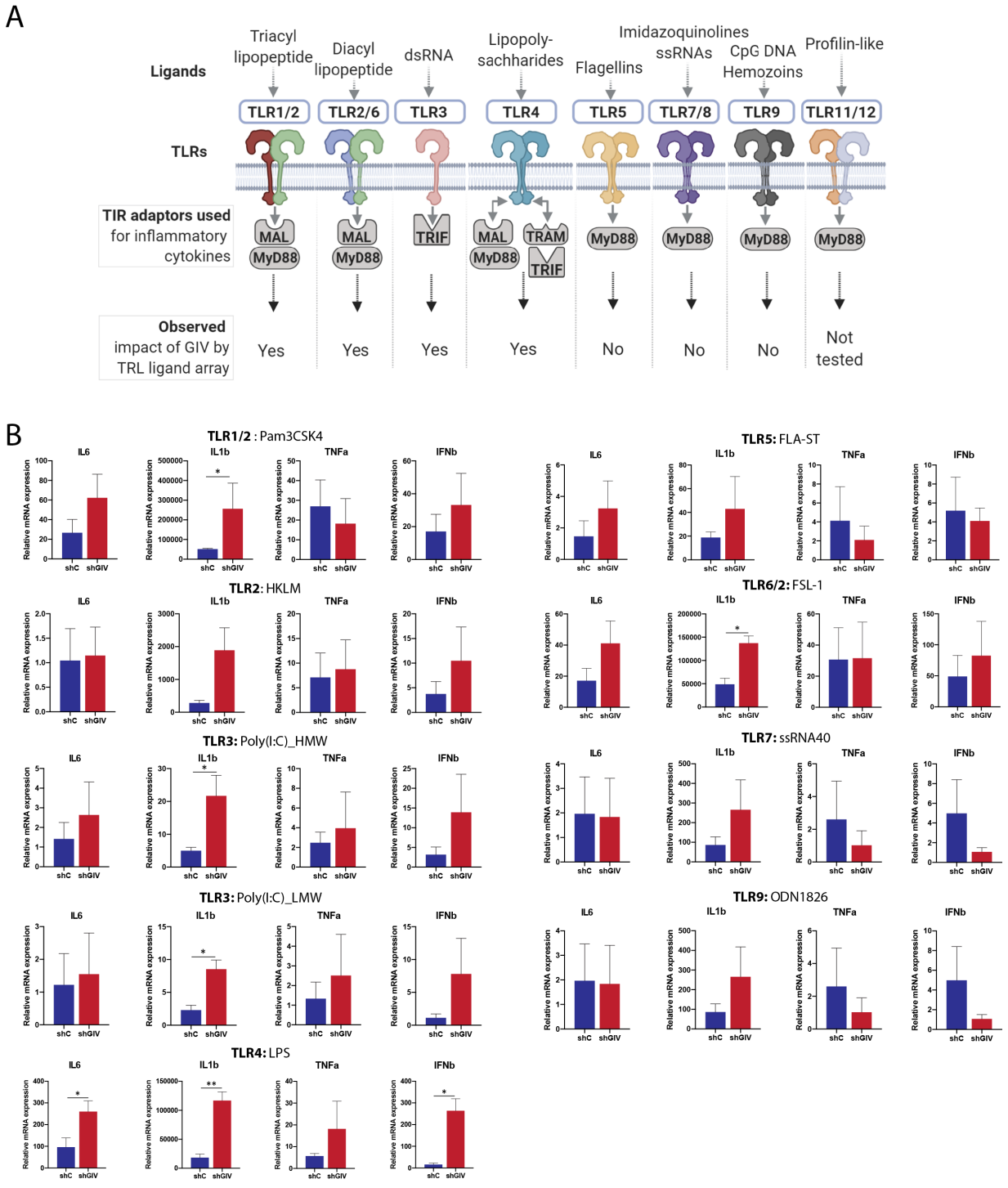

Figure 2.12: GIV impacts inflammatory responses downstream of TLRs that require the TIR-adaptors MAL, TRAM, and TRIF. (A) Schematic summarizing results from TLR-array assay highlighting GIV's impact on TLR responses that require MAL, TRAM, and TRIF TIR adaptors. (B) Bar graphs showing transcript levels of pro-inflammatory cytokines in WT or GIV-depleted macrophages in response to various TLR ligands after 6hrs. Results are from 3 independent experiments and displayed as mean $\pm$ S.E.M.. Students t-test was used to determine significance. (*;$p \leq 0.05$, **;$p \leq 0.01$, ***;$p \leq 0.001$, ****;$p \leq 0.0001$).

Figure 2.13: Identification of key contact sites between GIV's TILL and BB-loop of TLR4. (A) Homology model of GIV's TILL motif bound to the BB-loop of human TLR4. (B) Magnified view of GIV's TILL homotypic interface with TLR4's BB-Loop. (C) Three views of TILL-TIR homotypic interface showing position and orientation of key interactions. (D) Sequence alignment of TLR4 with other TLRs and TIR-adaptors highlighting residues in GIV-TLR4 interaction interface that may confer binding specificity. (E) Schematic of cell-penetrating TILL peptide design for disrupting GIV-TLR4 interaction. (F) Recombinant His-GIV-CT was used in GST pulldown assay with GST or GST-TLR4-TIR and increasing amounts of TILL-peptide or scrambled (SCR) control peptide. Bound GIV was visualized by immunoblot. Equal loading of GST proteins was confirmed by Ponceau S staining. (G) Endogenous TLR4 was immunoprecipitated from RAW lysates in the presence of either TILL-peptide or scrambled control. Bound complex of TLR4, GIV, and Gαi were visualized by immunoblot. Equal loading of IgG and anti-TLR4 were confirmed by Ponceau S staining. (H) Bar graphs displaying cytokine transcript levels (qPCR) in RAW macrophages stimulated with LPS (100ng/ml, 6hr) in the presence of either TILL-peptide or scrambled control. Results are from 3 independent experiments and displayed as mean $\pm$ S.E.M.. Students t-test was used to determine significance. (*;$p \leq 0.05$, **;$p \leq 0.01$, ***;$p \leq 0.001$, ****;$p \leq 0.0001$).

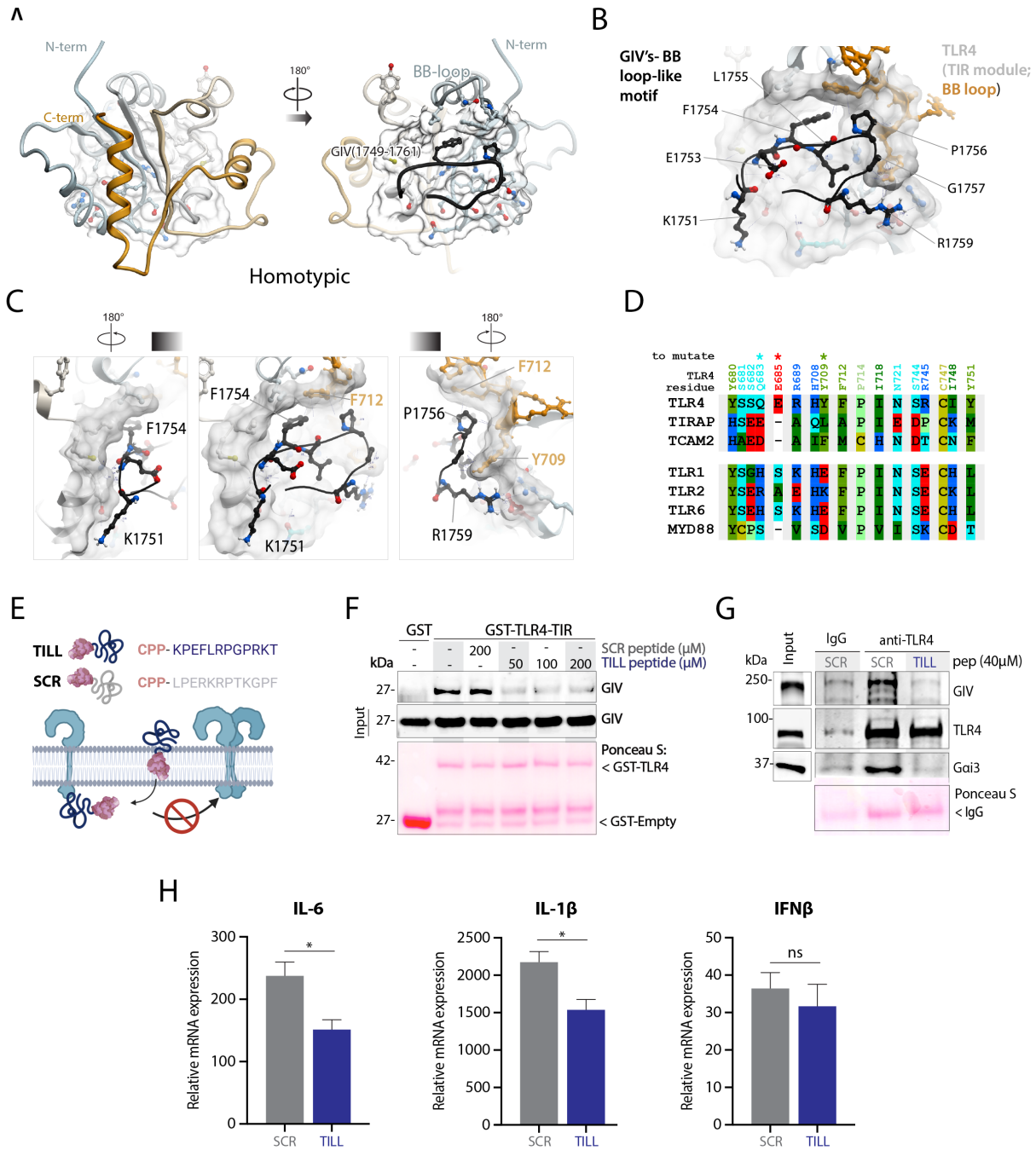
A
N-term
C-term
180°
BB-loop
N-term
GIV(1749-1761)
Homotypic
B
GIV's- BB loop-like motif
TLR4 (TIR module; BB loop)
L1755
F1754
E1753
K1751
P1756
G1757
R1759
C
180°
F1754
K1751
F712
F1754
K1751
180°
F712
P1756
Y709
R1759
D
to mutate
TLR4 residue
Y680 S682 Q683 E685 R689 H708 T709 F712 P714 I718 N721 S744 R745 C747 I748 Y751
TLR4 YSSQ E K HY F P I N SR CI Y
TIRAP HSEE - A QL A P I E DP CK M
TCAM2 HAED - A LF M C H N DT CN F
TLR1 YSSH S K HE F P I N SE CH L
TLR2 YSER A E HK F P I N SE CK L
TLR6 YSEH S K HE F P I N SE CH L
MYD88 YCPS - V SD V P V I SK CD T
E
TILL CPP- KPEFLRPGPRKT
SCR CPP- LPERKRPTKGPF
F
GST
GST-TLR4-TIR
SCR peptide (μM)
TILL peptide (μM)
kDa
200
50
100
200
27-
GIV
Input
27-
GIV
42-
Ponceau S:
< GST-TLR4
27-
< GST-Empty
G
Input
IgG
anti-TLR4
kDa
SCR
SCR
TILL
pep (40μM)
250-
GIV
100-
TLR4
37-
Gαi3
Ponceau S
< IgG
H
IL-6
IL-1β
IFNβ
Relative mRNA expression
300
200
100
0
*
SCR
TILL
2500
2000
1500
1000
500
0
*
50
40
30
20
10
0
ns

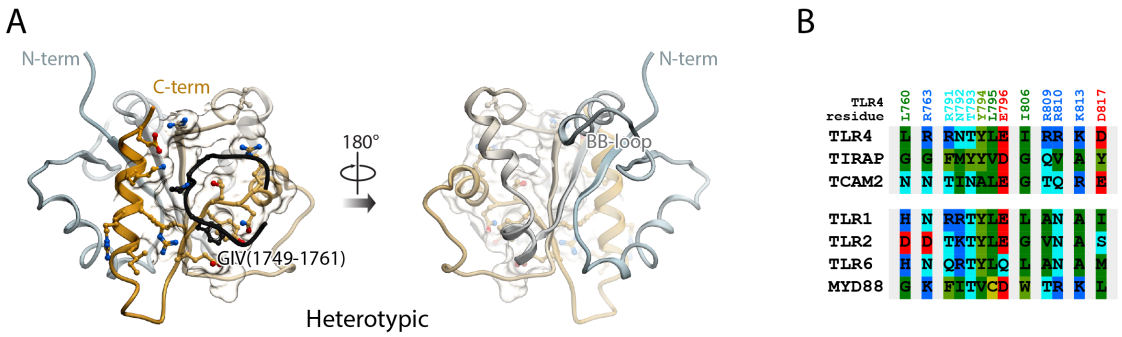

Figure 2.14: Heterotypic interaction model of GIV and TLR4-TIR. (A) Homology model of heterotypic interaction between GIV's TILL domain and the C-terminal helix of TLR4's TIR-domain. (B) Sequence alignment of TLR4 with other TLRs and TIR-adaptor proteins showing proposed contact residues between GIV and TLR4's C-terminal helix region.

Chapter 3

A Boolean Network of inflammatory bowel disease reveals a novel barrier-protective therapeutic target

Modeling diseases as networks has helped simplify an otherwise complex web of multicellular processes; however, an exclusive reliance on symmetric relationships in these networks overlooks the existence of asymmetry in data and loses relevant information that could otherwise inform drug discovery. Here we built a network in which clusters of genes are connected by directed edges that highlight asymmetric Boolean relationships. A Boolean network explorer (BoNE) was designed to analyze the massive Boolean implication network to detect, define and explore the fundamental timeseries underlying any biological data, and to unravel disease continuum states. Using machine learning we pinpoint the path of continuum states that most effectively predicts disease outcome, and exploit such knowledge for target identification, guiding

the choice of pre-clinical models for target validation and for designing organoid-based disease models. Evidence presented also rationalizes the use of BoNE for precision drug discovery and demonstrates the superiority of such approach over traditional approaches.

3.1 Introduction

The advent of high-throughput technologies has overseen an era of explosive growth in biological data. The transcriptome is one such data, which reflects the profile of gene expression. Building networks of robust relationships between genes has been popular approach to understand the underlying pathobiology of human diseases. First, relationships are identified between pairs of genes using symmetric computational frameworks such as linear regression, dimension reduction, and clustering. Subsequently, gene co-expression networks (GCNs) are built by focusing on pairwise gene similarity scores that meet a set statistical threshold. GCN-based analyses severely influenced by the above techniques for connecting two nodes with an edge (Margolin et al., 2006b, Margolin et al., 2006a, Shameer et al., 2015, Shen et al., 2017a, Shen et al., 2017b, van Someren et al., 2002, Butte and Kohane, 2000, Jordan et al., 2004, Tavazoie et al., 1999, Lee et al., 2004) have helped formalize Network Medicine as a field (Barabasi et al., 2011, Loscalzo and Barabasi, 2011) and deliver many successes [in drug repositioning, drug-target discovery, drug-drug interactions, side effect predictions, etc.; reviewed in (Harrold et al., 2013)]. Despite these successes, drugs that can predictably re-set the network in complex multi-component diseases are yet to emerge. The greatest challenges are: 1) Temporal evolution of network architecture during disease progression. 2) The unpredictable nature of biological robustness (Kitano, 2007a). 3) Pleiotropic nature of biological systems, in which multi-tissue, multi-component systems together influence drug targets and treatment efficacies.

4) Phenotypic heterogeneity influenced in each person by both nature (genetics, epigenetics, etc.) and nurture (diet, microbiome, habits, etc.), both variable at a spatiotemporal scale. These challenges have become apparent when modeling complex diseases in which cellular networks reflect adaptation to environmental challenges over time, with distinct continuum states (Kitano, 2007b). Here we explore node connectivity in the network using two fundamentally different principles— (i) asymmetric Boolean Implication relationships (Sahoo et al., 2008), and (ii) the concept of invariants in these relationships. We demonstrate how these two principles can aid the discovery of fundamental progressive timeseries events underlying complex human diseases and exploit such insights to deliver disease-modifying drugs. As an example of a complex, multi-factorial, chronic condition with urgent and unmet needs, we chose to tackle inflammatory bowel disease (IBD). IBD is an autoimmune disorder of the gut in which diverse components (microbes, genetics, environment and immune response) intersect in elusive ways and culminate in overt disease (Abraham and Cho, 2009). It is also heterogeneous with complex sub-disease phenotypes (i.e., strictures, fistula, abscesses, and colitis-associated cancers). Currently, patients are offered inflammation-reducing therapies that have only a 30-40% response-rate, and 40% of responders become refractory to treatment within one year (Ahluwalia, 2012). Little to nothing is available to fundamentally tackle the most widely recognized indicator/predictor of disease relapse, response and remission (D'Inca et al., 1999, Kiesslich et al., 2012, Fries et al., 2013, Florholmen, 2015, Chang et al., 2017, Shen et al., 2009), i.e., a compromised epithelial barrier.

3.2 Results and discussion

A Boolean implication network reveals continuum states in IBD

We created an asymmetric gene expression network of IBD using a computational method based on Boolean logic (Sahoo, 2012, Sahoo et al., 2008, Sahoo et al., 2010). We analyzed two publicly available colon-derived transcriptomic datasets from IBD patients (Arijs et al., 2009, Peters et al., 2017) to build the network. A Boolean Network Explorer (BoNE; see Supplementary Methods) computational tool was introduced which uses asymmetric properties of Boolean implication relationships (BIRs) to discover natural progressive time-series changes in major cellular compartments that initiate, propagate and perpetuate inflammation in IBD and are likely to be important for disease progression. BoNE provides an integrated platform for the construction, visualization and querying of a network of progressive changes much like a disease map (in this case, IBD-map) in three steps: First, the expression levels of all genes in these datasets were converted to binary values (high or low) using the StepMiner algorithm (Sahoo et al., 2007). Second, gene expression relationships between pairs of genes were classified into one-of-six possible BIRs, two symmetric and four asymmetric, and expressed as Boolean implication statements (Figure 3-1A). This offers a distinct vantage from conventional computational methods (Bayesian, Differential, etc.) that rely exclusively on symmetric linear relationships in networks. The other advantage of using BIRs is that they are robust to the noise of sample heterogeneity (i.e., healthy, diseased, genotypic, phenotypic, ethnic, interventions, disease severity) and every sample follows the same mathematical equation, and hence is likely to be reproducible in independent validation datasets. Third, genes with similar expression architectures, determined by sharing at least half of the equivalences among gene pairs, were grouped

into clusters and organized into a network by determining the overwhelming Boolean relationships observed between any two clusters (Sahoo et al., 2008, Sahoo et al., 2010) (Figure 3-1A). In the resultant Boolean implication network (BIN), clusters of genes are the nodes, and the BIR between the clusters are the directed edges; BoNE enables their discovery in an unsupervised way while remaining agnostic to the sample type. As expected, the IBD-Boolean implication network (Figure 3-1) showed scale-free architecture i.e., there are few large clusters, whereas the majority are smaller sized clusters. BoNE-enabled exploration of the Boolean paths (Figure 3-1B) revealed how some of the biggest clusters are connected by a series of BIRs (Green-Red arrows/Black-Blue lines, Figure 3-1C). Reactome pathway analysis of these clusters along the path continuum revealed the most important biological processes that they control (Figure 3-1C). Each cluster was then evaluated for whether they belong to the healthy or diseased side depending on whether the average gene expression value of a cluster in heathy samples is up or down, respectively. The clusters were then arranged sequentially from healthy on the left side to disease on the right side, allowing for the visualization of a time-series of biological processes during the initiation and progression of disease, i.e., yielding a map of IBD (Figure 3-1C). A time series of IBD-associated invariant events emerged— epithelial tight junctions (TJs) and other types of cell-cell junctions appeared leftmost on the healthy side (C1-2) of the IBD-map, levels of which are down-regulated early during disease initiation and are progressively lost. This is followed by bioenergetic stress (C3), culminating in inflammation and fibrosis mediated via the activation of both innate and adaptive immune components and pathways that lead to the formation, resorption and control cellular response to the extracellular matrix (ECM) (C4-6) (Figure 3-1C).

The IBD-Boolean implication network predicts therapeutic response

Next we introduced in BoNE machine learning that seeks to identify which of the gene clusters (nodes) connected by BIRs (edges) are most optimal in distinguishing healthy from diseased samples. BoNE computes a score that naturally orders the samples; this score can be thought of as a continuum of states. Among all possible permutations and combinations, clusters 1-2-3 (C1-3) emerged as the best in separating normal healthy from IBD-afflicted samples (Figure 3-1D) with the highest accuracy (Figure 3-1E). As expected of the invariant nature of the Boolean relationships, this C1-3 signature performed consistently well across seven independent validation cohorts (Figure 3-2A-B). Despite minimal overlaps between differentially regulated genes across these independent cohorts, conventional approaches e.g., differential and Bayesian performed equally well in separating the heathy and IBD-afflicted samples. By contrast, when it came to distinguishing responders from non-responders in a cohort of patients whose colons were analyzed by RNA-Seq prior to the initiation of treatment with TNFα-neutralizing mAbs [E-MTAB-7604; (Verstockt et al., 2019)], Boolean analysis was more accurate than the other two approaches [Figure 3-1F; ROC-AUC for Boolean, 0.86; Differential, 0.68; Bayesian, 0.61], indicating that the Boolean approach was superior in predicting therapeutic response. Additionally, BoNE revealed the ability of the C1-3 signature to segregate samples according to the aggressiveness of disease consistently across five additional validation cohorts (Figure 3-1G); it could separate active from inactive disease (Vanhove et al., 2015, Van der Goten et al., 2014), responders from non-responders receiving two different biologics, Infliximab (Arijs et al., 2009) or Vedolizumab (Arijs et al., 2018), and even distinguished those with quiescent disease with or without remote neoplasia (Pekow et al., 2013) (Figure 3-1G). These findings demonstrate the power of Boolean networks in accurately modeling gene expression

changes that occur during IBD pathogenesis and predicting clinical outcomes.

Network-rationalized selection of PRKAB1 as a barrier-protective target in IBD

Next we sought to exploit the predictive power of BoNE for rationalized target identification and drug discovery. The IBD-map (Figure 3-1C) and multiple validation studies (Figure 3-1F-G) concur that healthy controls and diseased patients in remission share a common signature– high expression of genes in C1-3 and low expression of genes in C4-6, whereas patients with active disease show the opposite pattern. Because the Boolean implication relationships between C1-3 and C4-6 are 'opposite', pharmacologic activation of gene products from C1-2-3 is predicted to both promote C1-2-3 (healthy) and inhibit C4-6 (disease) gene signatures thus 're-setting' the transcriptomic network towards a healthy profile. Gene ontology (GO) molecular function analysis of C1-3 identified high-priority 'druggable' classes of receptors, enzymes and signal transducers (Figure 3-3A), of which, 17 targets were identified as associated with GO biological function of 'response to stress'. Two of 17 were kinases, of which only one, PRKAB1(β1 subunit of the metabolic master regulator, AMPK) had commercially available and extensively validated specific and potent agonists with known structural basis (Xiao et al., 2013, Salatto et al., 2017, Cameron et al., 2016) (Figure 3-3A). When proteins encoded by C1-6 were analyzed for cooperativity between cellular processes within protein-protein interaction (PPI) networks using STRING (Szklarczyk et al., 2017), PRKAB1 and other subunits of AMPK appeared at the crossroads between 'pathogen-sensing', 'autophagy' and epithelial 'tight and adherens junctions' and 'polarity complexes', modules (Figure 3-4). As a plausible mechanism of action, we hypothesized that PRKAB1-agonists may augment epithelial tight junctions (TJs) in the presence of pathogens via its ability to activate a specialized signaling program in

epithelial cells, the stress polarity signaling (SPS) pathway (Aznar et al., 2016) (Figure 3-3B); the latter involves the phosphorylation of the polarity scaffold, Girdin (GRDN) at a single site (Ser245) by AMPK, an event that appears to be both necessary and sufficient for the strengthening of epithelial junctions under bioenergetic stress. Because the SPS-pathway is triggered exclusively as a stress response, and improves modular cooperativity within the PPI network, it fulfills the criteria of "creative elements" (Csermely, 2008); the latter are believed to be critical for the evolvability of complex systems and their pharmacological modulation is predicted to help survive unprecedented challenges/stressors. Next we asked how PRKAB1-agonists may impact the two progressive pathognomonic features of IBD: 1) Epithelial dysfunction and mesenchymal transition (EMT), which distinguishes active from inactive lesions (Zhao et al., 2015), and 2) inflammation and fibrosis. To answer that, we explored disease continuum paths within the IBD-network by accessing another feature of BoNE– given a set of genes in any process, it can identify and help visualize how their levels of expression change along a linear path based on the Boolean implication relationships. The EMT-continuum (Figure 3-3C) showed suppression of key TJ/polarity genes (OCLN, PARD3) is permissive to the upregulation of pro-inflammatory cytokines (i.e. IL6, IL23A, IL33, CXCL10), inflammatory trafficking molecules (i.e. ITGB1, ITGB7, ITGA4, S1PR1), pathogen sensing pathways (i.e. TLR2/4, NOD2, ELMO1), EMT genes (i.e. VIM, SNAI1/2), culminating in leakiness of the barrier, as evidenced by increase in the pore-forming leaky tetraspanin, CLDN2. The healing-inflammation continuum (Figure 3-3D) showed loss of C1-2 genes (PRKAB1, PPP1C1) is permissive to proinflammatory signaling factors (i.e. PRKCQ, JAK1, MRC1), cytokines (i.e. IL11, IL33, IL10, CXCL10), inflammatory trafficking molecules (i.e. ITGB1, ITGB7, ITGA4), pro-fibrotic factors (i.e. COL1A1, PRKCQ, ACTA2, TIMP2, TGFB1), and matrix metalloproteinases (i.e. MMP2, MMP9, MMP14, MMP1,

MMP3). PRKAB1 was present in both disease paths; its activation was predicted to re-set the pathogenic gene expression network in IBD by augmenting epithelial polarity and TJ integrity that are controlled by C1-3, and thereby restoring the integrity of the gut barrier and reducing its leakiness. Consequently, genes that fuel inflammation, EMT and fibrogenesis in clusters C4-6 are expected to be suppressed, and the two progressive pathophysiologic changes in IBD, namely, EMT and inflammation/fibrosis would be modified. Because many of the genes identified in the continuum analyses are known to contribute to IBD pathogenesis, findings further demonstrate the ability of Boolean analysis to identify key drivers of disease.

Tissue expression studies rationalize the use of PRKAB1-agonists in IBD

First, we noted that an IBD-associated SNP has been reported for PRKAB1, but no other subunit of AMPK (Figure 3-5). It was also the only subunit of AMPK that is downregulated in IBD (Figure 3-5). Target transcript analysis by quantitative PCR (qPCR) from human colon biopsies showed 5-fold decrease in PRKAB1 and a concomitant 4-fold increase in CLDN2 expression in IBD-afflicted tissues (Figure 3-3E). Analysis of two other independent cohorts also concurred, i.e., decreased expression of PRKAB1 transcripts in IBD was associated with a concomitant increased expression of CLDN2 in inflamed regions of the colon (Figure 3-6E). Furthermore, target expression analyses confirmed that low levels of PRKAB1 correlates with a higher degree of leakiness of the epithelial barrier (CLDN2), proinflammatory cytokines (MCP1, IL8, IL6 and TNFα) and higher expression of a mucosal gene signature that predicts non-response to anti-TNFα (Arijs et al., 2010). Target protein expression analyses studies were performed via three approaches. First, we noted that unlike its counterpart, AMPKβ2, PRKAB1-encoded AMPKβ1 is preferentially expressed in the gut (and not liver and skeletal muscle, two major sites

for the metabolic action of AMPK), as determined using two different antibodies [Human Protein Atlas (www.proteinatlas.org);]. Second, our immunohistochemistry (IHC) studies on human colon biopsies revealed that compared to healthy controls, patients with IBD display decreased AMPKβ1 (PRKAB1) and increased claudin-2 (CLDN2) staining at the apical side of the epithelial barrier (Figure 3-3F, (Figure 3-6A). Third, analysis of a previously published proteomics dataset from IBD-afflicted patients (Moriggi et al., 2017) further confirmed that diseased colons have high or low expression levels of AMPKβ1 depending on disease activity ((Figure 3-6B). We next asked if the proposed epithelium-specific mechanism of action of PRKAB1-agonists, i.e., their ability to activate the SPS-pathway, is relevant in IBD. IHC on FFPE colon biopsies from healthy and IBD-afflicted patients using a previously validated antibody revealed that the SPS-pathway is more frequently suppressed in IBD compared to healthy controls (Figure 3-3G-H), suggesting that this barrier-protective pathway may be compromised during IBD pathogenesis. Together, these expression studies further rationalize the selective activation of PRKAB1 as a therapeutic strategy to enhance the gut barrier function in IBD.

PRKAB1-agonists ameliorate colitis in a network-rationalized murine model

It is well known that mouse models of IBD capture one or few aspects of the multifaceted complex human disease; none recapitulate them all (Jiminez et al., 2015). We used BoNE to choose the murine model that most accurately recapitulates the barrier-defect transcript signature in human IBD, i.e., downregulation of genes in C1-3. When we analyzed multiple publicly available transcriptomes of the most commonly used chemical, immunological or genetically induced murine models of colitis, DSS-induced colitis emerged as the best (for both bulk colon and sorted epithelial cell-derived datasets), closely followed by TNBS, adoptive T-cell

transfer and Citrobacter-induced colitis, whereas genetic models were deemed inferior (Figure 3-7A). Because DSS acts by eroding the mucus barrier, exposing the epithelium to luminal stressors, resulting in loss of barrier integrity and triggering intestinal inflammation (Chassaing et al., 2014), we asked if PRKAB1-agonists can protect the barrier against stress-induced collapse, and if such protection is associated with activation of the SPS-pathway. Mice were treated intrarectally with DMSO alone (vehicle control), metformin, or PRKAB1-specific agonists while administering DSS in their drinking water (Figure 3-7B). All metrics of the disease, i.e., weight loss (Figure 3-7C), disease activity index (Figure 3-7D), histology score (Figure 3-7E-F) and fibrotic shortening of the colon (Figure3-7G) were significantly ameliorated by two PRKAB1-specific agonists, A-769662 (A7) and PF-06409577 (PF), whereas the non-specific AMPK-agonist, Metformin, did not (see Extended data; Figure 3-8). To obtain proof-of-mechanism for effective target (PRKAB1) activation and reversal of epithelial leakiness, we analyzed by IHC the colon tissues for activation of the SPS pathway (the proposed mechanism of action of PRKAB1 in the epithelium) and reduction of levels of claudin-2. Treatment with PRKAB1-specific agonists not only showed the most prominent activation of the SPS-pathway (as determined by anti-pS245GIV; Figure 3-7E) and near complete reversal of claudin-2, but also showed restoration of goblet cells (PAS staining), and ameliorated fibrosis (Trichrome stain) (Figure 3-8). These studies in a DSS-induced colitis model validate the use of PRKAB1-agonists as barrier-protective therapy and provide pre-clinical proof of concept and mechanism.

PRKAB1-agonists protect the epithelial barrier in organoid-based co-culture models

To define the epithelium-specific mechanism of action of PRKAB1-agonists, we used an in vitro enteroid derived monolayer (EDM) culture system (Sato et al., 2009), in which stem cells isolated from the colonic crypts of mice are grown as 3D organoids and subsequently plated onto trans-well inserts where they were differentiated into mature colonic epithelium (Figure 3-7H). These EDMs are known to contain diverse cell types and maintain a polarized architecture like what is seen in vivo (Noel et al., 2017), and allow for access to the apical and basolateral compartments and measurement of barrier function via trans-epithelial electrical resistance (TEER) and confocal microscopy. First, using organoids derived from colons of AMPKα1/α2-Villin-Cre KO (Um et al., 2010) mice, in which both the catalytic subunits of AMPK are depleted, we confirmed that PRKAB1-agonists require the catalytically active kinase to be able to stabilize the epithelial barrier (Figure 3-9C) and activate the SPS-pathway in polarized EDMs (Figure 3-9B, D). Next, we asked if PRKAB1-agonists can also stabilize/protect the epithelial barrier when exposed to live microbes. Once again, we used BoNE to confirm that EDMs infected with pathogenic microbes (E. coli and Shigella) but not probiotics could serve as models that recapitulate the barrier-defect transcript signature in human IBD (Figure 3-9E). We pre-treated murine EDMs with PRKAB1-agonists (PF; A7 and PF) and then challenged them with adherent invasive E. coli (AIEC)-LF82; this strain, originally isolated from a chronic ileal lesion from a CD patient (Boudeau et al., 1999). After 8 h of infection, control (untreated) monolayers showed a 60% reduction in TEER, whereas all PRKAB1-agonist treated conditions showed protection (Figure3-3I). Similar results were observed using lipopolysaccharide (LPS), a critical outer-membrane component of gram-negative bacteria (Figure 3-9G). As expected, decreasing

TEER after LF-82 infection was associated with junctional collapse, preferentially at tri-cellular TJs, that was prevented by pretreatment with the PRKAB1-agonist PF-06409577 (Figure 3-7J). Staining for pS245-GIV was observed at junctions exclusively after PF treatment, indicating that the stabilization of TJs via activation of the SPS-pathway may serve as the mechanism of action of PRKAB1-agonists. Thus, PRKAB1-agonists activate the SPS-pathway in gut epithelium and prevent disruption of the intestinal barrier when exposed to luminal stressors such as live microbes (pathogens) or microbial products (LPS).

PRKAB1-agonists restore the leaky barrier in IBD-derived organoids

To translate findings from mice to humans, and most importantly, to assess the impact of PRKAB1-agonists on the gut barrier of IBD-afflicted patients, we recruited a total of 18 patients (4 healthy, 4 UC and 10 CD), successfully generated organoids and EDMs from their colons (Figure 3-10A) and subsequently assessed them for barrier integrity. Barrier integrity, as determined by confocal microscopy on EDMs stained for the TJ-marker ZO1 and assessed for the frequency of disrupted ('burst') tri-cellular TJs (TTJ)/high power field, was impaired in both UC and CD, but not in monolayers prepared from healthy controls (Figure 3-10 A-B). TEER values were consistently lower in UC and CD EDMs compared to healthy controls (Figure 3-10C). Because the diseased organoids maintained what appeared to be an intrinsic defect in the epithelial barrier, we used these as models for testing the efficacy of PRKAB1-agonist PF-06409577 as barrier restorative and/or protective therapy. Treatment of both UC and CD-derived EDMs activated the SPS-pathway (pS245GIV signal; Figure 3-10D, H), repaired the 'burst' TTJs (Figure 3-10D-E, H-I), with just 25% increase in TEER across monolayers (Figure 3-10F, J). PF-06409577 also demonstrated barrier-protective efficacy when monolayers were challenged with AIEC-LF82 in

both healthy and IBD-derived EDMs (Figure 3-10G, K).

Next we assessed the efficacy of PRKAB1-agonist PF-06409577 using 25% increase in TEER as a criterion for response to barrier-restorative treatment. A majority (80%) of all diseased organoids responded to treatment with a single dose of 1 μM PF-06409577 (Figure 3-11 A). A multivariate analysis suggested that treatment is effective ($p < 0.001$) in IBD-organoids and that the effect of treatment is not confounded by age, gender, race, prior treatment history, and disease subtypes (Figure 3-11A). As expected, healthy organoids did not show significant changes in TEER. Findings are consistent with UC- and CD-alone networks which predicted that PRKAB1 is poised early in the disease continuum in both subtypes of IBD. Furthermore, combination of PRKAB1-agonists with anti-inflammatory agents is likely to show therapeutic synergy. These results provide proof-of-concept and mechanism in the human gut lining and demonstrate therapeutic response in a human pre-clinical model.

Boolean Network Explorer accurately separates successful and abandoned targets in IBD

Next we asked if BoNE can be exploited to statistically vet the probability of PRKAB1, or any novel target, to succeed in clinical trials. The primary source of trial failure has been and remains an inability to demonstrate efficacy (Hwang et al., 2016); many drugs that were effective in inbred mice lacked efficacy in heterogeneous cohorts of patients. A comprehensive review of literature identified five FDA-approved drugs, sixteen drug targets that were abandoned at different phases (I, II or III) in clinical trials, and seven currently ongoing trials (Figure 3-11B). We set a criterion that effective targets must appear on both Boolean paths (EMT and inflammation/fibrosis; Figure 3-3C-D). To make this process stringent, an additional criterion

was included, i.e., it must have a strong relationship with target (PRKAB1), meeting/exceeding the BooleanNet statistical threshold SThr $>$ 3 and pThr $<$ 0.1 (Sahoo et al., 2008); (Figure 3-11C). BoNE successfully distinguished the FDA-approved vs. the abandoned targets (ROC AUC 1.00; Accuracy 1.00; Figure 3-11D). By contrast, all targets were significant by differential analysis (high false positive rate; Figure 3-11D) and almost all the 'successes' were missed by Bayesian analysis (high false negative rate; Figure 3-11D). Findings indicate that BoNE can accurately assess the probability of a target to pass efficacy test in Phase III clinical trials. Given the retrospective nature of this analysis, these findings need to be confirmed within the framework of other randomized clinical trials, in conjunction with large-scale transcriptomic studies before BoNE can be used to pick 'winners' and 'losers' in IBD therapeutics.

3.3 Concluding remarks

Despite being at the forefront of biomedical research, therapies that can restore and/or protect the integrity of the gut barrier in IBD had not emerged. We have addressed this unmet need using a human-centered network-based drug discovery approach that differs from the current practice in three fundamental ways: 1) Target identification and prediction modeling that is guided by a Boolean implication network of continuum states in human disease; 2) Target validation in network-rationalized animal models that most accurately recapitulate the human disease; 3) Target validation in human pre-clinical organoid co-culture models, inspiring the concept of Phase '0' trials that have the potential to personalize the choice of therapies. The combined synergy of these approaches validates a first-in-class agent in addressing the broken gut barrier in IBD.

3.4 Materials and Methods

Computational Approaches

Inflammatory bowel disease (IBD) datasets used for network analysis

A large RNASeq dataset (Peters 2017, GSE83687, n = 143, 60 control, 32 Ulcerative Colitis, and 42 Crohn's disease) (Peters et al., 2017) and another large microarray dataset (Arijs 2018, GSE73661, n = 178, 12 Control, 166 biopsies from 67 Ulcerative Colitis patients) (Arijs et al., 2018) were downloaded from National Center for Biotechnology Information (NCBI) Gene Expression Omnibus website (GEO) (Edgar et al., 2002, Barrett et al., 2013, Barrett et al., 2007). Both Peters-2017 and Arijs-2018 dataset were processed using the Hegemon data analysis framework (Dalerba et al., 2011, Dalerba et al., 2016, Volkmer et al., 2012).

Preparation and validation of IBD datasets for analysis Both Peters-2017 and Arijs-2018 dataset were prepared for Boolean analysis by filtering genes that have reasonable dynamic range of expression values by analyzing the fraction of high and low values identified by the StepMiner algorithm (Sahoo et al., 2007). Any probeset or genes that contain less than 5% of high or low values are dropped from the analysis. To check if pairwise Boolean implication relationships are consistent between two datasets, every gene in Peters-2017 dataset is mapped to the best probeset (identified by the biggest dynamic range) in the Arijs-2018 dataset, and genes/probesets that do not match are dropped from the analysis. Since RNA-Seq expression values have slightly different characteristics than microarray expression values, the consistency of Boolean implication relationship was determined by using BooleanNet statistics in both datasets and a Pearson's correlation coefficient in the Arijs-2018 dataset. A Pearson's correlation coefficient > 0.5 was considered compatible with Equivalent, High $\implies$ High, and

Low $\implies$ Low Boolean implication relationships. Similarly, a Pearson's correlation coefficient $<$ -0.25 was considered compatible with Opposite, High $\implies$ Low, and Low $\implies$ High Boolean implication relationships.

Identification of Boolean implication relationships

Using IBD datasets, gene expression levels were converted to Boolean values (high and low) using StepMiner algorithm (Sahoo et al., 2007). The expression values are sorted from low to high and a rising step function is fitted to the series to identify the threshold. These relationships are called Boolean implication relationships (BIRs) because they are represented by logical implication ($\implies$) formula. BooleanNet statistics is used to assess the significance of the Boolean implication relationships (Sahoo et al., 2008). S $>$ 2.5 and p $<$ 0.1 are the thresholds (False Discovery Rate $<$ 0.001) used on the BooleanNet statistics during the IBD data analysis to identify Boolean implication relationships. A noise margin of 2-fold change is applied around the threshold to determine intermediate values and these values are ignored during Boolean analysis.

Boolean implication network construction

A Boolean implication network (BIN) is created by identifying all significant pairwise Boolean implication relationships (BIRs) that are consistent in both Peters-2017 GSE83687 and Arijs-2018 GSE73661 datasets (Arijs et al., 2009, Peters et al., 2017). The Boolean implication network contains the six possible Boolean relationships between genes in the form of a directed graph with nodes as genes and edges as the Boolean relationship between the genes. The nodes in the BIN are genes and the edges correspond to BIRs. Equivalent and

Opposite relationships are denoted by undirected edges and the other four types (low $\Longrightarrow$ low; high $\Longrightarrow$ low; low $\Longrightarrow$ high; high $\Longrightarrow$ high) of BIRs are denoted by having a directed edge between them. The network of equivalences seems to follow a scale-free trend; however, other asymmetric relations in the network do not follow scale-free properties. BIR is strong and robust when the sample sizes are usually more than 200. However, it is also possible to build BIN for smaller dataset such as the selected IBD GSE83687 dataset (n = 134). For smaller size dataset (number of samples less than 200) $S > 2.5$ and $p < 0.1$ are used. The IBD dataset was prepared for Boolean analysis by filtering genes that had a reasonable dynamic range of expression values. When the dynamic range of expression values was small, it was difficult to distinguish if the values were all low or all high or there were some high and some low values. Thus, it was determined to be best to ignore them during Boolean analysis. The filtering step was performed by analyzing the fraction of high and low values identified by the StepMiner algorithm (Sahoo et al., 2007). Any probe set or genes which contained less than 5% of high or low values were dropped from the analysis.

Clustered Boolean Implication network

Clustering was performed in the Boolean implication network to dramatically reduce the complexity of the network. A clustered Boolean implication network (CBIN) was created by clustering nodes in the original BIN by following the equivalent BIRs. One approach is to build connected components in a undirected graph of Boolean equivalences. However, because of noise the connected components become internally inconsistent e.g. two genes opposite to each other becomes part of the same connected component. In order to avoid such situation, we need to break the component by removing the weak links. To identify the weakest links, we first

computed a minimum spanning tree for the graph and computed Jaccard similarity coefficient for every edge in this tree. Ideally if two members are part of the same cluster they should share as many connections as possible. If they share less than half of their total individual connections (Jaccard similarity coefficient less than 0.5) the edges are dropped from further analysis. Thus, many weak equivalences were dropped using the above algorithm leaving the clusters internally consistent. We removed all edges that have Jaccard similarity coefficient less than 0.5 and built the connected components with the rest. The connected components were used to cluster the BIN which is converted to the nodes of the CBIN. The distribution of cluster sizes was plotted in a log-log scale to observe the characteristic of the Boolean network. The clusters sizes were distributed along a straight line in a log-log plot suggesting scale-free properties. A new graph was built that connected the individual clusters to each other using Boolean relationships. Link between two clusters (A, B) was established by using the top representative node from A that was connected to most of the member of A and sampling 6 nodes from cluster B and identifying the overwhelming majority of BIRs between the nodes from each cluster. A CBIN was created using the selected Peters-2017 GSE83687 and Arijs-2018 GSE73661 datasets. Each cluster was associated with healthy or disease samples based on where these gene clusters were highly expressed. The edges between the clusters represented the Boolean relationships that are color-coded as follows: orange for low $\implies$ high, dark blue for low $\implies$ low, green for high $\implies$ high, red for high $\implies$ low, light blue for equivalent and black for opposite.

Boolean paths

The asymmetric BIRs provide a unique dimension to the network that is fundamentally different from any other gene expression networks in the literature. Traversing a set of nodes

in a directed graph of the Boolean network constitutes a Boolean path that can be interpreted as follows. A simple Boolean path involves two nodes and the directed edge between them. For the nodes X and Y with X low $\implies$ Y low only quadrant 1 is sparse; the other quadrants 0, 2, and 3 are filled with samples. Assuming monotonicity in X and Y, the quadrants can be ordered in two possible ways: 0-2-3 and 3-2-0. The path corresponds to 0-2-3 begins with X low and Y low. This is interpreted as X turns on first and then Y turns on along a hypothetical biological path defined by the sample order. Similarly, Y turns off first and then X turns off in the path 3-2-0. A complex path in the Boolean network involves more than one Boolean implication relationships. Three Boolean implication relationships can be used to group samples into five bins and the bins can be ordered in two possible ways.

Discovery of Paths in Clustered Boolean Implication network

Discovery of paths start with a node that represents the biggest cluster in the CBIN. Since a path of high $\implies$ high, high $\implies$ low, and low $\implies$ low can be used to order samples, we try to identify paths of this type that intersects the big clusters in the network. We developed a simple, intuitive algorithm that traverses the nodes of the CBIN starting with the biggest cluster and greedily chooses next big cluster connected to the nodes visited in sequence. The emphasis on cluster sizes comes from the fundamental assumption that size determines importance and relevance. Therefore, we start from a big cluster (A1) and identify other clusters that form a chain of low $\implies$ low. Further, we identify other clusters that are either opposite to A1 or they have high $\implies$ low relationship with A1, and the biggest cluster (A2) among these clusters were chosen. In addition, a chain of low $\implies$ low relationship from A2 is identified. In each subsequent step, again the biggest cluster among the different choices was greedily chosen.

Finally equivalence relationship from each cluster is used to gather more genes in each cluster and the whole path is clustered based on equivalence relationships. Depth-first traversal (DFS) was used to follow the path of low $\Longrightarrow$ low where bigger clusters are visited first. The search was performed until a cluster was reached for which there is no low $\Longrightarrow$ low relationships. For example, starting with cluster S, the search will return S low $\Longrightarrow$ A1 low, A1 low $\Longrightarrow$ A2 low, and A2 low $\Longrightarrow$ A3 low if A3 doesn't have any low $\Longrightarrow$ low relationships. Similarly, a new starting point is considered S2 such that S2 is the biggest cluster X that have either S high $\Longrightarrow$ X low or S Opposite X. From cluster S2 another DFS was performed to retrieve the longest possible path of low $\Longrightarrow$ low. The search may return S2 low $\Longrightarrow$ B1 low, B1 low $\Longrightarrow$ B2 low if B2 doesn't have any low $\Longrightarrow$ low relationships. In summary, the most prominent Boolean path was discovered by starting with the largest cluster and then exploring edges that connected to the next largest cluster in a greedy manner. This process was repeated to explore paths that connects the big clusters in the network.

Scoring Boolean path for sample order

A score was computed for a specified Boolean path that can be used to order the sample which was consistent with the logical order. To compute the final score, first the genes present in each cluster were normalized and averaged. Gene expression values were normalized according to a modified Z-score approach centered around StepMiner threshold (formula = (expr - SThr)/3*stddev). Weighted linear combination of the averages from the clusters of a Boolean path was used to create a score for each sample. The weights along path either monotonically increased or decreased to make the sample order consistent with the logical order based on BIR. The samples were ordered based on the final weighted and linearly combined score. The

direction of the path was derived from the connection from a healthy cluster to a disease cluster.

Summary of genes in the clusters

Reactome pathway analysis of each cluster along the top continuum paths was performed to identify the enriched pathways (Fabregat et al., 2018). The pathway description was used to summarize at a high-level what kind of biological processes are enriched in a particular cluster.

Assessing association of IBD signature genes with AMPK subunits

The association between mRNA expression levels of various AMPK subunits and Claudins were tested in a cohort previously reported (Peters et al., 2017). This cohort included gene expression data from multiple publicly available NCBI-GEO data-series (GSE100833, GSE83550, GSE83687). To investigate the relationship between the mRNA expression levels of selected genes (i.e. PRKAB1 and CLDN2), we applied the Hegemon, "hierarchical exploration of gene expression microarrays on-line" tool (Dalerba et al., 2011). The Hegemon software is an upgrade of the BooleanNet software (Sahoo et al., 2008), where individual gene-expression arrays, after having been plotted on a two-axis chart based on the expression levels of any two given genes, can be stratified using the StepMiner algorithm (Sahoo et al., 2007) and compared for statistically significant differences in expression. We stratified the patient population of the NCBI-GEO discovery dataset in different gene-expression subgroups, based on the mRNA expression levels of various AMPK subunits, and compared expression of IBD associated genes between groups.

Generation of heat maps using gene clusters identified by Boolean analysis

To generate the IBD, UC and CD heatmaps first a Boolean path was constructed by following the largest clusters in the Boolean Network (Arijs et al., 2009, Peters et al., 2017). Genes along this path was selected to generate a heatmap that shows the gene expression values in different samples. To build heatmaps using the datasets from patients treated with either an anti-TNF (Infliximab; GSE16879), (Arijs et al., 2009) or anti-$\alpha 4\beta 7$ (Vedolizumab; GSE73661) (Arijs et al., 2018), the gene clusters (C1-2-3) along the major IBD-paths were used. Gene expression values were normalized according to a modified Z-score approach centered around StepMiner threshold (formula = (expr - SThr)/3*stddev). The samples were ordered according to average of the normalized gene expression values in the largest cluster along the Boolean path. The heatmap use red colors for the high values, white colors for the intermediate values and blue colors for low values. Gene names for few selected genes are highlighted on the left to show their expression patterns.

Identification of Epithelial-Mesenchymal and Inflammation-Fibrosis continuum

Top genes involved with Epithelial-Mesenchymal processes and inflammation-fibrosis processed are chosen from literature review. Given a list of genes BoNE computes a subgraph of the CBIN graph by identifying clusters that include one or more genes from this list. BoNE then search for a path in this subgraph as mentioned before with the original CBIN graph. The path identified is used to draw a model of the gene expression timeline. The continuum is identified by computing a score based on the path as described before.

Measurement of classification strength or prediction accuracy

Measurement of classification strength or prediction accuracy Receiver operating characteristic (ROC) curves were computed by simulating a score based on the ordering of samples that illustrates the diagnostic ability of binary classifier system as its discrimination threshold is varied along the sample order. The ROC curves were created by plotting the true positive rate (TPR) against the false positive rate (FPR) at various threshold settings. The area under the curve (often referred to as simply the AUC) is equal to the probability that a classifier will rank a randomly chosen IBD samples higher than a randomly chosen healthy samples. In addition to ROC AUC, other classification metrics such as accuracy ((TP + TN)/N; TP: True Positive; TN: True Negative; N: Total Number), precision (TP/(TP+FP); FP: False Positive), recall (TP/(TP+FN); FN: False Negative) and f1 (2 * (precision * recall)/(precision + recall)) scores were computed. Precision score represents how many selected items are relevant and recall score represents how many relevant items are selected. Fisher exact test is used to examine the significance of the association (contingency) between two different classification systems (one of them can be ground truth as a reference).

Experimental Approaches

Reagents and antibodies

Unless otherwise indicated, all reagents were of analytical grade and obtained from Sigma-Aldrich (St. Louis,MO). Custom-designed oligos were obtained from Valuegene (San Diego, CA). Antibodies against GIV that were used in this work include rabbit serum anti-GIV coiled-coil immunoglobulin G (GIV-ccAb for immunoblotting only) (Le-Niculescu et al., 2005),

and affinity-purified GIV-cc Ab (Cat ABT80; from EMD Millipore for immunoblotting). Mouse mAbs against anti-phospho-(p; Cell Signaling Technology, Danvers, MA) and total (t; Abcam, Cambridge, UK) AMPK, anti-Claudin-2 (Abcam), and anti-tubulin (Sigma,St. Louis, MO) were purchased from commercial sources. Rabbit polyclonal antibodies against phospho-S245 GIV were generated commercially by 21st Century Biochemicals (Marlborough, MA) and validated previously (Aznar et al., 2016). DAPI and anti-mouse Alexa Fluor 488 or 594–coupled goat secondary antibody for immunofluorescence were purchased from Invitrogen (Carlsbad, CA). Goat anti-rabbit and goat anti-mouse Alexa Fluor 680 or IRDye 800 F(ab')2 for immunoblotting were from LI-COR Biosciences (Lincoln, NE).

RNA extraction and quantitative-(q) PCR

Total RNA was isolated using the Quick-RNA MicroPrep Kit (Zymo Research, USA) according to the manufacture's instruction. RNA was converted into cDNA using the qScript^{TM} cDNA SuperMix (Quantabio). Quantitative RT-PCR (qRT-PCR) was carried out using 2x SYBR Green qPCR Master Mix (Biotool^{TM}, USA). The cycle threshold (Ct) of target genes was normalized to 18S rRNA gene. The fold change in the mRNA expression was determined using the $\Delta\Delta$ Ct method. Primers used in qPCR reactions were designed using NCBI Primer Blast software and Roche Universal Probe Library Assay Design software.

Immunoblotting

For immunoblotting, protein samples were separated by SDS-PAGE and transferred to PVDF membranes (Millipore, Burlington, MA). Membranes were blocked with PBST supplemented with 5% nonfat milk (or with 5% BSA when probing for phosphorylated proteins) before

incubation with primary antibodies. Infrared imaging with two-color detection and band densitometry quantifications were performed using the Odyssey imaging system (Li-Cor, Lincoln, NE). All Odyssey images were processed using ImageJ software (NIH, Bethesda, MD.) and assembled into figure panels using Photoshop and Illustrator software suits (Adobe Inc., San Jose, CA.).

Human subjects

Colonic biopsies used either for IHC studies or as source of stem cells for organoid culture were obtained from IBD patients undergoing colonoscopies a part of their routine care and follow-up at UC San Diego's Inflammatory Bowel Disease (IBD) Center. Patients were recruited and consented using a study proposal approved by the Institutional Review Board of University of California, San Diego. The clinical phenotype and information were curated based on histopathology reports from Clinical Pathology and Chart check, followed by consultation with a specialist at UC San Diego's IBD Center. For immunohistochemical analysis of human tissue specimens, archived formaldehyde-fixed paraffin-embedded (FFPE) human colonic biopsies from healthy controls, or patients with adenomas and/or carcinomas were obtained from the Gastroenterology Division, VA San Diego Healthcare System, following the protocol approved by the Human Research Protection Program (HRPP) Institutional Review Board (Project ID 1132632). For the purpose of generating adult healthy enteroids, a fresh biopsy was prospectively collected using small forceps from healthy subjects undergoing routine colonoscopy for colon cancer screening at the VA San Diego Healthcare System. For all the deidentified human subjects the information including age, ethnicity, gender, previous history of disease and medication were collected from the chart following the security and privacy rules outlined in the

HIPAA (Health Insurance Portability and Accountability Act of 1996) legislation.

Murine models

Intestinal crypts were isolated either from the proximal and the mid-colon of WT C57BL/6 or AMPK KO mice; generated from gender- and age-matched littermates of age 5-7 weeks. For DSS-colitis experiments, 7-8-wk old C57Bl/6 mice were obtained from Jackson Laboratories (Bay Harbor, ME). Animals were bred, housed, and euthanized according to University of California San Diego Institutional Animal Care and Use Committee (IACUC) policies and guidelines.

Isolation of organoids from murine and human colons

Colonic specimens of around 1-inch segment in the case of mice or superficial biopsies in the case of human subjects were collected using cold forceps. The specimens were washed in ice-cold PBS to remove fecal contamination, fat and blood vessels. When acquisition of samples and isolation of stem cells were performed in different facilities, specimens were transported from the site of sample acquisition to the laboratory in media containing DMEM/F12 with HEPES and L-glutamine, 10% FBS and 10 M Y27632 (ROCK inhibitor). Crypts were isolated by digesting with collagenase type I [2 mg/ml; Invitrogen, Carlsbad, CA] solution containing Gentamicin (50 μg/ml, Life Technologies, Carlsbad, CA) at 37° C by monitoring the digestion of epithelial units up to 80%. The tissue fragments were added to media (DMEM/F12 with HEPES, 10% FBS) to inactivate the collagenase and filtered with a 70 μM cell strainer as outlined before (Mahe et al., 2015, Sato et al., 2009, Miyoshi and Stappenbeck, 2013). Filtered tissue fragments were centrifuged down at 100 g for 5 min and the media was aspirated. The epithelial units were suspended in matrigel BD basement membrane matrix (Cat 356235, Corning Costar,

Corning, NY). Cell-matrigel suspension (15 μl) was placed at the center of the 24-well plate on ice and placed for 10 m in the incubator upside-down for polymerization. Subsequently, 500 μl of 50% conditioned media (CM) was added. CM was prepared from L-WRN cells (ATCC® CRL-3276™, from the laboratory of Thaddeus S. Stappenbeck (Miyoshi and Stappenbeck, 2013)) with Wnt3a, R-spondin and Noggin. Y27632 (ROCK inhibitor, 10 μM) and SB431542 (an inhibitor for TGF-β type I receptor, 10 μM) were added to the media. For human colon samples, the 50% conditioned media was supplemented with Nicotinamide (10 μM, Sigma-Aldrich, St. Louis, MO), N-acetyl cysteine (1 mM, Sigma-Aldrich), and SB202190 (10 μM, Sigma-Aldrich). The medium was changed every 2-3 d and the enteroids were expanded and frozen in liquid nitrogen. One important caveat to mention is that after extended passage ($>$ 10) of IBD patient-derived enteroids they begin to revert their phenotype to a 'healthy' state (i.e. less disruption of TJs, and higher TEER values). This is likely due to the stress-reducing culture conditions required to propagate the enteroids and therefore it is imperative to use low passage number enteroids when assessing IBD associated barrier defects.

Preparation of enteroid-derived monolayers (EDMs)

For both murine and human enteroids, polarized EDMs were prepared using a similar protocol outlined below. Single-cell suspensions from typsinized organoids in 5% conditioned media were added to matrigel diluted in cold PBS (1:30) as done before (den Hartog et al., 2016). 2-4 x 105 cells were plated in 24-well trans-well inserts (0.4μm pore size; Corning Costar, Corning, NY) and differentiated for 2 days in advanced DMEM/F12 media without Wnt3a but with R-Spondin, Noggin, B27 and N2 supplements and 10 μM ROCK inhibitor for mouse (Sato et al., 2009). For Human EDMs, media and supplements were obtained commercially (Cell

Applications Inc. San Diego, CA) and a proprietary cocktail was added to the above media.

Bacteria and bacterial culture

Adherent Invasive Escherichia coli strain LF82 (AIEC-LF82), isolated initially from the colon of Crohn's disease patients obtained from the lab of Arlette Darfeuille-Michaud (Darfeuille-Michaud et al., 2004). For bacterial culture, a single colony was inoculated into LB broth and grown for 8 h under aerobic conditions in an orbital shaking incubator at 150 rpm, followed by overnight culture under oxygen-limiting conditions, but without shaking, to maintain their pathogenicity. Cells were infected with a multiplicity of infection (moi) of 10-30 as done before (Suarez et al., 2018).

Immunofluorescence

Mouse and human enteroid-derived monolayers (EDMs) were fixed with cold methanol at -20C for 20min, washed once with PBS and equilibrated in blocking buffer (0.1% Triton X-100, 2 mg/ml BSA, in PBS) for 1 h. Samples were then incubated with primary and then secondary antibodies as described previously (Ghosh et al., 2008). Dilutions of antibodies and reagents were as follows: anti-phospho-Ser245-GIV (pS245-GIV; 1:250); anti-Occludin (1:250); DAPI (1:1000); goat anti-mouse (488 and 594 nm wavelength) Alexa-conjugated antibodies (1:500). Images were acquired using a Leica CTR4000 Confocal Microscope with a 63X objective. Z-stack images were obtained by imaging approximately 4-μm thick sections of cells in all channels. Cross-section and maximal projection images were obtained by automatic layering of individual slices from each Z-stack. Red-Green-Blue (RGB) graphic profiles were created by analyzing the distribution and intensity of pixels of these colors along a chosen line using

ImageJ software. All individual images were processed using Image J software and assembled for presentation using Photoshop and Illustrator software (Adobe).

Quantitative (q)PCR analysis of IBD patient samples

Colonic biopsy specimens were collected either from healthy human subjects enrolled for routine colonoscopy or with IBD subjects enrolled for colonoscopy at the UCSD IBD center. RNA isolation, cDNA preparation, and analysis of transcript levels for PRKAB1 and CLDN2 were done as described above. Results are displayed as mean S.E.M. and p-values calculated using a student two-tailed t-test.

Immunohistochemistry of patient colon samples

Formalin-fixed, paraffin-embedded (FFPE) tissue sections of 4 μM m thickness were cut and placed on glass slides coated with poly-L-lysine, followed by deparaffinization and hydration. Heat-induced epitope retrieval was performed using citrate buffer (pH 6.0) in a pressure cooker. Tissue sections were incubated with 0.3% hydrogen peroxidase for 15 m to block endogenous peroxidase activity, followed by incubation with primary antibodies for overnight in a humidified chamber at 4°C. Antibodies used for immunostaining; anti-pS245 GIV [1:50, anti-rabbit antibody], anti-AMPKβ1 [1:50, anti-rabbit], anti-Claudin-2-1 [1:250, anti-rabbit]. Immunostaining was visualized with a labeled streptavidin-biotin using 3,3-diaminobenzidine as a chromogen and counterstained with hematoxylin. Samples were quantitatively analyzed and scored based on presence (positive) or absence (negative) of staining. Data is displayed as frequency of staining score and a Chi-square test was used to determine significance.

Proteomic analysis of IBD patient samples

Proteomic dataset containing from healthy and UC patients was obtained from previously published work (Bennike et al., 2015). Samples were analyzed for expression of AMPK subunits and tight junction proteins (occludin). Results are displayed as mean S.E.M. and p-values calculated by 2-way ANOVA using Tukey's multiple comparisons test.

Activation of SPS-pathway in colon enteroids by PRKAB1 agonists

3D enteroids were incubated with various chemical activators of AMPK (metformin [1 mM], A-769662 [100 μM], PF-06409577 [1μM]) for 4 h. Enteroids were separated from matrigel by incubating with Cell Recovery Solution (Corning) for 1 h at 4°C with rotation followed by centrifugation at 200 x g for 5 m at 4°C. Media and dissolved matrigel was aspirated and remaining cell pellet was boiled in Laemelli's sample buffer for 10 m. Samples were analyzed by Western blot, as described above, using: anti-pS245-GIV (1:500, 21st Century Biochemicals, Marlboro, MA), anti-GIV-coiled-coil(CC) (1:500, EMD Millipore), anti-AMPKα and anti-phospho-AMPKα(Thr172) (1:1000, Cell Signaling Technologies, Danvers, MA), and anti-α tubulin (1:1000, Sigma-Aldrich). Quantification of burst tight-junctions was done by manual counting the number of total and burst tri-cellular junctions in 3 randomly chosen fields in each of three independent experiments. Data is expressed as frequency of burst tight junctions and a one-way ANOVA analysis was used to determine significance.

Measurement of Trans-Epithelial Electrical Resistance (TEER) in 2D-EDM

EDMs were cultured, as described above, on 24-well transwell inserts (0.4μm pore size; Corning Costar). EDMs were differentiated for 2 d before treatment with various chemical acti-

vators of AMPK (metformin [1 mM], A-769662 [100 μM], PF-06409577 [1 muM]) for 16 h. Cultures were then challenged with insults (LPS [500 ng/ml] or AIEC-LF-82 [moi=10]) and epithelial permeability was measured using an epithelial voltohmmeter Millicel-ERS resistance meter (Millipore) at 1 h intervals for 8 h. TEER was calculated by subtracting measured values from blank control wells and expressed as ohm x cm2. TEER values were normalized to t0 and expressed as percentage change relative to t0. Results are displayed as mean S.E.M. and p-values calculated by 2-way ANOVA using Tukey's multiple comparisons test.

Imaging tight junction (TJ) integrity of 2D-EDM by confocal microscopy

EDMs were plated on 24-well transwell inserts, as described above for TEER experiments. After treatment, infection, and measurement of TEER samples were washed once with PBS, pH 7.4 and fixed in 100% methanol (-20°C for 20 m), washed with PBS, and permeabilized/blocked (0.1% Triton-X 100, 2mg/ml BSA in PBS for 1 h at 22°C). Cells were stained using either anti-pS245 GIV (1:300, 21st Century) or anti-Occludin (1:300, Thermo-Fisher, Waltham, MA) overnight at 4°C in blocking solution. For secondary staining goat anti-mouse-Alexa488 (1:500, Life technologies, Carlsbad, CA), goat anti-rabbit-Alexa594 (1:500, Life technologies) and DAPI (1:1000) were prepared in blocking solution and stained for 1 h at 22°C. For imaging, the transwell membranes were cut out and placed cell-side-up on untreated glass microscope slides. ProlongGoldTM (20 μl) mounting media (Life technologies) was placed directly on transwell membranes and coverslips were mounted (15 mm, 1 thickness).

Dextran Sodium Sulfate (DSS) mouse model of colitis

Seven wk-old female C57BL/6 mice obtained from Jackson Laboratories (Bay Harbor, ME) were given either normal drinking water (control) or 2.5% dextran sodium sulfate (DSS) for 5 d, followed by an additional 4 d recovery period with normal drinking water. Water levels were monitored to determine the volume of water consumed by all groups. Weight was monitored daily. Treatment with AMPK agonists (metformin [50 mg/kg/d], A769662 [6 mg/kg/d], PF-06409577 [10 mg/kg/d]) was administered once per day (d0 through d9) via intrarectal injection (50 μl total volume). All compounds were dissolved in 4% DMSO (vehicle). Post-injection, mice were hung upside-down for 30 sec to ensure injection solution was retained in colon. Mice were sacrificed on the 9th day, and colon length was assessed. Colon samples were collected for assessing the levels of mRNA (by qPCR) or proteins (by immunohistochemistry on FFPE tissues) for target genes/proteins. Disease activity index (DAI) was calculated using by scoring stool consistency (0-4), rectal bleeding (0-4), and weight loss (0-4) as previously published (Kim et al., 2012). Results are displayed as mean S.E.M. and p-values calculated by 2-way ANOVA using Tukey's multiple comparisons test. Immunohistochemical analysis was done as described above. Antibodies used for immunostaining; anti-pS245 GIV (1:50, anti-rabbit antibody generated commercially by 21st Century Biochemicals, and extensively validated previously(Aznar et al., 2016)), anti-claudin-2 (1:100, anti-rabbit, Abcam, Cambridge, UK), anti-myeloperoxidase (1:30, anti-rabbit, Abcam). Immunostaining was visualized with a labeled streptavidin-biotin using 3,3-diaminobenzidine as a chromogen and counterstained with hematoxylin. Samples were quantitatively analyzed and scored based on the intensity of staining using the following scale; 0 to 3, where 0 = no staining, 1 = light brown, 2 = brown, and 3 = dark brown. For Periodic Acid Schiff (PAS) staining FFPE tissue sections were first cut into slides, deparaffinized, and rehy-

drated before immersion into PAS for 5 m at 22°C. Slides were then washed, and immersed in Schiff's reagent for 15 m at 22°C. Slides were counterstained in Hematoxylin solution for 3 min, before dehydration and mounting. Hematoxylin and Eosin (HE) stained slides were evaluated for presence of neutrophilic and mononuclear infiltrates, submucosal edema, surface erosions, inflammatory exudates, and presence of crypt abscesses and scored as done previously (Das et al., 2015). Scoring was carried out by two independent pathologists.

Statistical analyses

Statistical significance between datasets with three or more experimental groups was determined using one-way (or two-way in the case of DSS weight analysis) analysis of variance (ANOVA) including a Tukey's test for multiple comparisons. Statistical difference between two experimental groups was determined using a two-tailed unpaired t-test or two-tailed Mann-Whitney test (patient sample transcript analysis). For analysis of frequency of SPS-pathway activation in human patient biopsies, a two-tailed Fisher's exact test was used to calculate significance. For all tests, a p-value of 0.05 was used as the cutoff to determine significance. All experiments were repeated a least three times, and p-values are indicated in each figure. All statistical analysis was performed using GraphPad prism 8.

Acknowledgements

This work was supported by National Institutes for Health (NIH) grants CA238042, AI141630, CA100768 and CA160911 (to P.G), DK107585, CTSA/NCATS grant UL1TR001442 pilot award program and DiaComp Pilot and Feasibility award (to SD), R00-CA151673 (to DS). PG and SD were also supported by the Helmsley Charitable Trust and Foundation for the

Crohn's disease project grant. Y.M and L.S were supported by National Institutes for Health (NIH) training grant (DK 0070202). Y.M was also supported by an NIH CTSA-funded career-development award (1TL1TR001443). SRI was supported by the postdoctoral fellowship grant from NIH (3R01DK107585-02S1).

Chapter 3 in part a reprint of material submitted to be published in: Sahoo DS*, **Swanson L***, Sayed IM*, Katkar GD, Ibeawuchi SR, Lim BB, Mittal Y, Pranadinata RF, Tindle C, Fuller M, Stec DL, Chang JT, Sandborn WJ, Das S, Ghosh P. 2020. "Modeling disease continuum states from a clustered Boolean implication network". *under review*. The dissertation author was the primary author.

Figure 3.1: Generation and validation of Boolean Network map of IBD. (A) We applied Boolean Network Explorer (BoNE) to analyze two IBD datasets: GSE83687 and GSE73661 (Arijs et al., 2018, Peters et al., 2017). The Boolean network (middle) contains the six possible Boolean relationships (right) in the form of a directed graph with genes having similar expression profiles organized into clusters, and relationships between gene clusters represented as color-coded edges. (B) Schematic illustrating how Boolean cluster relationships are used to chart disease paths (Top); and individual gene expression changes along a boolean path, illustrating gene expression dynamics within the normal to IBD continuum (bottom). (C) Reactome pathway analysis of each cluster along the top continuum paths were performed to identify the signaling pathways and cellular processes that are enriched during IBD progression. (D) Heatmap of the expression profile of genes in GSE83687 using Boolean clusters (C1-2-3) superimposed on sample type (top bar) demonstrates the accuracy of Boolean analysis in sample segregation into normal and IBD. (E) Selection of Boolean path using machine learning. Linear regression on Test dataset 3 (GSE6731) was used to select the best path that can separate normal and IBD samples. (F) Direct comparison of Boolean, Differential and Bayesian analysis in predicting responders (R) and non-responders (NR) to anti-TNFα treatment in E-MTAB-7604 (n=11) dataset. (G) Prediction of active UC vs inactive UC (GSE59071, GSE48958), responder vs. non-responder to treatment with anti-TNFα (GSE16879) and anti-α47 (GSE73661) mAbs, quiescent UC without or with remote neoplasia (GSE37283, N=20) by using Boolean analysis.

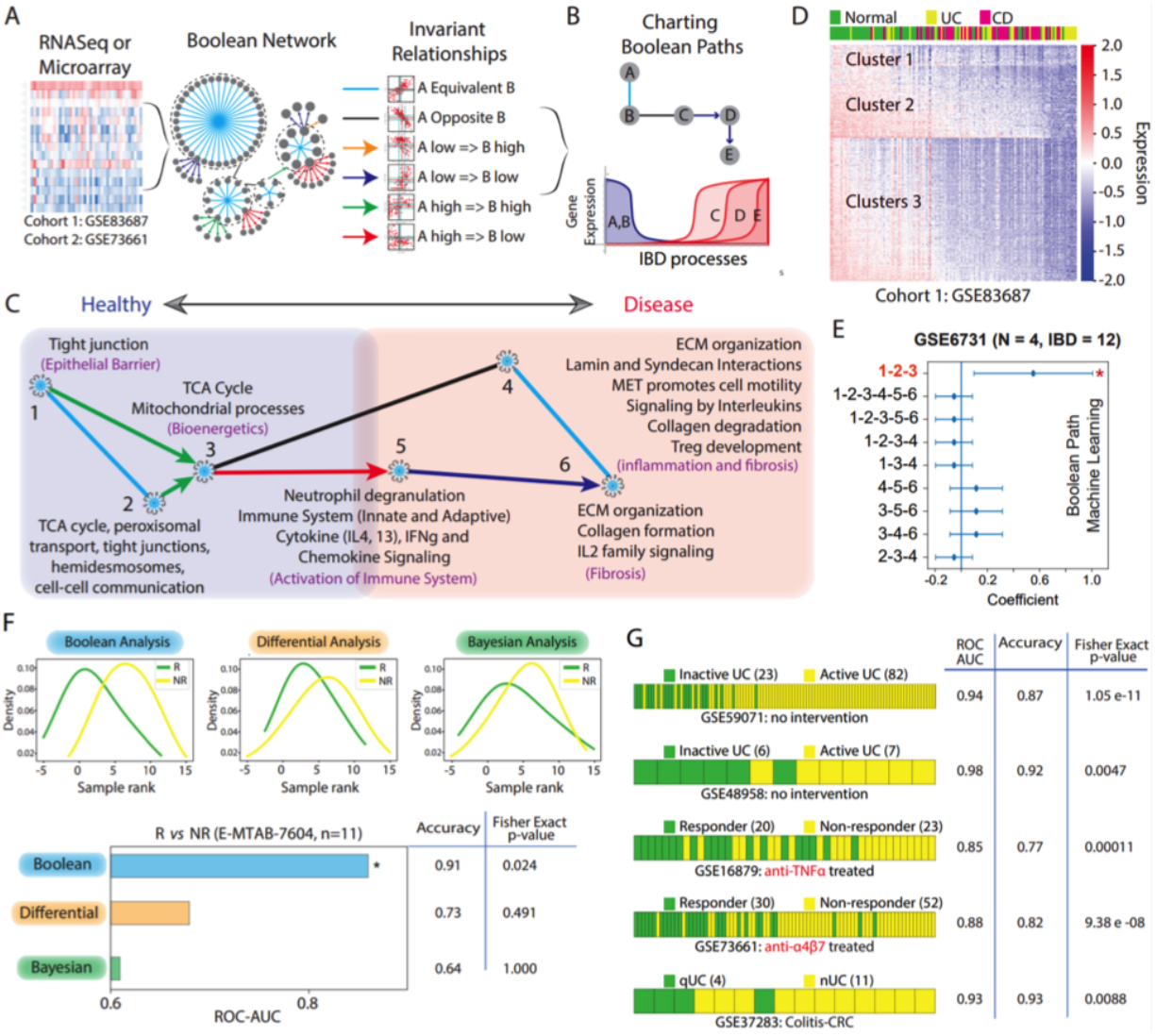
A
RNASeq or Microarray
Boolean Network
Invariant Relationships
A Equivalent B
A Opposite B
A low => B high
A low => B low
A high => B high
A high => B low
Cohort 1: GSE83687
Cohort 2: GSE73661
B
Charting Boolean Paths
A
B
C
D
E
Gene Expression
A,B
C D E
IBD processes
D
Normal
UC
CD
Cluster 1
Cluster 2
Clusters 3
Expression
Cohort 1: GSE83687
C
Healthy
Disease
Tight junction
(Epithelial Barrier)
TCA Cycle
Mitochondrial processes
(Bioenergetics)
TCA cycle, peroxisomal transport, tight junctions, hemidesmosomes, cell-cell communication
Neutrophil degranulation
Immune System (Innate and Adaptive)
Cytokine (IL4, 13), IFNg and Chemokine Signaling
(Activation of Immune System)
ECM organization
Lamin and Syndecan Interactions
MET promotes cell motility
Signaling by Interleukins
Collagen degradation
Treg development
(inflammation and fibrosis)
ECM organization
Collagen formation
IL2 family signaling
(Fibrosis)
E
GSE6731 (N = 4, IBD = 12)
1-2-3
1-2-3-4-5-6
1-2-3-5-6
1-2-3-4
1-3-4
4-5-6
3-5-6
3-4-6
2-3-4
Boolean Path Machine Learning
Coefficient
F
Boolean Analysis
Differential Analysis
Bayesian Analysis
Density
Sample rank
R
NR
R vs NR (E-MTAB-7604, n=11)
Accuracy
Fisher Exact p-value
Boolean
Differential
Bayesian
0.91
0.024
0.73
0.491
0.64
1.000
ROC-AUC
G
ROC AUC
Accuracy
Fisher Exact p-value
Inactive UC (23)
Active UC (82)
GSE59071: no intervention
0.94
0.87
1.05 e-11
Inactive UC (6)
Active UC (7)
GSE48958: no intervention
0.98
0.92
0.0047
Responder (20)
Non-responder (23)
GSE16879: anti-TNFα treated
0.85
0.77
0.00011
Responder (30)
Non-responder (52)
GSE73661: anti-α4β7 treated
0.88
0.82
9.38 e -08
qUC (4)
nUC (11)
GSE37283: Colitis-CRC
0.93
0.93
0.0088

A

Cohort	GSE#	# of Samples (N, IBD)	ROC AUC	Accuracy	Fisher Exact p value
Test 1	GSE83687	(60, 74)	0.81	0.75	5.13 e-09
Test 2	GSE73661	(12, 166)	0.98	0.94	8.11 e-10
Validation 1	GSE6731	(4, 12)	1.00	0.94	0.003
Validation 2	GSE75214	(11, 82)	0.99	0.95	1.30 e-09
Validation 3	GSE16879	(6, 43)	1.00	1.00	7.15 e-08
Validation 4	GSE59071	(11, 105)	0.97	0.96	5.48 e-08
Validation 5	GSE48958	(8, 13)	0.91	0.76	0.007
Validation 6	GSE37283	(5, 15)	0.71	0.5	0.26
Validation 7	GSE109142	(20, 206)	0.97	0.95	7.23 e-12

B

Figure 3.2: Path C1-2-3 predicts healthy vs disease samples. (A) BoNE identified path C1-2-3 by machine learning that performed best in separating healthy vs disease samples in two training datasets: GSE83687 and GSE73661. C1-2-3 path score is applied to seven other validation datasets to predict healthy vs disease samples: GSE6731, GSE75214, GSE16879, GSE59071, GSE48958, GSE37283, and GSE109142. The strength of the classification is measured by number of samples, ROC AUC, Accuracy, and Fisher exact p-values. (B) Detailed classification report is provided in terms of heatmap of the sample ordering, precision (TP/(TP+FP)), recall (TP/(TP+FN)), and f1-score (2 * (precision * recall)/(precision + recall)) for all the datasets.

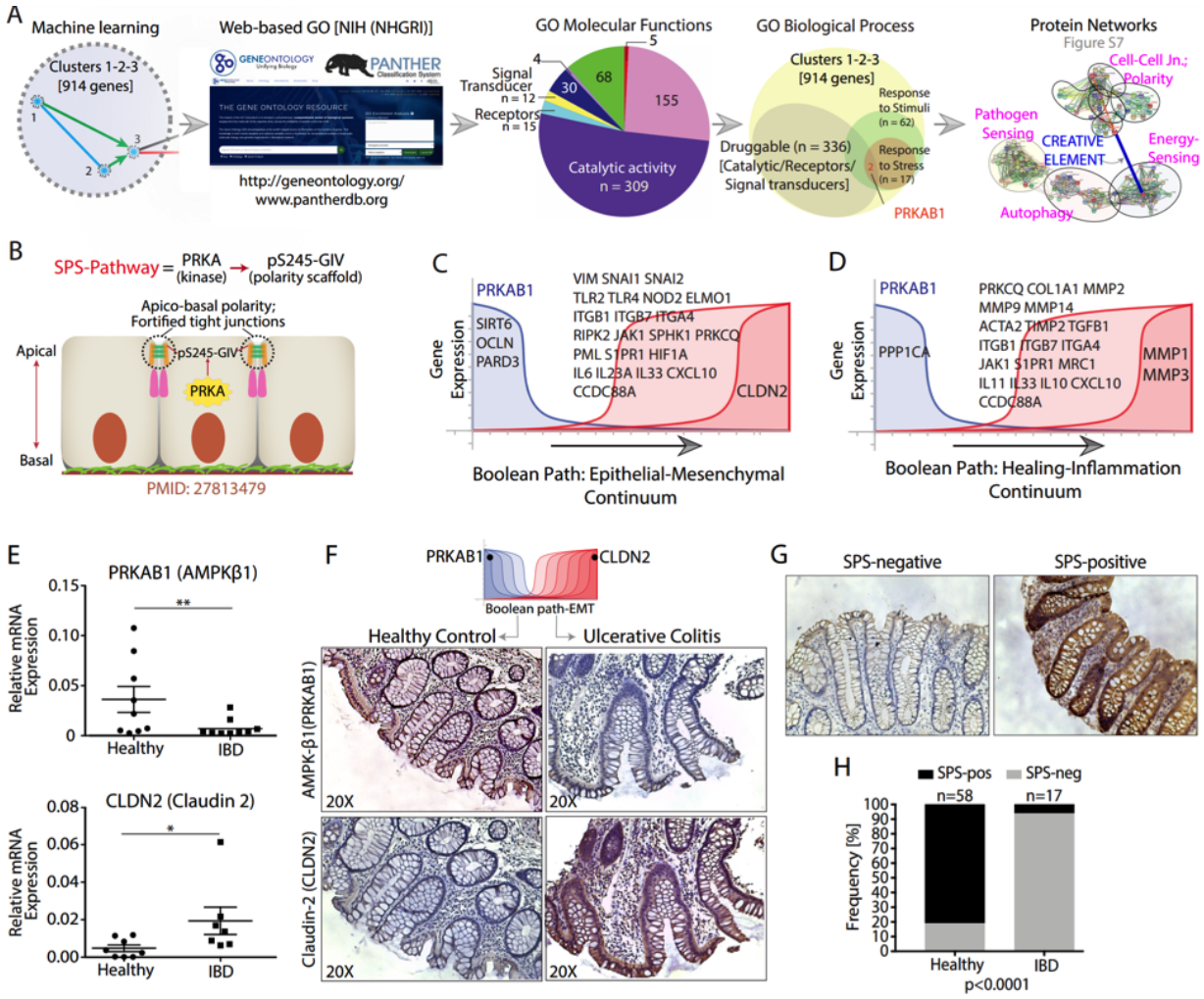

Figure 3.3: Identification of PRKAB1 as a therapeutic target to promote intestinal barrier function. (A) Computational workflow for identification of PRKAB1 as a druggable target for promoting a barrier protective transcriptional program within the IBD network. (B) Schematic summarizing key components of the SPS-pathway used in fortifying tight junctions and promoting apical-basal polarity. (C-D) Detailed view of two prominent disease paths identifying down regulation of PRKAB1 as a shared early event in IBD pathogenesis. (E) Scatter plots of PRKAB1 and CLDN2 transcript levels (qPCR) from colon biopsies of IBD patients or healthy controls. Scatter plots show mean S.E.M. and two-tailed Mann-Whitney test using p=0.05 cutoff was used to calculate significance. (F) IHC of IBD patient colon biopsies assessed for expression of PRKAB1 and CLDN2. Representative images are shown (Expanded selection of IHC in Figure3-S4). (G) Activation status of SPS-pathway was analyzed in FFPE colon biopsies from UC/CD patients using an anti-pS245-GIV antibody. Representative images are shown. (H) Bar graphs showing frequency of SPS pathway activation in healthy vs. IBD patients. Two-sided Fisher's exact test was used to calculate significance.

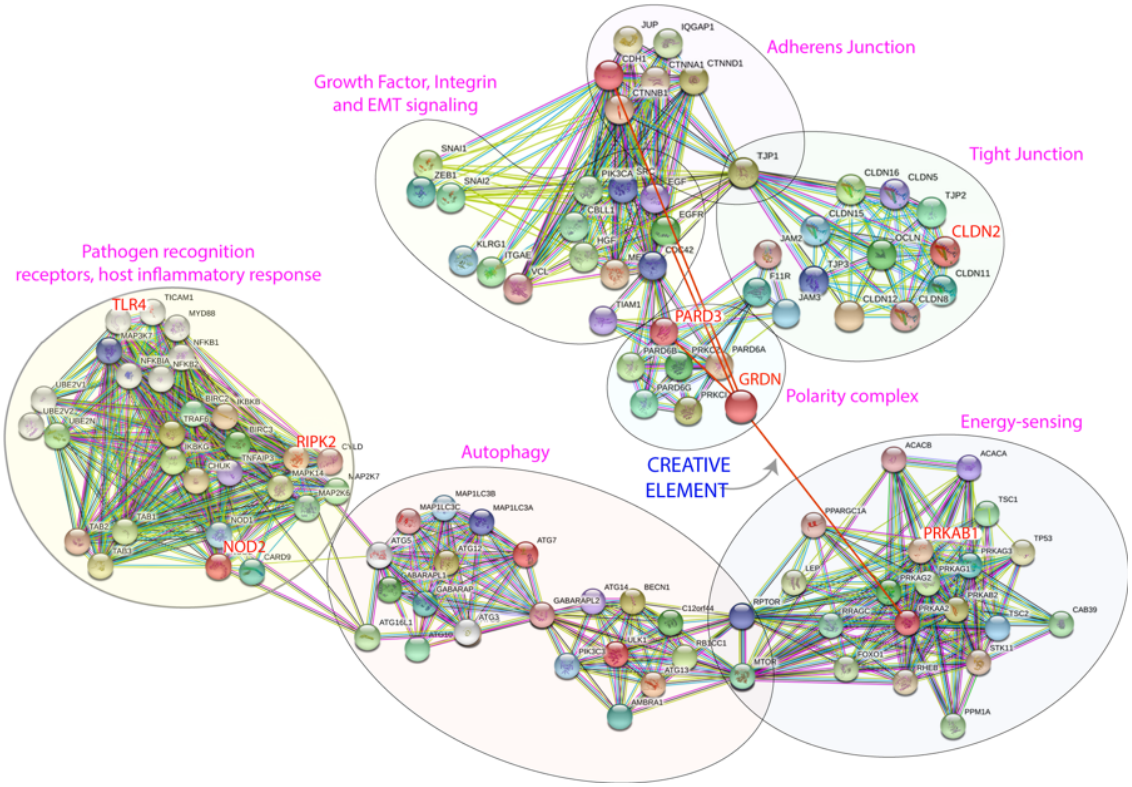

Figure 3.4: Protein-protein interaction network reveals that the stress-polarity signaling (SPS)-pathway is a creative element within that network:Protein-protein interaction (PPI) network built using STRING software (https://string-db.org/) shows the major modules and inter-module links between pathogen-sensing pathways (left most) to epithelial cell-cell adhesions (top right). A stress polarity signaling (SPS) pathway which involves the phosphorylation of the polarity scaffold, Girdin (GRDN), by the metabolic kinase AMPK (of which PRKAB1 is a subunit) has been described as both necessary and sufficient for the strengthening of epithelial junctions under bioenergetic stress (Aznar et al., 2016). Because this event is triggered exclusively as a stress response and helps connect distinct modules of PPI, it fulfills the criteria of “creative elements” within this network (Csermely, 2008).

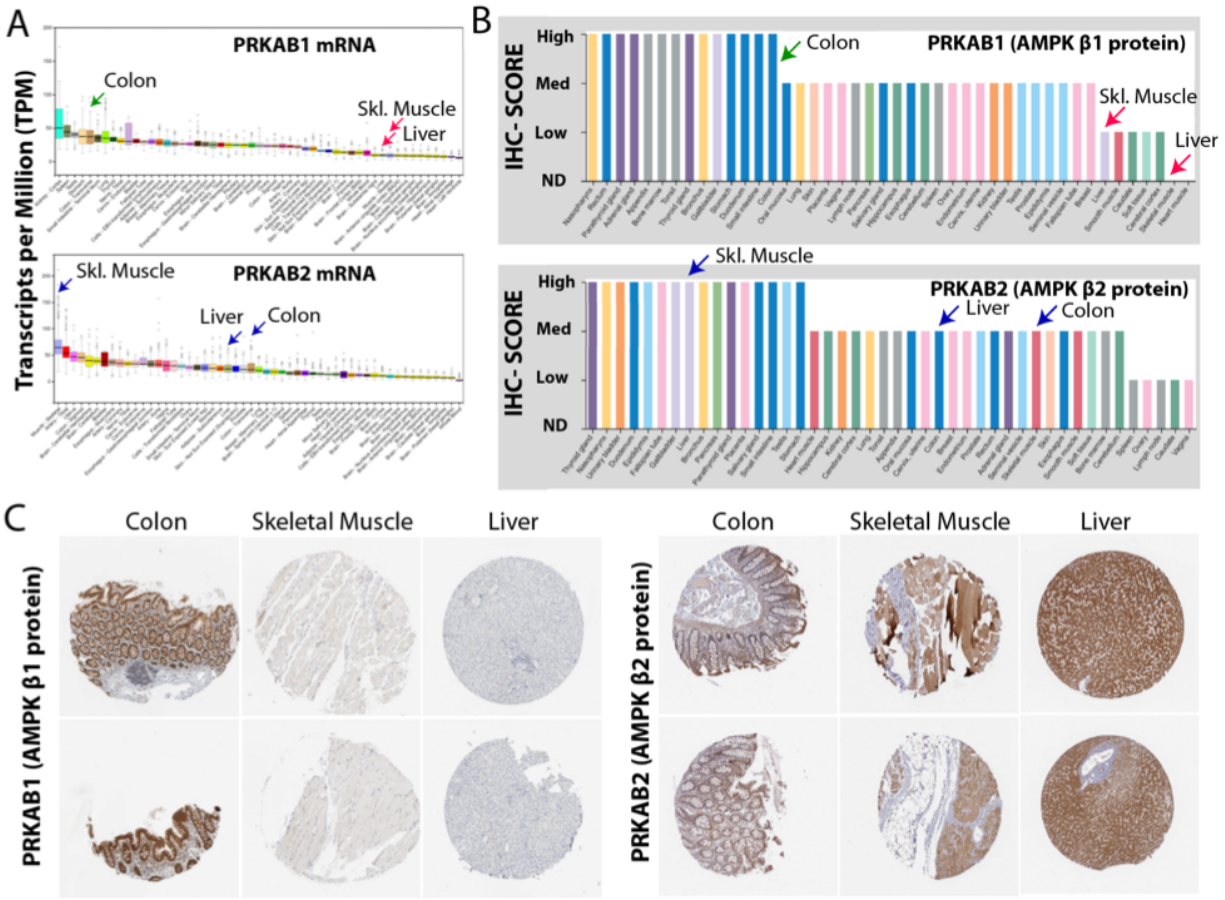

Figure 3.5: (A) Boxplots showing PRKAB1 subunit of AMPK mRNA is expressed at high levels in the colon (green arrow), but low levels in liver and skeletal muscle(red arrows), where PRKAB2 subunit is expressed in all three tissues with highest expression in skeletal muscle (blue arrows). (B) Bar graph summarizing protein expression data determined by IHC on colon biopsies. PRKAB1 is highly expressed in the colon (green arrow) compared to liver and skeletal muscle (red arrows) compared to PRKAB2, which shows no preferential expression between tissues (blue arrow). (C) Representative tissue IHC images used for protein expression analysis. All data curated from Human Protein Atlas (www.proteinatlas.org).

Figure 3.6: IHC of FFPE colon biopsies and colon-derived proteomics analysis confirms Boolean relationships of PRKAB1 at the protein level: (A) Expression of PRKAB1 and CLDN2 analyzed by IHC on FFPE IBD patient colon biopsies from various stages of disease severity. (B) Proteomic datasets (Bennike et al., 2015) from healthy and UC patients were analyzed for PRKAB1 expression. Samples were sub-divided into PRKAB1 high vs. low and assessed for expression of the TJ protein occludin. Claudin-2 peptides were not detected reliably in this study, and hence, not analyzed. Data displayed as scatter plots showing mean S.E.M. and one-way ANOVA using Tukey's multiple comparisons test and p0.05 cutoff was used to determine significance.

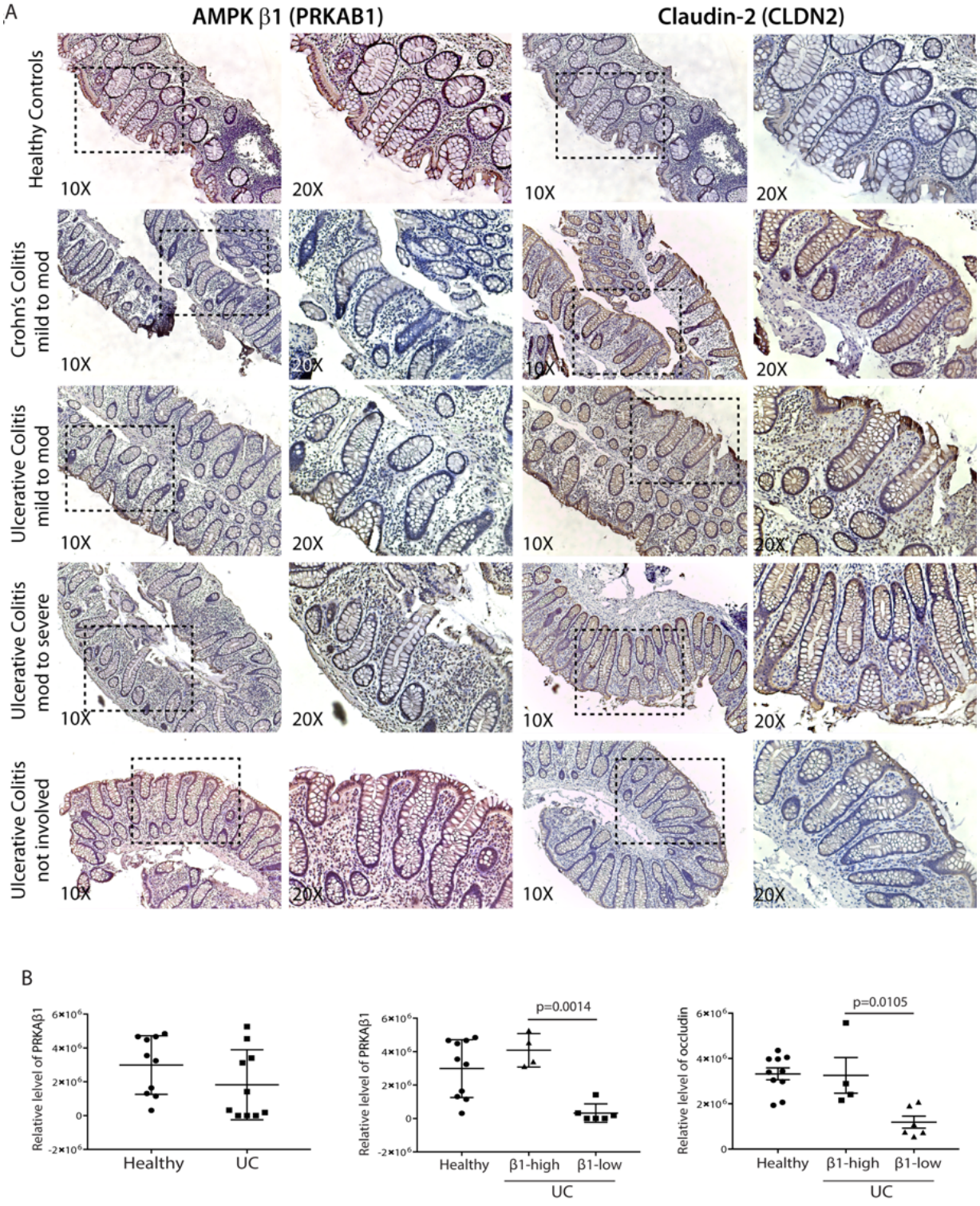
A
AMPK β1 (PRKAB1)
Claudin-2 (CLDN2)
Healthy Controls
Crohn's Colitis mild to mod
Ulcerative Colitis mild to mod
Ulcerative Colitis mod to severe
Ulcerative Colitis not involved
10X
20X
B
Relative lelvel of PRKAβ1
Healthy
UC
p=0.0014
β1-high
β1-low
Relative lelvel of occludin
p=0.0105

Figure 3.7: PRKAB1 specific agonists protect the gut barrier against DSS-induced colitis and microbe-mediated junctional collapse. (A) Table summarizing ROC/AUC analysis of various mouse models of colitis for their ability to model gut barrier defect transcript signature identified in C1-C3 of the Boolean network. Bulk = whole distal colon; epi = sorted epithelial cells. (B) Schematic outlining experimental design of DSS colitis model used to test the efficacy of PRKAB1 agonist PF-06409577. (C) Line graph showing body weight change monitored daily during the course of acute DSS colitis. (D) Line graph of disease activity index (DAI) using stool consistency (0-4), rectal bleeding (0-4), and weight loss (0-4) as scoring criteria. (E) Representative images of colon tissue stained with HE or immunostained for activation of SPS-pathway (pS245 GIV). (F) Scatter plot of histomorphological evaluation of inflammation by HE stained colon tissues using inflammatory cell infiltrate (1-3), and epithelial architecture (1-3) as scoring criteria. (G) Scatter plot of colon length assessed at d9 of DSS experiment. (H) Schematic of the stem cell based organoid model and the generation of differentiated enteroid-derived monolayers (EDMs) for co-culture studies with microbes. (I) Bar graph showing change in TEER in EDMs pre-treated with PF-06409577 after exposure to adherent invasive E. coli (AIEC; LF-82 strain) for 8 h. (J) Bar graph quantifying frequency of burst tight-junctions (fluorescent microscopy for occluding) observed in EDMs treated as in (I). Quantification was done on 3 randomly chosen fields in each of three independent experiments. All data displayed as mean S.E.M. and one-way ANOVA using Tukey's multiple comparisons test and p0.05 cutoff was used to determine significance; *; p0.05, **; p0.01, ***; p0.001, ****; p0.0001.

A

Datasets of Mouse Models of Colitis [ROC AUC]	Chemical		Infectious	T cell-mediated	Genetic		
	DSS	TNBS	Citrobacter	T-cell transfer (ACT)	IL10-/-	TNFR1	TNFR2
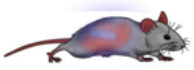	GSE42768 [0.90- bulk] E-MTAB-5249 [1.00 - epi]	GSE53835 [0.97]	GSE90577 [0.85]	GSE87317 [0.88] GSE27302 [1.00]	GSE39859 [0.87- epi; 0.62 - bulk]	GSE107933 [0.67]	GSE65408 [0.33]
	Fig S13	Fig S14	Fig S15	Fig S16	Fig S17	Fig S18	Fig S19

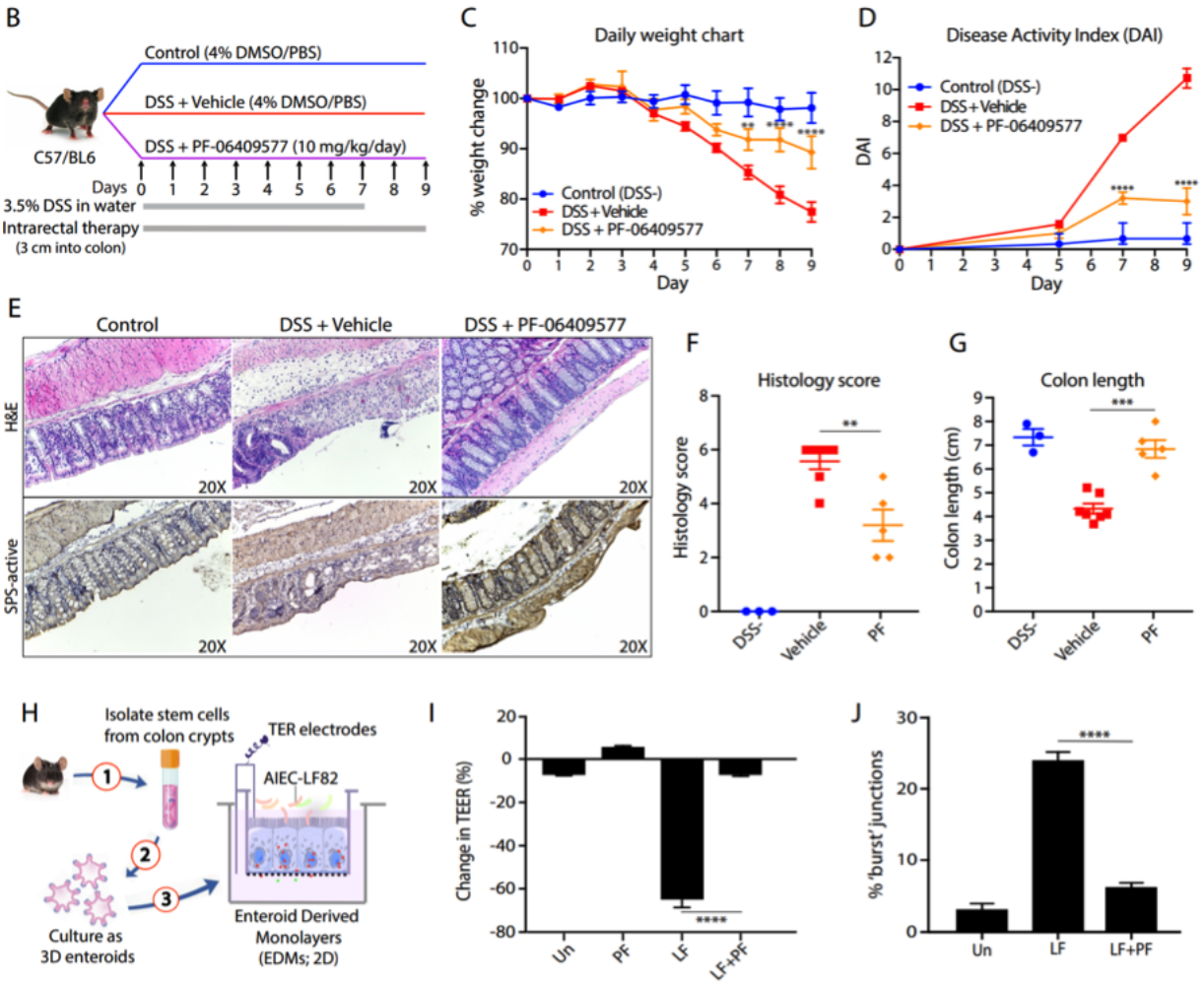

Figure 3.8: Extended dataset demonstrating the efficacy of 1-selective AMPK agonists in an acute DSS colitis: (A) Schematic outlining experimental design of DSS colitis model used to test efficacy of PRKAB1 agonists. (B) Line graph showing body weight change monitored daily during acute DSS colitis. (C) Scatter plot showing maximum weight loss (observed on d9) in DSS experiment. (D) Line graph of disease activity index (DAI) scored using stool consistency (0-4), rectal bleeding (0-4), and weight loss (0-4). (E) Scatter plot of colon length assessed at d9 of DSS experiment. (F) Scatter plot of histomorphological evaluation of inflammation by hematoxylin and eosin (HE) stained colon tissues using inflammatory cell infiltrate (1-3), and epithelial architecture (1-3) as scoring criteria. (G) Representative images of colon tissue stained with HE, or immunostained for activation of SPS-pathway (pS245 GIV) or upregulation of Claudin-2. Tissues were also stained to assess goblet cells loss (PAS staining) and fibrotic collagen deposition (Trichrome stain). All data shown as mean S.E.M. and one (C, E, F) or two-way (B, D) ANOVA using Tukey's multiple comparisons test and p 0.05 cutoff was used to determine significance;(*; p 0.05, **; p 0.01, ***; p 0.001, ****; p 0.0001).

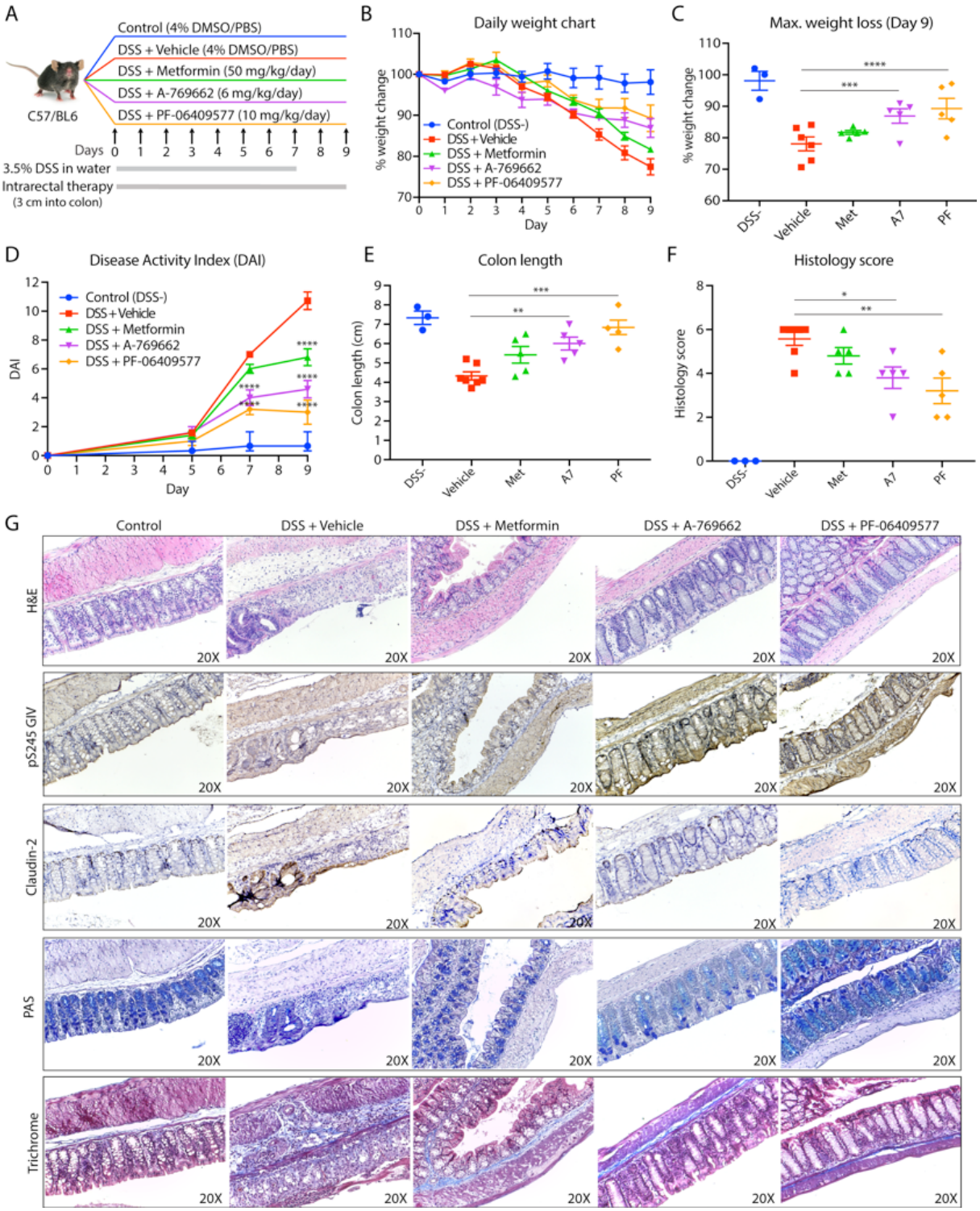
A
Control (4% DMSO/PBS)
DSS + Vehicle (4% DMSO/PBS)
DSS + Metformin (50 mg/kg/day)
DSS + A-769662 (6 mg/kg/day)
DSS + PF-06409577 (10 mg/kg/day)
C57/BL6
Days 0 1 2 3 4 5 6 7 8 9
3.5% DSS in water
Intrarectal therapy
(3 cm into colon)
B
Daily weight chart
% weight change
Control (DSS-)
DSS + Vehicle
DSS + Metformin
DSS + A-769662
DSS + PF-06409577
Day
C
Max. weight loss (Day 9)
% weight change
DSS-
Vehicle
Met
A7
PF
D
Disease Activity Index (DAI)
DAI
Day
E
Colon length
Colon length (cm)
F
Histology score
Histology score
G
Control
DSS + Vehicle
DSS + Metformin
DSS + A-769662
DSS + PF-06409577
H&E
pS245 GIV
Claudin-2
PAS
Trichrome
20X

Figure 3.9: Murine colon-derived organoid monolayers confirm that pharmacologic activation of PRKAB1 protects the epithelial barrier by IBD-associated microbes: (A) Schematic of the stem cell-based organoid model and generation of enteroid-derived monolayers (EDMs). (B) Immunoblots of 3D enteroid whole cell lysates isolated from WT or AMPK KO mice treated with pharmacologic agonists of AMPK for 4 h (1 mM Metformin; 100 μM A-769662; 1 μM PF-06409557). (C) Line graph showing TEER kinetics over 24 h of WT or AMPKα1/2-/- EDM pre-treated or not with PF for 16 h. Black asterisks (*) = WT vs. AMPK KO comparisons; red asterisks (*) = untreated vs. PF pre-treatment. (D) EDMs treated as in (C) were assessed for TJ integrity (occludin) and SPS-pathway activation (pS245 GIV) using confocal microscopy at 24h. (E) ROC/AUC plots rationalizing the use of monolayer-microbe co-culture systems to model pathologic shifts. (F) EDMs pre-treated with indicated AMPK agonists for 16 h were assessed for TJ integrity (occludin) and SPS-pathway activation (pS245 GIV) after exposure to adherent invasive E. coli (AIEC-LF82 strain) for 8h using confocal microscopy. (G-H) Bar graphs showing change in TEER in EDMs pre-treated with indicated AMPK agonists [Met = metformin. A7 = A-769662; PF = PF-06409557] and subsequently exposed to adherent invasive E. coli (AIEC-LF82 strain) (G), or LPS (H) at 8 h post-infection. (I) Bar graph quantifying frequency of burst TJs observed in EDMs treated as in (F). Quantification was done on 3 randomly chosen fields in each of three independent experiments. All data displayed as mean S.E.M. and one-way ANOVA using Tukey's multiple comparisons test and p 0.05 cutoff was used to determine significance; *, p 0.05; **, p 0.01; ****, p 0.0001.

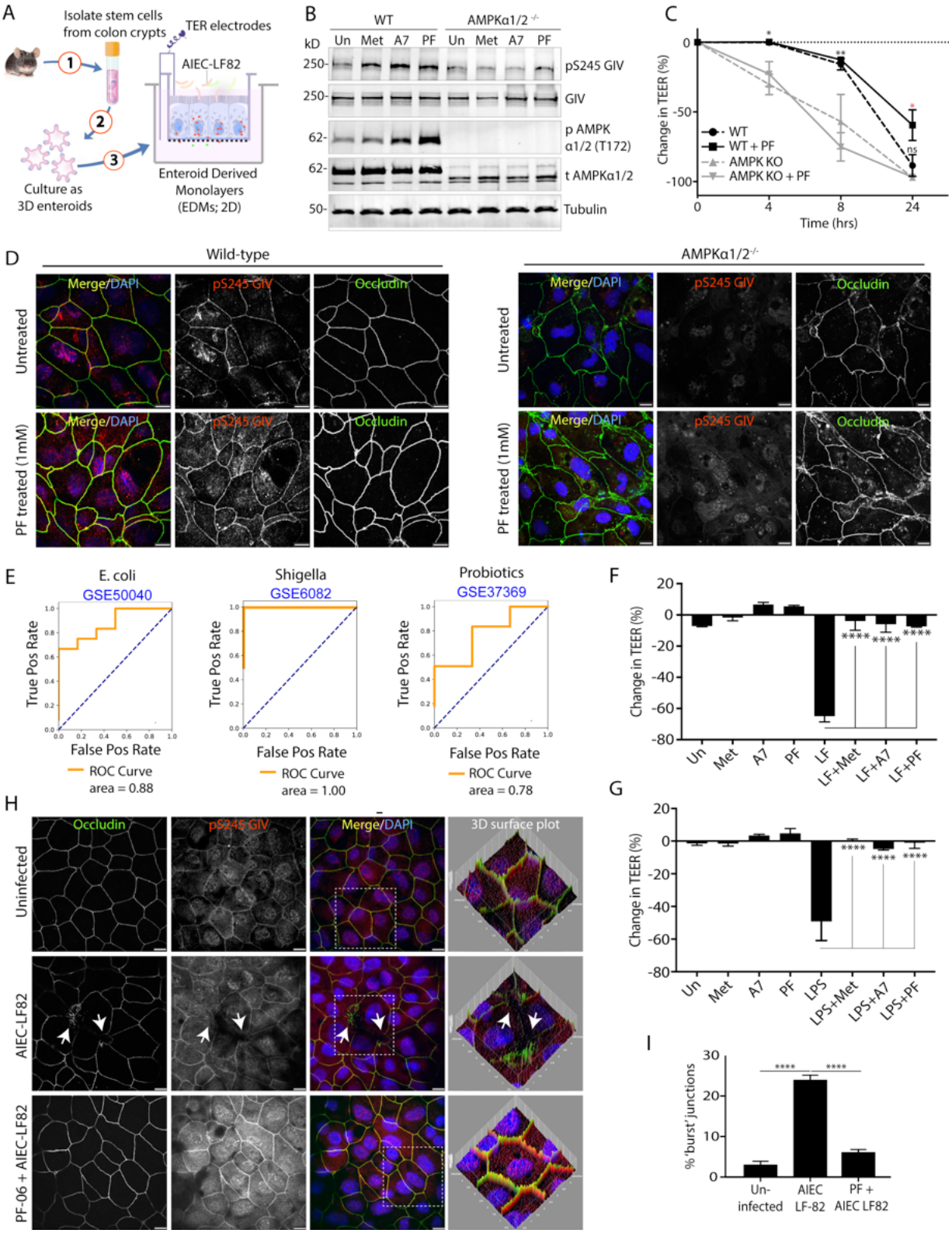
A
Isolate stem cells from colon crypts
TER electrodes
AIEC-LF82
Culture as 3D enteroids
Enteroid Derived Monolayers (EDMs; 2D)
B
WT
AMPKα1/2 -/-
kD
Un Met A7 PF Un Met A7 PF
250-
pS245 GIV
GIV
p AMPK α1/2 (T172)
62-
t AMPKα1/2
50-
Tubulin
C
Change in TEER (%)
WT
WT + PF
AMPK KO
AMPK KO + PF
Time (hrs)
D
Wild-type
AMPKα1/2 -/-
Untreated
PF treated (1mM)
Merge/DAPI
pS245 GIV
Occludin
E
E. coli
GSE50040
Shigella
GSE6082
Probiotics
GSE37369
True Pos Rate
False Pos Rate
ROC Curve
area = 0.88
area = 1.00
area = 0.78
F
Change in TEER (%)
Un Met A7 PF LF LF+Met LF+A7 LF+PF
G
Change in TEER (%)
Un Met A7 PF LPS LPS+Met LPS+A7 LPS+PF
H
Uninfected
AIEC-LF82
PF-06 + AIEC-LF82
3D surface plot
I
% 'burst' junctions
Un-infected
AIEC LF-82
PF + AIEC LF82

Figure 3.10: PRKAB1 agonist PF-06409577 restores and protects the epithelial barrier in diseased human organoids. (A) Light micrographs of 3D enteroids (left column), brightfield micrographs of 2D enteroids (center column), and immunofluorescent micrographs of the TJ marker ZO-1 on 2D enteroids (right column) isolated from healthy human colons or from colons of actively inflamed UC and CD patients. White arrowheads identify disrupted TJs. (B) Bar graph showing quantification of disrupted tri-cellular tight-junctions (TTJs) of healthy (n=2), UC (n=2), and CD (n=3) patient derived EDMs. (C) Bar graph of absolute TEER values of UC and CD EDMs. (D-F) Immunofluorescent micrographs (D), bar graph of quantification of TTJ disruption (E), and bar graph showing change in TEER (F) in UC patient EDMs treated, or not, with PF-06409577 (PF) for 16h. (G) Bar graph showing change in TEER in UC patient EDMs treated, or not, with PF and exposed to LF-82 for 8h. (H-J) Immunofluorescent micrographs (H), bar graph showing quantification of TTJ disruption (I), and bar graph showing change in TEER (J) in CD patient EDMs treated, or not, with PF for 16h. (K) Bar graph showing change in TEER in CD patient EDMs treated, or not, with PF and exposed to LF-82 for 8h. For UC and CD patient experiments, frequency of disrupted TJs was calculated from 3 randomly chosen fields. All TEER results were from 3 independent experiments. All data shown as mean S.E.M. and one-way ANOVA using Tukey's multiple comparisons test and p0.05 cutoff was used to determine significance;(*; p0.05, **; p0.01, ***; p0.001, ****; p0.0001).

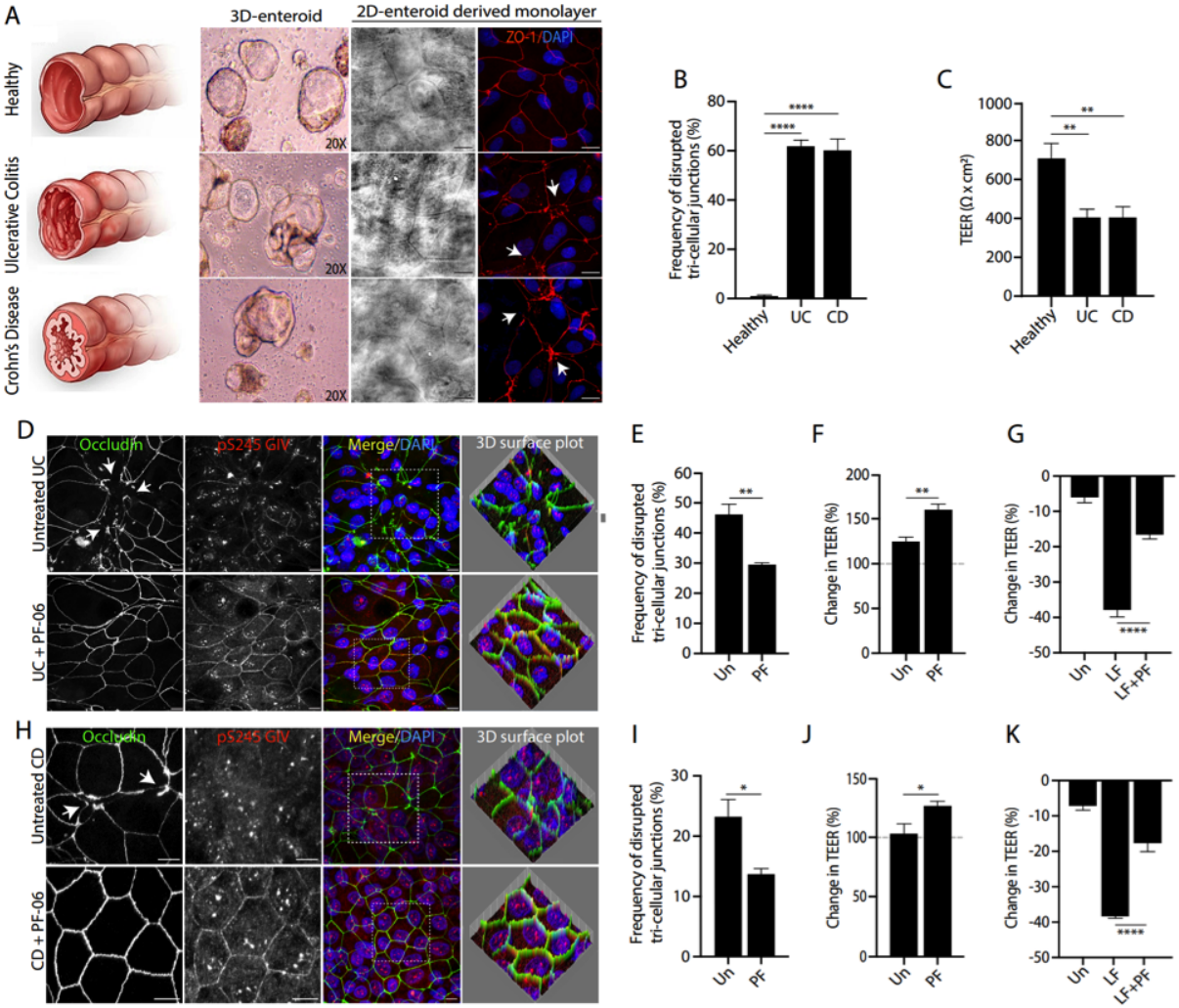
A
3D-enteroid
2D-enteroid derived monolayer
Healthy
Ulcerative Colitis
Crohn's Disease
ZO-1/DAPI
20X
B
Frequency of disrupted tri-cellular junctions (%)
Healthy
UC
CD
C
TEER (Ω x cm²)
D
Occludin
pS245 GIV
Merge/DAPI
3D surface plot
Untreated UC
UC + PF-06
E
F
G
Change in TEER (%)
Un
PF
LF
LF+PF
H
Untreated CD
CD + PF-06
I
J
K

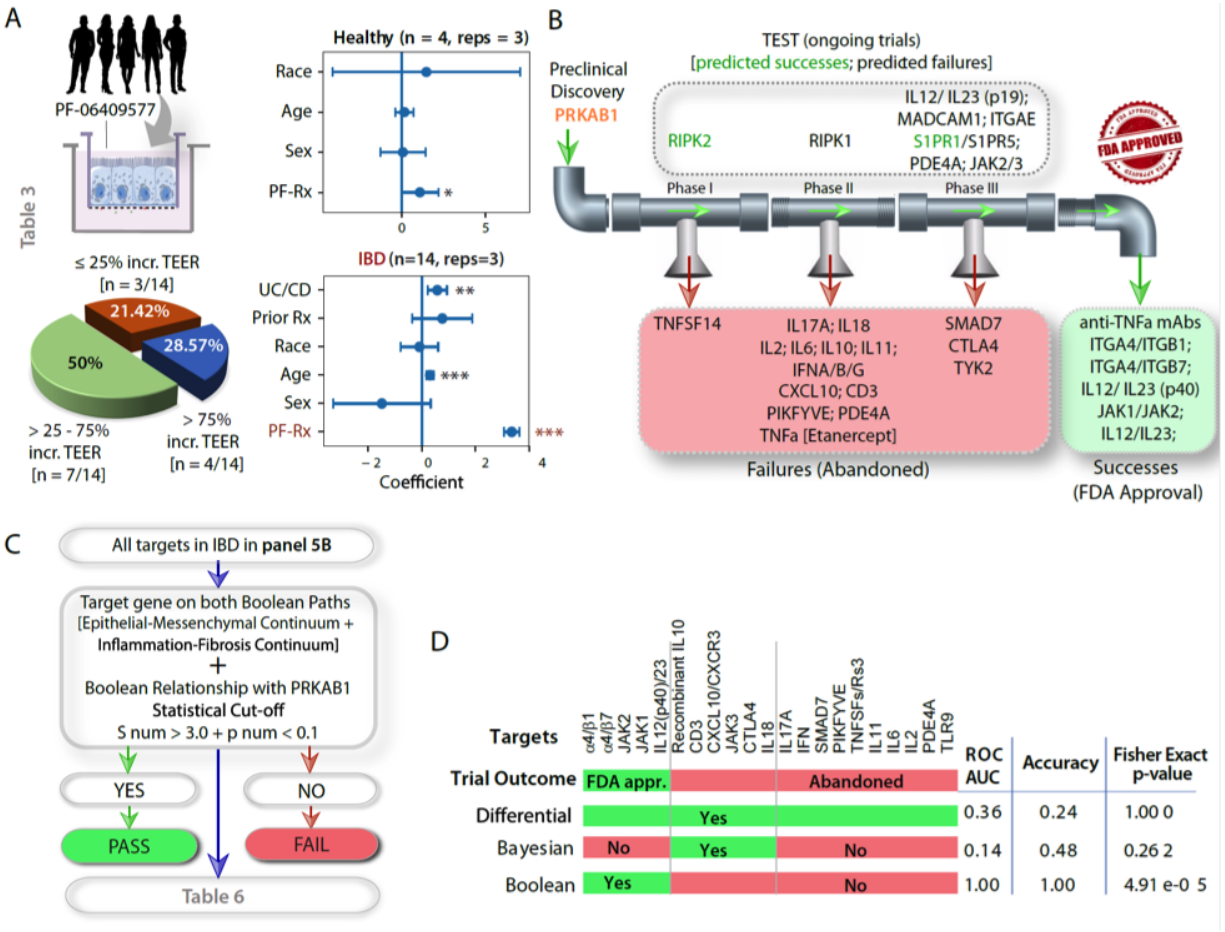

Figure 3.11: Diseased organoids and the Boolean Network Explorer predict clinical therapeutic efficacy in humans. (A) Left top: Enteroid monolayers from healthy and IBD-afflicted patients were treated with PRKAB1-agonist PF-06409577 (PF-Rx) and assessed for therapeutic response, i.e., >25% increase in TEER. Left bottom: Pie chart showing the fraction of IBD-derived EDMs in each category of response. Right. Multivariate analysis models the TEER measurement before the treatment as a linear combination of TEER measurement after treatment, age, gender, race, treatment history. Coefficient of each variables with 95% confidence intervals. n = number of patients; reps = average number of repeat TEER measurements/patient; *, p0.05; **, p0.01; ***, p0.001; ****, p0.0001. (B) Drug targets arranged by their status in clinical trials. Ongoing trials (top); Abandoned trials (red box); FDA-approved drugs that are considered a success (green box). (C) Computational steps for prediction of success and failure. The targets are checked for consistency in both Epithelial-Mesenchymal and inflammation-fibrosis Boolean paths and a strong PRKAB1 high $\implies$ X low Boolean implication relationship ($S > 3$, $p < 0.1$). (D) Prediction of outcomes in clinical trials by Boolean analysis compared to Differential and Bayesian analyses.

Chapter 4

Conclusion: New insights into regulation of inflammatory responses and treatment of inflammatory diseases.

The immune system is a complex network composed of many cell types positioned throughout the body with the collective goal of maintaining homeostasis and protecting against infection. Decades of research has identified many subsets of immune cells, and the various mechanisms they employ to defend the body. These discoveries have translated into revolutionary therapeutics that modulate immune function and have transformed the way we think about modern medicine. However, our understanding of the complex regulatory mechanisms that control immune responses is still far from complete. My dissertation work has focused on the

discovery and characterization of two novel regulatory mechanisms for immune function, and their potential as therapeutic targets in the treatment of inflammatory and infectious disease. In this remainder of this section I will discuss how each of these discoveries have advanced the field of immune regulation, their impact on targeting the immune system therapeutically, and potential future directions for the work.

4.1 GIV, a new player in the field of immune regulation

The bulk of my dissertation work was dedicated to the characterization of GIV as a negative regulator of TLR4 signaling and its impact on macrophage inflammatory responses. Before I joined the Ghosh Lab, nearly a decade of research on guanine nucleotide exchange modulators (GEMs) had established the ability of GIV, the prototypical member of the GEM family, to act as a central hub of signal transduction downstream of a variety of cell surface receptors. All GEMs have two critical features; 1) a GEM motif that allows the binding and modulation of G-protein activity, and 2) a series of short-linear interaction motifs (SLIMs) within its C-terminus that facilitate the binding to various cell surface receptors. These two features give GEMs the unique ability to link G-protein signaling to a diverse array of receptors, not just G-protein coupled receptors (GPCRs). The impact of this signaling paradigm has been explored in a wide range of biological processes and its dysregulation is associated with the pathogenesis of a number of diseases, many of which have an inflammatory component (i.e. liver fibrosis, diabetes, and cancer). However, the role of GEMs in modulating inflammatory signaling pathways and their impact on immune function had not been investigated.

My work has identified GIV as a novel regulator of macrophage inflammatory responses through its ability to interact with TLR4 using a putative TIR-like loop motif within its C-terminus.

Binding of GIV to TLR4 has two effects on TLR4 signaling; 1) recruitment of G-proteins to TLR4 receptor tail and subsequent modulation of cAMP levels during LPS stimulation, and 2) inhibition of TLR4 homodimerization and/or TIR-adaptor recruitment potentially through competition for shared binding interfaces. The consequence of both of these processes is negative regulation of TLR4 signaling and pro-inflammatory responses in macrophages. However, we have not yet identified the contributions of each of these mechanisms on the modulation of macrophage inflammatory responses. Future work using mutations in GIV that selectively ablate the G-protein modulation function or TLR4 binding ability of GIV will allow us to dissect these mechanisms in more detail. Another future direction is determining the spatial and temporal dynamics of GIV-mediated regulation of TLR4 signaling. We know that GIV can interact with TLR4 under resting conditions but have not conducted experiments to assess if GIV dissociates from TLR4 upon LPS stimulation to accommodate TLR4 homodimerization and TIR-adaptor recruitment. Another area of interest is the role of GIV in other immune cell types. I found that GIV is expressed in a number of immune cells including dendritic cells, neutrophils, and B-cells, but its function is still unexplored. Understanding the conserved, and divergent, mechanisms of immune regulation across cells types will be critical for a full understanding of GIV's role in regulating immune function.

My work has also demonstrated the importance of GIV's function in macrophages during inflammation driven disease using animal models of acute sepsis and inflammatory bowel disease. In both cases, selective depletion of GIV from myeloid cells exacerbates disease, likely through increased sensitivity of macrophage inflammatory responses to microbial antigens. However, we have not fully explored the cellular mechanisms responsible for these observations. Future studies will investigate GIV's role in microbial clearance during infection,

macrophage chemotaxis, macrophage polarization state, and transition to the resolution/healing phase of an inflammatory response. It is also likely that GIV-dependent macrophage regulation impacts a number of other inflammatory diseases and ongoing studies in the lab are now exploring GIV's role in arthritis, liver fibrosis, and cancer progression. I have also provided initial proof-of-principle studies for therapeutically targeting GIV to correct pathogenic inflammation in macrophages. Using a cell-penetrable peptide (CPPs) designed to mimic GIV's TIR-like loop (TILL) module, I was able to reduce inflammatory cytokine production in macrophages stimulated with LPS. Ongoing studies in the lab are now testing GIV-TILL CPPs as a therapeutic intervention in animal models of inflammatory disease.

Overall, my work has defined a new player in immune regulation and inflammatory disease. As the first body of work to characterize the function of GEMs in the immune system I feel that I have managed to open more doors than I was able to close, and that we have only begun to realize the importance of GEMs in immune function. It is my hope that this dissertation work will lay the foundation for future studies that can add to our understanding of GEMs in immunobiology and harness this knowledge to develop new therapeutic approaches for inflammatory diseases.

4.2 Changing the game in therapeutic target identification for inflammatory bowel disease

Another part of my dissertation work was the development and validation of a new drug discovery platform using computational networks based on Boolean logic principles. This was a highly collaborative effort that combined expertise in computational modeling (Sahoo Lab),

organoid cell culture systems (Das Lab), and therapeutic targeting of signaling pathways (Ghosh Lab) to identify and validate new treatment strategies for inflammatory bowel disease (IBD). Together, we were able to model the continuum of transcriptional changes that occur in the gut during the development and progression of IBD, identify key processes/targets in this progression, and validate these targets in vitro and in vivo using both mouse and human model systems. This strategy yielded a number of novel therapeutic targets predicted to improve impaired gut barrier function, a main driver of disease initiation and propagation in IBD. My contribution was to help identify potential targets of interest, determine potential mechanisms of action, and validate these targets experimentally using mouse models of IBD and organoid cell culture models derived from IBD patients. We found that pharmacologic activation of the beta-subunit of AMPK (PRKAB1) improved gut barrier function through activation of a stress-polarity pathway that bolsters tight-junction integrity in the intestinal epithelium. We were able to demonstrate that activation of this pathway was not only able to prevent loss of barrier function during microbial infection and chemically induced colitis models, but was also able to repair disrupted tight-junctions in IBD patient-derived organoids. Going forward, we hope to translate these proof-of-principle studies into IBD therapeutics that target PRKAB1.

Although this initial work focused on developing barrier protective therapeutics for IBD, the implications for rational drug discovery using Boolean powered disease networks are far-reaching. Most chronic diseases arise through progressive changes in genetic sequence (mutations), transcriptional landscape, and cellular function that ultimately result in disease. Understanding how and when these steps occur and the critical nodes that connect these steps will allow us to design therapies that target the disease at its weakest points. Ongoing work in the collaboration aims to model disease progression in a number of diseases including arthritis,

Alzheimer's disease, liver disease, and various cancers. I look forward to seeing this initiative progress and bring new therapeutics for these challenging diseases to the clinic.

4.3 Final thoughts

Through my dissertation work I have had the opportunity to learn and grow as a scientist while making contributions to the fields of immunobiology and therapeutic drug discovery. It is my hope that my contributions can lay the groundwork for future studies investigating the role of GEMs in immune regulation and will lead to therapeutics that can help patients suffering from inflammatory diseases.

Bibliography

ABAGYAN, R., BATALOV, S., CARDOZO, T., TOTROV, M., WEBBER, J. & ZHOU, Y. 1997. Homology modeling with internal coordinate mechanics: deformation zone mapping and improvements of models via conformational search. *Proteins,* Suppl 1**,** 29-37.

ABAGYAN, R. & TOTROV, M. 1994. Biased probability Monte Carlo conformational searches and electrostatic calculations for peptides and proteins. *J Mol Biol,* 235**,** 983-1002.

ABRAHAM, C. & CHO, J. H. 2009. Inflammatory bowel disease. *N Engl J Med,* 361**,** 2066-78.

AHLUWALIA, J. P. 2012. Immunotherapy in inflammatory bowel disease. *Med Clin North Am,* 96**,** 525-44, x.

ARIJS, I., DE HERTOGH, G., LEMAIRE, K., QUINTENS, R., VAN LOMMEL, L., VAN STEEN, K., LEEMANS, P., CLEYNEN, I., VAN ASSCHE, G., VERMEIRE, S., GEBOES, K., SCHUIT, F. & RUTGEERTS, P. 2009. Mucosal gene expression of antimicrobial peptides in inflammatory bowel disease before and after first infliximab treatment. *PLoS One,* 4**,** e7984.

ARIJS, I., DE HERTOGH, G., LEMMENS, B., VAN LOMMEL, L., DE BRUYN, M., VANHOVE, W., CLEYNEN, I., MACHIELS, K., FERRANTE, M., SCHUIT, F., VAN ASSCHE, G., RUTGEERTS, P. & VERMEIRE, S. 2018. Effect of vedolizumab (anti-alpha4beta7-integrin) therapy on histological healing and mucosal gene expression in patients with UC. *Gut,* 67**,** 43-52.

ARIJS, I., QUINTENS, R., VAN LOMMEL, L., VAN STEEN, K., DE HERTOGH, G., LEMAIRE, K., SCHRAENEN, A., PERRIER, C., VAN ASSCHE, G., VERMEIRE, S., GEBOES, K., SCHUIT, F. & RUTGEERTS, P. 2010. Predictive value of epithelial gene expression profiles for response to infliximab in Crohn's disease. *Inflamm Bowel Dis,* 16**,** 2090-8.

ASAI, M., ASAI, N., MURATA, A., YOKOTA, H., OHMORI, K., MII, S., ENOMOTO, A., MURAKUMO, Y. & TAKAHASHI, M. 2012. Similar phenotypes of Girdin germ-line and conditional knockout mice indicate a crucial role for Girdin in the nestin lineage. *Biochem Biophys Res Commun,* 426**,** 533-8.

AZNAR, N., PATEL, A., ROHENA, C. C., DUNKEL, Y., JOOSEN, L. P., TAUPIN, V., KUFAREVA, I., FARQUHAR, M. G. & GHOSH, P. 2016. AMP-activated protein kinase fortifies epithelial tight junctions during energetic stress via its effector GIV/Girdin. *Elife,* 5.

BARABASI, A. L., GULBAHCE, N. & LOSCALZO, J. 2011. Network medicine: a network-based approach to human disease. *Nat Rev Genet,* 12**,** 56-68.

BARRETT, T., TROUP, D. B., WILHITE, S. E., LEDOUX, P., RUDNEV, D., EVANGELISTA, C., KIM, I. F., SOBOLEVA, A., TOMASHEVSKY, M. & EDGAR, R. 2007. NCBI GEO: mining tens of millions of expression profiles--database and tools update. *Nucleic Acids Res,* 35**,** D760-5.

BARRETT, T., WILHITE, S. E., LEDOUX, P., EVANGELISTA, C., KIM, I. F., TOMASHEVSKY, M., MARSHALL, K. A., PHILLIPPY, K. H., SHERMAN, P. M., HOLKO, M., YEFANOV, A., LEE, H., ZHANG, N., ROBERTSON, C. L., SEROVA, N., DAVIS, S. & SOBOLEVA, A. 2013. NCBI GEO: archive for functional genomics data sets--update. *Nucleic Acids Res,* 41**,** D991-5.

BEAS, A. O., TAUPIN, V., TEODOROF, C., NGUYEN, L. T., GARCIA-MARCOS, M. & FARQUHAR, M. G. 2012. Gαs promotes EEA1 endosome maturation and shuts down proliferative signaling through interaction with GIV (Girdin). *Mol Biol Cell.*

BENNIKE, T. B., CARLSEN, T. G., ELLINGSEN, T., BONDERUP, O. K., GLERUP, H., BOGSTED, M., CHRISTIANSEN, G., BIRKELUND, S., STENSBALLE, A. & ANDERSEN, V. 2015. Neutrophil Extracellular Traps in Ulcerative Colitis: A Proteome Analysis of Intestinal Biopsies. *Inflamm Bowel Dis,* 21**,** 2052-67.

BEYER, M., MALLMANN, M. R., XUE, J., STARATSCHEK-JOX, A., VORHOLT, D., KREBS, W., SOMMER, D., SANDER, J., MERTENS, C., NINO-CASTRO, A., SCHMIDT, S. V. & SCHULTZE, J. L. 2012. High-resolution transcriptome of human macrophages. *PLoS One,* 7**,** e45466.

BHANDARI, D., LOPEZ-SANCHEZ, I., TO, A., LO, I. C., AZNAR, N., LEYME, A., GUPTA, V., NIESMAN, I., MADDOX, A. L., GARCIA-MARCOS, M., FARQUHAR, M. G. & GHOSH, P. 2015. Cyclin-dependent kinase 5 activates guanine nucleotide exchange factor GIV/Girdin to orchestrate migration-proliferation dichotomy. *Proc Natl Acad Sci U S A,* 112**,** E4874-83.

BOUDEAU, J., GLASSER, A. L., MASSERET, E., JOLY, B. & DARFEUILLE-MICHAUD, A. 1999. Invasive ability of an Escherichia coli strain isolated from the ileal mucosa of a patient with Crohn's disease. *Infect Immun,* 67**,** 4499-509.

BRINT, E. K., XU, D., LIU, H., DUNNE, A., MCKENZIE, A. N., O'NEILL, L. A. & LIEW, F. Y. 2004. ST2 is an inhibitor of interleukin 1 receptor and Toll-like receptor 4 signaling and maintains endotoxin tolerance. *Nat Immunol,* 5**,** 373-9.

BUTTE, A. J. & KOHANE, I. S. 2000. Mutual information relevance networks: functional genomic clustering using pairwise entropy measurements. *Pac Symp Biocomput***,** 418-29.

CAMERON, K. O., KUNG, D. W., KALGUTKAR, A. S., KURUMBAIL, R. G., MILLER, R., SALATTO, C. T., WARD, J., WITHKA, J. M., BHATTACHARYA, S. K., BOEHM, M., BORZILLERI, K. A., BROWN, J. A., CALABRESE, M., CASPERS, N. L., COKORINOS, E., CONN, E. L., DOWLING, M. S., EDMONDS, D. J., ENG, H., FERNANDO, D. P., FRISBIE, R., HEPWORTH, D., LANDRO, J., MAO, Y., RAJAMOHAN, F., REYES, A. R., ROSE, C. R., RYDER, T., SHAVNYA, A., SMITH, A. C., TU, M., WOLFORD, A. C. & XIAO, J. 2016. Discovery and Preclinical Characterization of 6-Chloro-5-[4-(1-hydroxycyclobutyl)phenyl]-1H-indole-3-carboxylic Acid (PF-06409577), a Direct Activator of Adenosine Monophosphate-activated Protein Kinase (AMPK), for the Potential Treatment of Diabetic Nephropathy. *J Med Chem,* 59**,** 8068-81.

CARLSSON, E., DING, J. L. & BYRNE, B. 2016. SARM modulates MyD88-mediated TLR activation through BB-loop dependent TIR-TIR interactions. *Biochim Biophys Acta,* 1863**,** 244-53.

CHANG, J., LEONG, R. W., WASINGER, V. C., IP, M., YANG, M. & PHAN, T. G. 2017. Impaired Intestinal Permeability Contributes to Ongoing Bowel Symptoms in Patients With Inflammatory Bowel Disease and Mucosal Healing. *Gastroenterology,* 153**,** 723-731 e1.

CHASSAING, B., AITKEN, J. D., MALLESHAPPA, M. & VIJAY-KUMAR, M. 2014. Dextran sulfate sodium (DSS)-induced colitis in mice. *Curr Protoc Immunol,* 104**,** Unit 15 25.

CIRL, C., WIESER, A., YADAV, M., DUERR, S., SCHUBERT, S., FISCHER, H., STAPPERT, D., WANTIA, N., RODRIGUEZ, N., WAGNER, H., SVANBORG, C. & MIETHKE, T. 2008. Subversion of Toll-like receptor signaling by a unique family of bacterial Toll/interleukin-1 receptor domain-containing proteins. *Nat Med,* 14**,** 399-406.

CSERMELY, P. 2008. Creative elements: network-based predictions of active centres in proteins and cellular and social networks. *Trends Biochem Sci,* 33**,** 569-76.

D'INCA, R., DI LEO, V., CORRAO, G., MARTINES, D., D'ODORICO, A., MESTRINER, C., VENTURI, C., LONGO, G. & STURNIOLO, G. C. 1999. Intestinal permeability test as a predictor of clinical course in Crohn's disease. *Am J Gastroenterol,* 94**,** 2956-60.

DALERBA, P., KALISKY, T., SAHOO, D., RAJENDRAN, P. S., ROTHENBERG, M. E., LEYRAT, A. A., SIM, S., OKAMOTO, J., JOHNSTON, D. M., QIAN, D., ZABALA, M., BUENO, J., NEFF, N. F., WANG, J., SHELTON, A. A., VISSER, B., HISAMORI, S., SHIMONO, Y., VAN DE WETERING, M., CLEVERS, H., CLARKE, M. F. & QUAKE, S. R. 2011. Single-cell dissection of transcriptional heterogeneity in human colon tumors. *Nat Biotechnol,* 29**,** 1120-7.

DALERBA, P., SAHOO, D., PAIK, S., GUO, X., YOTHERS, G., SONG, N., WILCOX-FOGEL, N., FORGO, E., RAJENDRAN, P. S., MIRANDA, S. P., HISAMORI, S., HUTCHISON, J., KALISKY, T., QIAN, D., WOLMARK, N., FISHER, G. A., VAN DE RIJN, M. & CLARKE, M. F. 2016. CDX2 as a Prognostic Biomarker in Stage II and Stage III Colon Cancer. *N Engl J Med,* 374**,** 211-22.

DARFEUILLE-MICHAUD, A., BOUDEAU, J., BULOIS, P., NEUT, C., GLASSER, A. L., BARNICH, N., BRINGER, M. A., SWIDSINSKI, A., BEAUGERIE, L. & COLOMBEL, J. F. 2004. High

prevalence of adherent-invasive Escherichia coli associated with ileal mucosa in Crohn's disease. *Gastroenterology,* 127**,** 412-21.

DAS, S., SARKAR, A., CHOUDHURY, S. S., OWEN, K. A., CASTILLO, V., FOX, S., ECKMANN, L., ELLIOTT, M. R., CASANOVA, J. E. & ERNST, P. B. 2015. ELMO1 has an essential role in the internalization of Salmonella Typhimurium into enteric macrophages that impacts disease outcome. *Cell Mol Gastroenterol Hepatol,* 1**,** 311-324.

DAUPHINEE, S. M., VOELCKER, V., TEBAYKINA, Z., WONG, F. & KARSAN, A. 2011. Heterotrimeric Gi/Go proteins modulate endothelial TLR signaling independent of the MyD88-dependent pathway. *Am J Physiol Heart Circ Physiol,* 301**,** H2246-53.

DEN HARTOG, G., CHATTOPADHYAY, R., ABLACK, A., HALL, E. H., BUTCHER, L. D., BHATTACHARYYA, A., ECKMANN, L., HARRIS, P. R., DAS, S., ERNST, P. B. & CROWE, S. E. 2016. Regulation of Rac1 and Reactive Oxygen Species Production in Response to Infection of Gastrointestinal Epithelia. *PLoS Pathog,* 12**,** e1005382.

DIVANOVIC, S., TROMPETTE, A., ATABANI, S. F., MADAN, R., GOLENBOCK, D. T., VISINTIN, A., FINBERG, R. W., TARAKHOVSKY, A., VOGEL, S. N., BELKAID, Y., KURT-JONES, E. A. & KARP, C. L. 2005. Negative regulation of Toll-like receptor 4 signaling by the Toll-like receptor homolog RP105. *Nat Immunol,* 6**,** 571-8.

DUNKEL, Y., ONG, A., NOTANI, D., MITTAL, Y., LAM, M., MI, X. & GHOSH, P. 2012. STAT3 protein up-regulates Galpha-interacting vesicle-associated protein (GIV)/Girdin expression, and GIV enhances STAT3 activation in a positive feedback loop during wound healing and tumor invasion/metastasis. *J Biol Chem,* 287**,** 41667-83.

EDGAR, R., DOMRACHEV, M. & LASH, A. E. 2002. Gene Expression Omnibus: NCBI gene expression and hybridization array data repository. *Nucleic Acids Res,* 30**,** 207-10.

FABREGAT, A., JUPE, S., MATTHEWS, L., SIDIROPOULOS, K., GILLESPIE, M., GARAPATI, P., HAW, R., JASSAL, B., KORNINGER, F., MAY, B., MILACIC, M., ROCA, C. D., ROTHFELS, K., SEVILLA, C., SHAMOVSKY, V., SHORSER, S., VARUSAI, T., VITERI, G., WEISER, J., WU, G., STEIN, L., HERMJAKOB, H. & D'EUSTACHIO, P. 2018. The Reactome Pathway Knowledgebase. *Nucleic Acids Res,* 46**,** D649-D655.

FAN, H., ZINGARELLI, B., PECK, O. M., TETI, G., TEMPEL, G. E., HALUSHKA, P. V., SPICHER, K., BOULAY, G., BIRNBAUMER, L. & COOK, J. A. 2005. Lipopolysaccharide- and gram-positive bacteria-induced cellular inflammatory responses: role of heterotrimeric Galpha(i) proteins. *Am J Physiol Cell Physiol,* 289**,** C293-301.

FERLITO, M., ROMANENKO, O. G., GUYTON, K., ASHTON, S., SQUADRITO, F., HALUSHKA, P. V. & COOK, J. A. 2002. Implication of Galpha i proteins and Src tyrosine kinases in endotoxin-induced signal transduction events and mediator production. *J Endotoxin Res,* 8**,** 427-35.

FLORHOLMEN, J. 2015. Mucosal healing in the era of biologic agents in treatment of inflammatory bowel disease. *Scand J Gastroenterol,* 50**,** 43-52.

FRIES, W., BELVEDERE, A. & VETRANO, S. 2013. Sealing the broken barrier in IBD: intestinal permeability, epithelial cells and junctions. *Curr Drug Targets,* 14**,** 1460-70.

GAFFEN, S. L. 2009. Structure and signalling in the IL-17 receptor superfamily. *Nat Rev Immunol,* 9**,** 556.

GARCIA-MARCOS, M., GHOSH, P., EAR, J. & FARQUHAR, M. G. 2010. A Structural Determinant That Renders Gαi Sensitive to Activation by GIV/Girdin Is Required to Promote Cell Migration*. *J Biol Chem.*

GARCIA-MARCOS, M., GHOSH, P. & FARQUHAR, M. G. 2009. GIV is a nonreceptor GEF for G alpha i with a unique motif that regulates Akt signaling. *Proc Natl Acad Sci U S A,* 106**,** 3178-83.

GARCIA-MARCOS, M., GHOSH, P. & FARQUHAR, M. G. 2015. GIV/ Girdin transmits signals from multiple receptors by triggering trimeric G protein activation. *J Biol Chem*.

GHOSH, P. 2015a. G protein coupled growth factor receptor tyrosine kinase: no longer an oxymoron. *Cell Cycle,* 14**,** 2561-5.

GHOSH, P. 2015b. Heterotrimeric G proteins as emerging targets for network based therapy in cancer: End of a long futile campaign striking heads of a Hydra. *Aging (Albany NY),* 7**,** 469-74.

GHOSH, P., GARCIA-MARCOS, M., BORNHEIMER, S. J. & FARQUHAR, M. G. 2008. Activation of Galphai3 triggers cell migration via regulation of GIV. *J Cell Biol,* 182**,** 381-93.

GHOSH, P., RANGAMANI, P. & KUFAREVA, I. 2017. The GAPs, GEFs, GDIs and...now, GEMs: New kids on the heterotrimeric G protein signaling block. *Cell Cycle,* 16**,** 607-612.

GILMAN, A. G. 1987. G proteins: transducers of receptor-generated signals. *Annu Rev Biochem,* 56**,** 615-49.

GUPTA, V., BHANDARI, D., LEYME, A., AZNAR, N., MIDDE, K. K., LO, I. C., EAR, J., NIESMAN, I., LOPEZ-SANCHEZ, I., BLANCO-CANOSA, J. B., VON ZASTROW, M., GARCIA-MARCOS, M., FARQUHAR, M. G. & GHOSH, P. 2016. GIV/Girdin activates Galphai and inhibits Galphas via the same motif. *Proc Natl Acad Sci U S A,* 113**,** E5721-30.

HARROLD, J. M., RAMANATHAN, M. & MAGER, D. E. 2013. Network-based approaches in drug discovery and early development. *Clin Pharmacol Ther,* 94**,** 651-8.

HAYANO, S., TAKEFUJI, M., MAEDA, K., NODA, T., ICHIMIYA, H., KOBAYASHI, K., ENOMOTO, A., ASAI, N., TAKAHASHI, M. & MUROHARA, T. 2015. Akt-dependent Girdin phosphorylation regulates repair processes after acute myocardial infarction. *J Mol Cell Cardiol,* 88**,** 55-63.

HEADLAND, S. E. & NORLING, L. V. 2015. The resolution of inflammation: Principles and challenges. *Semin Immunol,* 27**,** 149-60.

HWANG, T. J., CARPENTER, D., LAUFFENBURGER, J. C., WANG, B., FRANKLIN, J. M. & KESSELHEIM, A. S. 2016. Failure of Investigational Drugs in Late-Stage Clinical Development and Publication of Trial Results. *JAMA Intern Med,* 176**,** 1826-1833.

ICHIMIYA, H., MAEDA, K., ENOMOTO, A., WENG, L., TAKAHASHI, M. & MUROHARA, T. 2015. Girdin/GIV regulates transendothelial permeability by controlling VE-cadherin trafficking through the small GTPase, R-Ras. *Biochem Biophys Res Commun,* 461**,** 260-7.

JANG, J. H., SHIN, H. W., LEE, J. M., LEE, H. W., KIM, E. C. & PARK, S. H. 2015. An Overview of Pathogen Recognition Receptors for Innate Immunity in Dental Pulp. *Mediators Inflamm,* 2015**,** 794143.

JANG, T. H. & PARK, H. H. 2014. Crystal structure of TIR domain of TLR6 reveals novel dimeric interface of TIR-TIR interaction for toll-like receptor signaling pathway. *J Mol Biol,* 426**,** 3305-3313.

JIMINEZ, J. A., UWIERA, T. C., DOUGLAS INGLIS, G. & UWIERA, R. R. 2015. Animal models to study acute and chronic intestinal inflammation in mammals. *Gut Pathog,* 7**,** 29.

JORDAN, I. K., MARINO-RAMIREZ, L., WOLF, Y. I. & KOONIN, E. V. 2004. Conservation and coevolution in the scale-free human gene coexpression network. *Mol Biol Evol,* 21**,** 2058-70.

KARIN, M. 1995. The regulation of AP-1 activity by mitogen-activated protein kinases. *J Biol Chem,* 270**,** 16483-6.

KIESSLICH, R., DUCKWORTH, C. A., MOUSSATA, D., GLOECKNER, A., LIM, L. G., GOETZ, M., PRITCHARD, D. M., GALLE, P. R., NEURATH, M. F. & WATSON, A. J. 2012. Local barrier dysfunction identified by confocal laser endomicroscopy predicts relapse in inflammatory bowel disease. *Gut,* 61**,** 1146-53.

KIM, J. J., SHAJIB, M. S., MANOCHA, M. M. & KHAN, W. I. 2012. Investigating intestinal inflammation in DSS-induced model of IBD. *J Vis Exp*.

KITANO, H. 2007a. A robustness-based approach to systems-oriented drug design. *Nat Rev Drug Discov,* 6**,** 202-10.

KITANO, H. 2007b. Towards a theory of biological robustness. *Mol Syst Biol,* 3**,** 137.

KOBAYASHI, K., HERNANDEZ, L. D., GALAN, J. E., JANEWAY, C. A., JR., MEDZHITOV, R. & FLAVELL, R. A. 2002. IRAK-M is a negative regulator of Toll-like receptor signaling. *Cell,* 110**,** 191-202.

LE-NICULESCU, H., NIESMAN, I., FISCHER, T., DEVRIES, L. & FARQUHAR, M. G. 2005. Identification and characterization of GIV, a novel Galpha i/s-interacting protein found on COPI, endoplasmic reticulum-Golgi transport vesicles. *J Biol Chem,* 280**,** 22012-20.

LEE, I., DATE, S. V., ADAI, A. T. & MARCOTTE, E. M. 2004. A probabilistic functional network of yeast genes. *Science,* 306**,** 1555-8.

LI, C., ZIENKIEWICZ, J. & HAWIGER, J. 2005. Interactive sites in the MyD88 Toll/interleukin (IL) 1 receptor domain responsible for coupling to the IL1beta signaling pathway. *J Biol Chem,* 280**,** 26152-9.

LIEW, F. Y., XU, D., BRINT, E. K. & O'NEILL, L. A. 2005. Negative regulation of toll-like receptor-mediated immune responses. *Nat Rev Immunol,* 5**,** 446-58.

LO, I. C., GUPTA, V., MIDDE, K. K., TAUPIN, V., LOPEZ-SANCHEZ, I., KUFAREVA, I., ABAGYAN, R., RANDAZZO, P. A., FARQUHAR, M. G. & GHOSH, P. 2015. Activation of Galphai at the Golgi by GIV/Girdin imposes finiteness in Arf1 signaling. *Dev Cell,* 33**,** 189-203.

LOPEZ-SANCHEZ, I., DUNKEL, Y., ROH, Y. S., MITTAL, Y., DE MINICIS, S., MURANYI, A., SINGH, S., SHANMUGAM, K., AROONSAKOOL, N., MURRAY, F., HO, S. B., SEKI, E., BRENNER, D. A. & GHOSH, P. 2014. GIV/Girdin is a central hub for profibrogenic signalling networks during liver fibrosis. *Nat Commun,* 5**,** 4451.

LOSCALZO, J. & BARABASI, A. L. 2011. Systems biology and the future of medicine. *Wiley Interdiscip Rev Syst Biol Med,* 3**,** 619-27.

LU, Y. C., YEH, W. C. & OHASHI, P. S. 2008. LPS/TLR4 signal transduction pathway. *Cytokine,* 42**,** 145-151.

LUCAS, T., WAISMAN, A., RANJAN, R., ROES, J., KRIEG, T., MULLER, W., ROERS, A. & EMING, S. A. 2010. Differential roles of macrophages in diverse phases of skin repair. *J Immunol,* 184**,** 3964-77.

LYSAKOVA-DEVINE, T., KEOGH, B., HARRINGTON, B., NAGPAL, K., HALLE, A., GOLENBOCK, D. T., MONIE, T. & BOWIE, A. G. 2010. Viral inhibitory peptide of TLR4, a peptide derived from vaccinia protein A46, specifically inhibits TLR4 by directly targeting MyD88 adaptor-like and TRIF-related adaptor molecule. *J Immunol,* 185**,** 4261-71.

MAHE, M. M., SUNDARAM, N., WATSON, C. L., SHROYER, N. F. & HELMRATH, M. A. 2015. Establishment of human epithelial enteroids and colonoids from whole tissue and biopsy. *J Vis Exp*.

MARGOLIN, A. A., NEMENMAN, I., BASSO, K., WIGGINS, C., STOLOVITZKY, G., DALLA FAVERA, R. & CALIFANO, A. 2006a. ARACNE: an algorithm for the reconstruction of gene regulatory networks in a mammalian cellular context. *BMC Bioinformatics,* 7 Suppl 1**,** S7.

MARGOLIN, A. A., WANG, K., LIM, W. K., KUSTAGI, M., NEMENMAN, I. & CALIFANO, A. 2006b. Reverse engineering cellular networks. *Nat Protoc,* 1**,** 662-71.

MATZINGER, P. 2002. The danger model: a renewed sense of self. *Science,* 296**,** 301-5.

MEDZHITOV, R. 2001. Toll-like receptors and innate immunity. *Nat Rev Immunol,* 1**,** 135-45.

MIYACHI, H., MII, S., ENOMOTO, A., MURAKUMO, Y., KATO, T., ASAI, N., KOMORI, K. & TAKAHASHI, M. 2014. Role of Girdin in intimal hyperplasia in vein grafts and efficacy of atelocollagen-mediated application of small interfering RNA for vein graft failure. *J Vasc Surg,* 60**,** 479-489 e5.

MIYACHI, H., TAKAHASHI, M. & KOMORI, K. 2015. A Novel Approach against Vascular Intimal Hyperplasia Through the Suppression of Girdin. *Ann Vasc Dis,* 8**,** 69-73.

MIYOSHI, H. & STAPPENBECK, T. S. 2013. In vitro expansion and genetic modification of gastrointestinal stem cells in spheroid culture. *Nat Protoc,* 8**,** 2471-82.

MOGENSEN, T. H. 2009. Pathogen Recognition and Inflammatory Signaling in Innate Immune Defenses. *Clin Microbiol Rev.*

MORIGGI, M., PASTORELLI, L., TORRETTA, E., TONTINI, G. E., CAPITANIO, D., BOGETTO, S. F., VECCHI, M. & GELFI, C. 2017. Contribution of Extracellular Matrix and Signal Mechanotransduction to Epithelial Cell Damage in Inflammatory Bowel Disease Patients: A Proteomic Study. *Proteomics,* 17.

MORRIS, A. J. & MALBON, C. C. 1999. Physiological regulation of G protein-linked signaling. *Physiol Rev,* 79**,** 1373-430.

MOYNAGH, P. N. 2005. TLR signalling and activation of IRFs: revisiting old friends from the NF-kappaB pathway. *Trends Immunol,* 26**,** 469-76.

MUNGUIA, J. & NIZET, V. 2017. Pharmacological Targeting of the Host-Pathogen Interaction: Alternatives to Classical Antibiotics to Combat Drug-Resistant Superbugs. *Trends Pharmacol Sci,* 38**,** 473-88.

MURRAY, P. J. 2017. Macrophage Polarization. *Annu Rev Physiol,* 79**,** 541-566.

MUZIO, M., BOSISIO, D., POLENTARUTTI, N., D'AMICO, G., STOPPACCIARO, A., MANCINELLI, R., VAN'T VEER, C., PENTON-ROL, G., RUCO, L. P., ALLAVENA, P. & MANTOVANI, A. 2000. Differential expression and regulation of toll-like receptors (TLR) in human leukocytes: selective expression of TLR3 in dendritic cells. *J Immunol,* 164**,** 5998-6004.

NOEL, G., BAETZ, N. W., STAAB, J. F., DONOWITZ, M., KOVBASNJUK, O., PASETTI, M. F. & ZACHOS, N. C. 2017. A primary human macrophage-enteroid co-culture model to investigate mucosal gut physiology and host-pathogen interactions. *Sci Rep,* 7**,** 45270.

NYMAN, T., STENMARK, P., FLODIN, S., JOHANSSON, I., HAMMARSTROM, M. & NORDLUND, P. 2008. The crystal structure of the human toll-like receptor 10 cytoplasmic domain reveals a putative signaling dimer. *J Biol Chem,* 283**,** 11861-5.

O'NEILL, L. A. 2008. Bacteria fight back against Toll-like receptors. *Nat Med.* United States.

OHNISHI, H., TOCHIO, H., KATO, Z., ORII, K. E., LI, A., KIMURA, T., HIROAKI, H., KONDO, N. & SHIRAKAWA, M. 2009. Structural basis for the multiple interactions of the MyD88 TIR domain in TLR4 signaling. *Proc Natl Acad Sci U S A,* 106**,** 10260-5.

ORTEGA-GÓMEZ, A., PERRETTI, M. & SOEHNLEIN, O. 2013. Resolution of inflammation: an integrated view. *EMBO Mol Med,* 5**,** 661-74.

PAN, B., SHEN, J., CAO, J., ZHOU, Y., SHANG, L., JIN, S., CAO, S., CHE, D., LIU, F. & YU, Y. 2015. Interleukin-17 promotes angiogenesis by stimulating VEGF production of cancer cells via the STAT3/GIV signaling pathway in non-small-cell lung cancer. *Sci Rep,* 5**,** 16053.

PARK, H. S., JUNG, H. Y., PARK, E. Y., KIM, J., LEE, W. J. & BAE, Y. S. 2004. Cutting edge: direct interaction of TLR4 with NAD(P)H oxidase 4 isozyme is essential for lipopolysaccharide-induced production of reactive oxygen species and activation of NF-kappa B. *J Immunol,* 173**,** 3589-93.

PEKOW, J., DOUGHERTY, U., HUANG, Y., GOMETZ, E., NATHANSON, J., COHEN, G., LEVY, S., KOCHERGINSKY, M., VENU, N., WESTERHOFF, M., HART, J., NOFFSINGER, A. E., HANAUER, S. B., HURST, R. D., FICHERA, A., JOSEPH, L. J., LIU, Q. & BISSONNETTE, M. 2013. Gene signature distinguishes patients with chronic ulcerative colitis harboring remote neoplastic lesions. *Inflamm Bowel Dis,* 19**,** 461-70.

PETERS, L. A., PERRIGOUE, J., MORTHA, A., IUGA, A., SONG, W. M., NEIMAN, E. M., LLEWELLYN, S. R., DI NARZO, A., KIDD, B. A., TELESCO, S. E., ZHAO, Y., STOJMIROVIC, A., SENDECKI, J., SHAMEER, K., MIOTTO, R., LOSIC, B., SHAH, H., LEE, E., WANG, M., FAITH, J. J., KASARSKIS, A., BRODMERKEL, C., CURRAN, M., DAS, A., FRIEDMAN, J. R., FUKUI, Y., HUMPHREY, M. B., IRITANI, B. M., SIBINGA, N., TARRANT, T. K., ARGMANN, C., HAO, K., ROUSSOS, P., ZHU, J., ZHANG, B., DOBRIN, R., MAYER, L. F. & SCHADT, E. E. 2017. A functional genomics predictive network model identifies regulators of inflammatory bowel disease. *Nat Genet,* 49**,** 1437-1449.

PIAO, W., SHIREY, K. A., RU, L. W., LAI, W., SZMACINSKI, H., SNYDER, G. A., SUNDBERG, E. J., LAKOWICZ, J. R., VOGEL, S. N. & TOSHCHAKOV, V. Y. 2015. A Decoy Peptide that Disrupts TIRAP Recruitment to TLRs Is Protective in a Murine Model of Influenza. *Cell Rep,* 11**,** 1941-52.

POLTORAK, A., HE, X., SMIRNOVA, I., LIU, M. Y., VAN HUFFEL, C., DU, X., BIRDWELL, D., ALEJOS, E., SILVA, M., GALANOS, C., FREUDENBERG, M., RICCIARDI-CASTAGNOLI, P., LAYTON, B. & BEUTLER, B. 1998. Defective LPS signaling in C3H/HeJ and C57BL/10ScCr mice: mutations in Tlr4 gene. *Science,* 282**,** 2085-8.

PROUDFOOT, A. E. 2002. Chemokine receptors: multifaceted therapeutic targets. *Nat Rev Immunol,* 2**,** 106-15.

QIN, J., QIAN, Y., YAO, J., GRACE, C. & LI, X. 2005. SIGIRR inhibits interleukin-1 receptor- and toll-like receptor 4-mediated signaling through different mechanisms. *J Biol Chem,* 280**,** 25233-41.

RAETZ, C. R. & WHITFIELD, C. 2002. Lipopolysaccharide endotoxins. *Annu Rev Biochem,* 71**,** 635-700.

REPPE, K., TSCHERNIG, T., LUHRMANN, A., VAN LAAK, V., GROTE, K., ZEMLIN, M. V., GUTBIER, B., MULLER, H. C., KURSAR, M., SCHUTTE, H., ROSSEAU, S., PABST, R., SUTTORP, N. & WITZENRATH, M. 2009. Immunostimulation with macrophage-activating lipopeptide-2 increased survival in murine pneumonia. *Am J Respir Cell Mol Biol,* 40**,** 474-81.

SACLIER, M., YACOUB-YOUSSEF, H., MACKEY, A. L., ARNOLD, L., ARDJOUNE, H., MAGNAN, M., SAILHAN, F., CHELLY, J., PAVLATH, G. K., MOUNIER, R., KJAER, M. & CHAZAUD, B. 2013. Differentially activated macrophages orchestrate myogenic precursor cell fate during human skeletal muscle regeneration. *Stem Cells,* 31**,** 384-96.

SAHOO, D. 2012. The power of boolean implication networks. *Front Physiol,* 3**,** 276.

SAHOO, D., DILL, D. L., GENTLES, A. J., TIBSHIRANI, R. & PLEVRITIS, S. K. 2008. Boolean implication networks derived from large scale, whole genome microarray datasets. *Genome Biol,* 9**,** R157.

SAHOO, D., DILL, D. L., TIBSHIRANI, R. & PLEVRITIS, S. K. 2007. Extracting binary signals from microarray time-course data. *Nucleic Acids Res,* 35**,** 3705-12.

SAHOO, D., SEITA, J., BHATTACHARYA, D., INLAY, M. A., WEISSMAN, I. L., PLEVRITIS, S. K. & DILL, D. L. 2010. MiDReG: a method of mining developmentally regulated genes using Boolean implications. *Proc Natl Acad Sci U S A,* 107**,** 5732-7.

SALATTO, C. T., MILLER, R. A., CAMERON, K. O., COKORINOS, E., REYES, A., WARD, J., CALABRESE, M. F., KURUMBAIL, R. G., RAJAMOHAN, F., KALGUTKAR, A. S., TESS, D. A., SHAVNYA, A., GENUNG, N. E., EDMONDS, D. J., JATKAR, A., MACIEJEWSKI, B. S., AMARO, M., GANDHOK, H., MONETTI, M., CIALDEA, K., BOLLINGER, E., KREEGER, J. M., COSKRAN, T. M., OPSAHL, A. C., BOUCHER, G. G., BIRNBAUM, M. J., DASILVA-JARDINE, P. & ROLPH, T. 2017. Selective Activation of AMPK beta1-Containing Isoforms Improves Kidney Function in a Rat Model of Diabetic Nephropathy. *J Pharmacol Exp Ther,* 361**,** 303-311.

SASAKI, K., KAKUWA, T., AKIMOTO, K., KOGA, H. & OHNO, S. 2015. Regulation of epithelial cell polarity by PAR-3 depends on Girdin transcription and Girdin-Galphai3 signaling. *J Cell Sci,* 128**,** 2244-58.

SATO, T., VRIES, R. G., SNIPPERT, H. J., VAN DE WETERING, M., BARKER, N., STANGE, D. E., VAN ES, J. H., ABO, A., KUJALA, P., PETERS, P. J. & CLEVERS, H. 2009. Single Lgr5 stem cells build crypt-villus structures in vitro without a mesenchymal niche. *Nature,* 459**,** 262-5.

SCANNELL, M., FLANAGAN, M. B., DESTEFANI, A., WYNNE, K. J., CAGNEY, G., GODSON, C. & MADERNA, P. 2007. Annexin-1 and peptide derivatives are released by apoptotic cells and stimulate phagocytosis of apoptotic neutrophils by macrophages. *J Immunol,* 178**,** 4595-605.

SHAMEER, S., LOGAN-KLUMPLER, F. J., VINSON, F., COTTRET, L., MERLET, B., ACHCAR, F., BOSHART, M., BERRIMAN, M., BREITLING, R., BRINGAUD, F., BUTIKOFER, P., CATTANACH, A. M., BANNERMAN-CHUKUALIM, B., CREEK, D. J., CROUCH, K., DE KONING, H. P., DENISE, H., EBIKEME, C., FAIRLAMB, A. H., FERGUSON, M. A., GINGER, M. L., HERTZ-FOWLER, C., KERKHOVEN, E. J., MASER, P., MICHELS, P. A., NAYAK, A., NES, D. W., NOLAN, D. P., OLSEN, C., SILVA-FRANCO, F., SMITH, T. K., TAYLOR, M. C., TIELENS, A. G., URBANIAK, M. D., VAN HELLEMOND, J. J., VINCENT, I. M., WILKINSON, S. R., WYLLIE, S., OPPERDOES, F. R., BARRETT, M. P. & JOURDAN, F. 2015. TrypanoCyc: a community-led biochemical pathways database for Trypanosoma brucei. *Nucleic Acids Res,* 43**,** D637-44.

SHEN, C., DING, Y., TANG, J., XU, X. & GUO, F. 2017a. An Ameliorated Prediction of Drug-Target Interactions Based on Multi-Scale Discrete Wavelet Transform and Network Features. *Int J Mol Sci,* 18.

SHEN, L., SU, L. & TURNER, J. R. 2009. Mechanisms and functional implications of intestinal barrier defects. *Dig Dis,* 27**,** 443-9.

SHEN, Y., ALVAREZ, M. J., BISIKIRSKA, B., LACHMANN, A., REALUBIT, R., PAMPOU, S., COKU, J., KARAN, C. & CALIFANO, A. 2017b. Systematic, network-based characterization of therapeutic target inhibitors. *PLoS Comput Biol,* 13**,** e1005599.

SLACK, J. L., SCHOOLEY, K., BONNERT, T. P., MITCHAM, J. L., QWARNSTROM, E. E., SIMS, J. E. & DOWER, S. K. 2000. Identification of two major sites in the type I interleukin-1 receptor cytoplasmic region responsible for coupling to pro-inflammatory signaling pathways. *J Biol Chem,* 275**,** 4670-8.

SONG, J., DUNCAN, M. J., LI, G., CHAN, C., GRADY, R., STAPLETON, A. & ABRAHAM, S. N. 2007. A novel TLR4-mediated signaling pathway leading to IL-6 responses in human bladder epithelial cells. *PLoS Pathog,* 3**,** e60.

SUAREZ, K., LIM, E., SINGH, S., PEREIRA, M., JOOSEN, L. P., IBEAWUCHI, S.-R., DUNKEL, Y., MITTAL, Y., HO, S. B., CHATTOPADHYAY, R., GUMA, M., BOLAND, B. S., DULAI, P. S., SANDBORN, W. J., GHOSH, P. & DAS, S. 2018. Dysregulation of the engulfment pathway in the gut fuels Inflammatory Bowel Disease. *BIORXIV,* 280172.

SUN, L. & YE, R. D. 2012. Role of G protein-coupled receptors in inflammation. *Acta Pharmacol Sin,* 33**,** 342-50.

SZKLARCZYK, D., MORRIS, J. H., COOK, H., KUHN, M., WYDER, S., SIMONOVIC, M., SANTOS, A., DONCHEVA, N. T., ROTH, A., BORK, P., JENSEN, L. J. & VON MERING, C. 2017. The STRING database in 2017: quality-controlled protein-protein association networks, made broadly accessible. *Nucleic Acids Res,* 45**,** D362-D368.

TAVAZOIE, S., HUGHES, J. D., CAMPBELL, M. J., CHO, R. J. & CHURCH, G. M. 1999. Systematic determination of genetic network architecture. *Nat Genet,* 22**,** 281-5.

TOSHCHAKOV, V. Y., SZMACINSKI, H., COUTURE, L. A., LAKOWICZ, J. R. & VOGEL, S. N. 2011. Targeting TLR4 signaling by TLR4 Toll/IL-1 receptor domain-derived decoy

peptides: identification of the TLR4 Toll/IL-1 receptor domain dimerization interface. *J Immunol,* 186**,** 4819-27.

TOSHCHAKOV, V. Y. & VOGEL, S. N. 2007. Cell-penetrating TIR BB loop decoy peptides a novel class of TLR signaling inhibitors and a tool to study topology of TIR-TIR interactions. *Expert Opin Biol Ther,* 7**,** 1035-50.

UM, J. H., PARK, S. J., KANG, H., YANG, S., FORETZ, M., MCBURNEY, M. W., KIM, M. K., VIOLLET, B. & CHUNG, J. H. 2010. AMP-activated protein kinase-deficient mice are resistant to the metabolic effects of resveratrol. *Diabetes,* 59**,** 554-63.

VAN DER GOTEN, J., VANHOVE, W., LEMAIRE, K., VAN LOMMEL, L., MACHIELS, K., WOLLANTS, W. J., DE PRETER, V., DE HERTOGH, G., FERRANTE, M., VAN ASSCHE, G., RUTGEERTS, P., SCHUIT, F., VERMEIRE, S. & ARIJS, I. 2014. Integrated miRNA and mRNA expression profiling in inflamed colon of patients with ulcerative colitis. *PLoS One,* 9**,** e116117.

VAN SOMEREN, E. P., WESSELS, L. F., BACKER, E. & REINDERS, M. J. 2002. Genetic network modeling. *Pharmacogenomics,* 3**,** 507-25.

VANHOVE, W., PEETERS, P. M., STAELENS, D., SCHRAENEN, A., VAN DER GOTEN, J., CLEYNEN, I., DE SCHEPPER, S., VAN LOMMEL, L., REYNAERT, N. L., SCHUIT, F., VAN ASSCHE, G., FERRANTE, M., DE HERTOGH, G., WOUTERS, E. F., RUTGEERTS, P., VERMEIRE, S., NYS, K. & ARIJS, I. 2015. Strong Upregulation of AIM2 and IFI16 Inflammasomes in the Mucosa of Patients with Active Inflammatory Bowel Disease. *Inflamm Bowel Dis,* 21**,** 2673-82.

VE, T., VAJJHALA, P. R., HEDGER, A., CROLL, T., DIMAIO, F., HORSEFIELD, S., YU, X., LAVRENCIC, P., HASSAN, Z., MORGAN, G. P., MANSELL, A., MOBLI, M., O'CARROLL, A., CHAUVIN, B., GAMBIN, Y., SIERECKI, E., LANDSBERG, M. J., STACEY, K. J., EGELMAN, E. H. & KOBE, B. 2017. Structural basis of TIR-domain-assembly formation in MAL- and MyD88-dependent TLR4 signaling. *Nat Struct Mol Biol,* 24**,** 743-751.

VE, T., WILLIAMS, S. J. & KOBE, B. 2015. Structure and function of Toll/interleukin-1 receptor/resistance protein (TIR) domains. *Apoptosis,* 20**,** 250-61.

VERSTOCKT, B., VERSTOCKT, S., DEHAIRS, J., BALLET, V., BLEVI, H., WOLLANTS, W. J., BREYNAERT, C., VAN ASSCHE, G., VERMEIRE, S. & FERRANTE, M. 2019. Low TREM1 expression in whole blood predicts anti-TNF response in inflammatory bowel disease. *EBioMedicine,* 40**,** 733-742.

VOLKMER, J. P., SAHOO, D., CHIN, R. K., HO, P. L., TANG, C., KURTOVA, A. V., WILLINGHAM, S. B., PAZHANISAMY, S. K., CONTRERAS-TRUJILLO, H., STORM, T. A., LOTAN, Y., BECK, A. H., CHUNG, B. I., ALIZADEH, A. A., GODOY, G., LERNER, S. P., VAN DE RIJN, M., SHORTLIFFE, L. D., WEISSMAN, I. L. & CHAN, K. S. 2012. Three differentiation states risk-stratify bladder cancer into distinct subtypes. *Proc Natl Acad Sci U S A,* 109**,** 2078-83.

WALD, D., QIN, J., ZHAO, Z., QIAN, Y., NARAMURA, M., TIAN, L., TOWNE, J., SIMS, J. E., STARK, G. R. & LI, X. 2003. SIGIRR, a negative regulator of Toll-like receptor-interleukin 1 receptor signaling. *Nat Immunol,* 4**,** 920-7.

WANG, H., MISAKI, T., TAUPIN, V., EGUCHI, A., GHOSH, P. & FARQUHAR, M. G. 2015. GIV/girdin links vascular endothelial growth factor signaling to Akt survival signaling in podocytes independent of nephrin. *J Am Soc Nephrol,* 26**,** 314-27.

WELLS, T. N., POWER, C. A. & PROUDFOOT, A. E. 1998. Definition, function and pathophysiological significance of chemokine receptors. *Trends Pharmacol Sci,* 19**,** 376-80.

WYNN, T. A., CHAWLA, A. & POLLARD, J. W. 2013. Origins and Hallmarks of Macrophages: Development, Homeostasis, and Disease. *Nature,* 496**,** 445-55.

WYNN, T. A. & VANNELLA, K. M. 2016. Macrophages in tissue repair, regeneration, and fibrosis. *Immunity,* 44**,** 450-62.

XIAO, B., SANDERS, M. J., CARMENA, D., BRIGHT, N. J., HAIRE, L. F., UNDERWOOD, E., PATEL, B. R., HEATH, R. B., WALKER, P. A., HALLEN, S., GIORDANETTO, F., MARTIN, S. R., CARLING, D. & GAMBLIN, S. J. 2013. Structural basis of AMPK regulation by small molecule activators. *Nat Commun,* 4**,** 3017.

XU, Y., TAO, X., SHEN, B., HORNG, T., MEDZHITOV, R., MANLEY, J. L. & TONG, L. 2000. Structural basis for signal transduction by the Toll/interleukin-1 receptor domains. *Nature,* 408**,** 111-5.

YE, R. D. 2001. Regulation of nuclear factor kappaB activation by G-protein-coupled receptors. *J Leukoc Biol,* 70**,** 839-48.

ZHAO, X., FAN, J., ZHI, F., LI, A., LI, C., BERGER, A. E., BOORGULA, M. P., BARKATAKI, S., COURNEYA, J. P., CHEN, Y., BARNES, K. C. & CHEADLE, C. 2015. Mobilization of epithelial mesenchymal transition genes distinguishes active from inactive lesional tissue in patients with ulcerative colitis. *Hum Mol Genet,* 24**,** 4615-24.